

1 REVISION #2—07 May 2020—*American Mineralogist*

2
3 **An evolutionary system of mineralogy, part II: Interstellar and solar**
4 **nebula primary condensation mineralogy (> 4.565 Ga)**

5
6 **SHAUNNA M. MORRISON¹ AND ROBERT M. HAZEN^{1,*}**

7 ¹Earth and Planets Laboratory, Carnegie Institution for Science,
8 5251 Broad Branch Road NW, Washington DC 20015, U. S. A.
9

10
11 **ABSTRACT**

12 The evolutionary system of mineralogy relies on varied physical and chemical attributes,
13 including trace elements, isotopes, solid and fluid inclusions, and other information-rich
14 characteristics, to understand processes of mineral formation and to place natural condensed
15 phases in the deep-time context of planetary evolution. Part I of this system reviewed the earliest
16 refractory phases that condense at $T > 1000$ K within the turbulent expanding and cooling
17 atmospheres of highly evolved stars. Part II considers the subsequent formation of primary
18 crystalline and amorphous phases by condensation in three distinct mineral-forming environments,
19 each of which increased mineralogical diversity and distribution prior to the accretion of
20 planetesimals > 4.5 billion years ago:

- 21 1) *Interstellar molecular solids*: Varied crystalline and amorphous molecular solids containing
22 primarily H, C, O, and N are observed to condense in cold, dense molecular clouds in the
23 interstellar medium ($10 < T < 20$ K; $P < 10^{-13}$ atm). With the possible exception of some
24 nano-scale organic condensates preserved in carbonaceous meteorites, the existence of

25 these phases is documented primarily by telescopic observations of absorption and emission
26 spectra of interstellar molecules in radio, microwave, or infrared wavelengths.

27 2) *Nebular and circumstellar ice*: Evidence from infrared observations and laboratory
28 experiments suggest that cubic H₂O (“cubic ice”) condenses as thin crystalline mantles on
29 oxide and silicate dust grains in cool, distant nebular and circumstellar regions where T
30 ~100 K.

31 3) *Primary condensed phases of the inner solar nebula*: The earliest phase of nebular
32 mineralogy saw the formation of primary refractory minerals that solidified through high-
33 temperature condensation ($1100 < T < 1800$ K; $10^{-6} < P < 10^{-2}$ atm) in the solar nebula
34 more than 4.565 billion years ago. These earliest mineral phases originating in our solar
35 system formed prior to the accretion of planetesimals and are preserved in calcium-
36 aluminum-rich inclusions, ultra-refractory inclusions, and amoeboid olivine aggregates.

37

38

39 *E-mail: rhazen@carnegiescience.edu

40 **Keywords:** classification; mineral evolution; natural kinds; vapor deposition; condensation;

41 nebular mineralogy; interstellar mineralogy; chondrite meteorites

42

INTRODUCTION

43 The incremental, episodic emergence of mineral diversity and distribution through more than
44 13 billion years of cosmic evolution provides the basis for an “evolutionary system” of mineral
45 classification—one that emphasizes the formation of solid phases by a progression of physical,
46 chemical, and ultimately biological processes (Hazen et al. 2008; Hazen and Ferry 2010; Hazen
47 2019; Hazen and Morrison 2020). This system amplifies the official classification protocols of the
48 International Mineralogical Association’s Commission on New Minerals, Nomenclature and
49 Classification (IMA, CNMNC; e.g., Burke 2006; Mills et al. 2009; Schertl et al. 2018), which
50 defines each mineral “species” on the basis of its unique combination of end-member composition
51 and idealized crystal structure. More than 5500 approved mineral species are now recognized by
52 the IMA system (rruff.info/ima; accessed 27 March 2020).

53 By design, the IMA classification system is predicated on identifying the minimum amount of
54 information (as measured in bits; e.g., Krivovichev 2012, 2013) required to distinguish one species
55 from another. Consequently, IMA procedures cannot capture the information-rich complexity of
56 natural mineral specimens—their trace and minor elements, fractionated isotopes, structural
57 defects, varied magnetic and electrical properties, external morphologies, solid and fluid
58 inclusions, spectral features, petrologic environment, ages of both formation and subsequent
59 diagenetic episodes, and myriad other attributes that have the potential to tell the story of each
60 individual sample’s origin and alteration via interactions with a succession of environments
61 through deep time. We conclude that IMA protocols are insufficient to classify minerals in their
62 evolutionary contexts.

63 Accordingly, we propose an “evolutionary system of mineralogy” that amplifies and modifies
64 the IMA scheme in three ways, each of which is informed by those information-rich aspects of

65 natural mineral specimens—attributes that are the essence of historical science discovery in the
66 “messy, uncontrollable world of nature” (Cleland 2013; see also Cleland 2011). We split some
67 IMA species into two or more “natural kinds”—subdivisions that recognize fundamentally
68 different idiosyncratic combinations of attributes that arise from distinct paragenetic modes. Thus,
69 for example, we view isotopically anomalous nanoscale diamond condensed from a high-
70 temperature, low-pressure carbon-rich vapor in the expanding atmosphere of an exploding star as
71 intrinsically different from macroscopic Type I “gem” diamond crystallized in high-temperature,
72 high-pressure, carbon-saturated aqueous fluids in Earth’s mantle, which in turn differs from
73 diamond formed by the impact of an asteroid on near-surface carbonaceous material (Hazen 2019).
74 Such splitting of IMA species into multiple “natural kinds” is appropriate for many of Earth’s
75 commonest mineral species, including calcite, hydroxylapatite, pyrite, and quartz, all of which
76 have both abiotic and biotic paragenetic modes.

77 In other instances, we propose lumping two or more IMA species into a single “natural kind.”
78 Notable examples of species that are lumped according to their evolutionary contexts occur in
79 chemically diverse structural groups of rock-forming silicates, including amphibole, mica,
80 pyroxene, and tourmaline group minerals, for which a given specimen formed in a single
81 geological setting and in one continuous phase domain may display a range of zoning and solid
82 solution that overlaps the compositional ranges of two or more end-member species as defined by
83 IMA protocols. Other examples of IMA species that we lump into a single natural kind include
84 groups of isostructural rare earth element minerals, some Mg-Fe oxides and silicates, and natural
85 metal alloys, for which small variations in the ratios of crystal chemically similar elements that
86 occur within one paragenetic environment may require multiple IMA end-member mineral
87 species.

88 Thirdly, the evolutionary system catalogues a variety of non-crystalline or aperiodic condensed
89 phases, including glasses (e.g., stellar amorphous carbon, impact maskelynite, volcanic obsidian)
90 and mixed-phase nano-materials (bauxite, coal, and limonite, for example)—materials not usually
91 considered in the current IMA scheme (e.g., Hazen et al. 2013, Table 3), though many of these
92 phases were included in the revolutionary third edition of James Dwight Dana's *System of*
93 *Mineralogy* (Dana 1850), from which the modern IMA formalisms have evolved.

94

95 *Meteorite minerals*

96 An important illustration of the demonstrable benefits and potential pitfalls of the IMA system
97 is provided by the diversity, distribution, and modes of formation of meteorite minerals, as
98 reviewed by Rubin and Ma (2017, 2020), who tabulate more than 400 types of minerals known
99 from meteorites, the majority of which (including dozens of intriguing micro- or nano-scale phases
100 discovered by Dr. Chi Ma) have been approved as official IMA species. However, more than 50
101 of the listed meteorite phases are not officially recognized by the IMA (see rruff.info/ima; accessed
102 27 March 2020), because they fail to meet IMA criteria for legitimate species owing to a range of
103 reasons.

104 At least a dozen minerals in Rubin and Ma's list, including native Mo, Nb, and Re; carbides of
105 Fe, Mo, and Zr; Ca and Nb oxides, and other primarily micron-scale phases, may eventually
106 receive approval but have not yet been accepted by the IMA. However, many of Rubin and Ma's
107 listed phases do not meet IMA requirements for end-member compositional variants of natural
108 crystalline phases. In some cases, they list phases that effectively split IMA species as a
109 consequence of additional minor elements. For example, they record "Ti-rich" and "V-rich"
110 varieties of magnetite (in addition to magnetite), "pleonaste" (a varietal name for Mg-Fe²⁺ oxide

111 spinel), “sodium phlogopite,” “Ca-armalcolite,” and “carbonate-fluorapatite.” They also split
112 graphite into two polytypes—graphite 2H and graphite 3R.

113 On the other hand, in some instances Rubin and Ma (2017, 2020) lump mineral species into
114 broadly inclusive mineral groups—e.g., apatite, feldspar, mica, olivine, and orthopyroxene. They
115 also implicitly lump two or more approved minerals with end-member compositions into one solid
116 solution; for example, their list includes “magnesiowüstite,” which is an unapproved name for the
117 solid solution between periclase (MgO) and wüstite (FeO), both of which end members are also
118 listed. Similarly, IMA-approved magnesite (MgCO₃) and siderite (FeCO₃) are listed along with
119 “breunnerite,” an obsolete, though useful, name for Mg-dominant rhombohedral carbonates in the
120 magnesite-siderite solid solution. “Plagioclase” also appears in the tabulation along with the two
121 end members of the albite-anorthite solid solution. Similarly, “biotite,” “Au-dominated alloys,”
122 and “PGE-dominated alloys” are names for chemically complex phase regions that encompass
123 multiple approved IMA species.

124 Finally, Rubin and Ma (2017, 2020) catalog several amorphous or composite nanophases that
125 are excluded from the current IMA list (illite, martinsite, and maskelynite, for example). In these
126 particulars, Rubin and Ma’s tabulation of meteorite minerals mirrors the evolutionary system of
127 mineralogy, as it underscores both the need for the exacting IMA nomenclature and the desirability
128 of additional classification protocols to address complex natural condensed phases – varied split,
129 lumped, and non-crystalline phases that are critical to describing the diverse modes of mineral
130 formation in the natural world.

131 The potential benefits of the evolutionary system are further highlighted by Rubin and Ma
132 (2017), who list 17 different processes by which the hundreds of documented meteorite minerals
133 have formed ([Table 1](#)). They note, “Some meteoritic minerals form by only a single mechanism

134 (e.g., ringwoodite and ahrensite by high-pressure shock metamorphism of olivine); other minerals
 135 form by several mechanisms (e.g., olivine by condensation around red giant and AGB stars,
 136 condensation in the solar nebula, crystallization in [high-temperature nebular] melts,
 137 crystallization in chondrule melts, thermal metamorphism, crystallization from impact melts,
 138 condensation within impact plumes, crystallization in magmatic bodies on differentiated asteroids,
 139 annealing of amorphous material, and aqueous alteration)” (Rubin and Ma 2017, page 339). They
 140 emphasize that, “In this overview, no attempt has been made to describe every mode of formation
 141 of every meteoritic mineral. That monumental task would require a multi-volume book-length
 142 treatment.”

143 We suggest that such varied modes of formation usually result in diagnostic sets of attributes
 144 that point to multiple natural kinds—the mineralogical key to understanding the evolution of
 145 planetary systems. Our multi-part endeavor, though far from the encyclopedic “monumental task”
 146 envisioned by Rubin and Ma for meteorite minerals, nevertheless will attempt to enumerate
 147 mineral natural kinds in the context of their paragenetic modes.

148

149 **Table 1.** Seventeen paragenetic modes of meteorite minerals, after Rubin and Ma (2017). Note that these modes of
 150 formation are not mutually exclusive. “Part” refers to proposed divisions of the evolutionary system of mineralogy,
 151 which will appear in multiple, ongoing contributions.

152

153	Mode #	Description	Part
154	1	Condensation in the gaseous envelopes of stars (stellar mineralogy)	I
155	2	Condensation in the solar nebula	II
156	3	Crystallization in CAI and AOA melts	II
157	4	Crystallization in chondrule melts	III
158	5	Exsolution during cooling of CAIs	II
159	6	Exsolution during cooling of chondrules	III
160	7	Annealing of amorphous material	I, II, & III
161	8	Thermal metamorphism and exsolution	V
162	9	Aqueous alteration, hydrothermal alteration, and metasomatism	V
163	10	Shock metamorphism	IV
164	11	Condensation within impact plumes	IV
165	12	Crystallization from melts in differentiated bodies	IV
166	13	Condensation from late-stage vapors in differentiated bodies	IV
167	14	Exsolution, inversion, and subsolidus redox effects in cooling igneous rocks	IV

168	15	Solar heating near perihelion	III,V
169	16	Atmospheric passage	V
170	17	Terrestrial weathering*	VI+
171	<hr/> *Includes biological alteration, to be discussed in later contributions. <hr/>		
172			

173 *Pre-terrestrial stages of mineral formation*

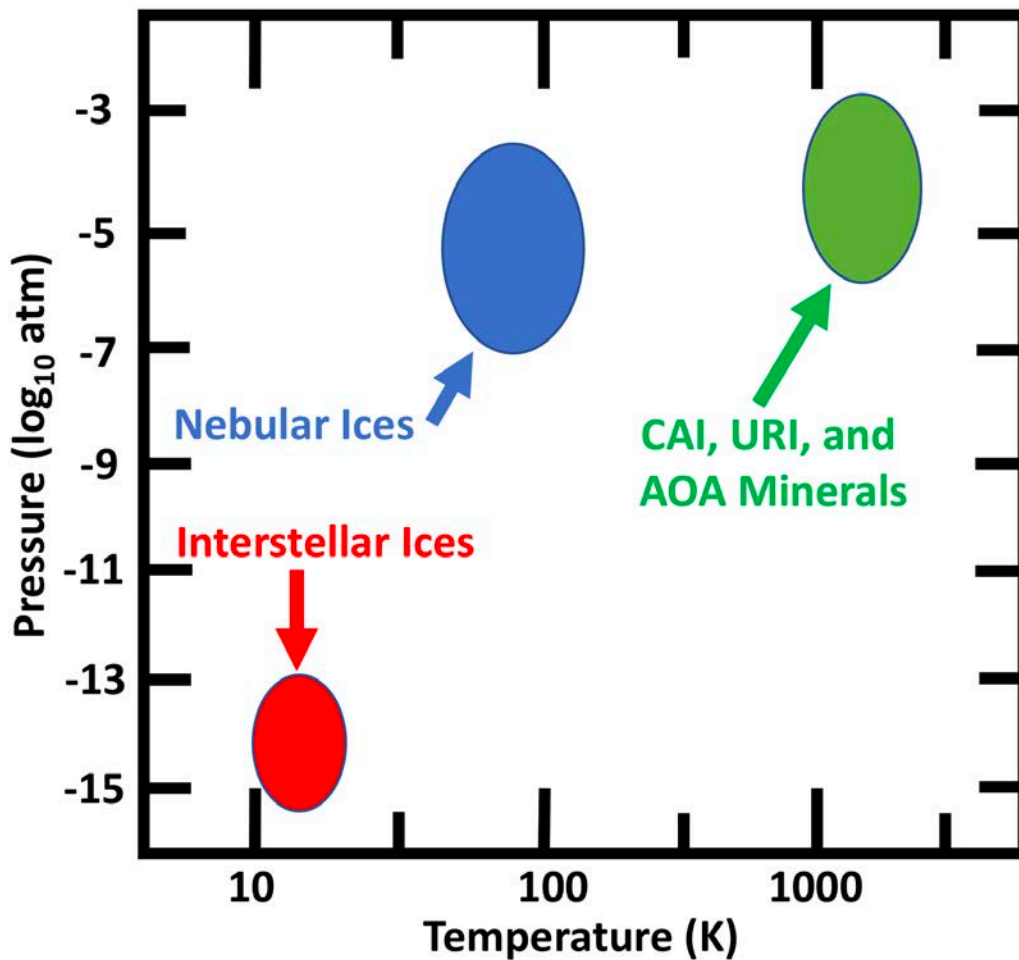
174 In Part I of this series, Hazen and Morrison (2020) described the earliest phase of mineral
175 evolution commencing more than 13 billion years ago – the condensation of more than 40 kinds
176 of extremely refractory nanoscale minerals, representing 22 IMA-approved mineral species, as
177 well as two as yet unapproved crystalline phases and amorphous forms of carbon, alumina, and
178 silicates (i.e., Mode #1 of Rubin and Ma’s 17 modes of meteorite mineralization; Table 1). These
179 varied phases were dispersed as micro- and nanoscale dust grains into the interstellar medium,
180 along with hydrogen, helium, and other atomic and molecular species. A variety of highly evolved
181 stars, including C- and O-rich asymptotic giant branch (AGB) stars, classical novae, and type II
182 supernovae, seeded the interstellar environment with copious quantities of gas and mineral dust.
183 Significant fractions of those raw materials eventually concentrated in subsequent generations of
184 stars and their companion planets.

185 Here in Part II we examine the next two episodes of cosmic mineral evolution, which
186 encompass the primary condensation, melt crystallization, and initial solid-state transformation on
187 cooling (e.g., exsolution, reversible phase transitions, and element ordering) of a variety of
188 crystalline and amorphous phases from the dust and gaseous remnants of stars. These processes
189 include modes of formation #2, #3, and #5 in Table 1, as well as additional processes that lead to
190 interstellar and circumstellar condensed phases that are observed through telescopic spectral
191 observations but are not preserved in meteorites.

192 In particular, we consider a few kinds of condensed molecular phases, sometimes collectively
193 known as “ices,” though in this review the term ice refers exclusively to crystalline H₂O.
194 Condensed molecular solids are observed by astronomical spectroscopy to form in the extremely
195 low-temperature, high-vacuum conditions of “cool, dense” interstellar molecular clouds – the
196 nurseries of new generations of stars. Perturbations to a molecular cloud can lead to a Jeans
197 instability – a local density increase, followed by gravitationally-induced collapse of the molecular
198 cloud into a solar nebula, and ultimately star system formation (Jeans 1902; Mizuno et al. 1994;
199 Longair 2008). In the case of our solar system, more than 99.8 percent of the solar nebula’s mass
200 formed the Sun, commencing ~4.567 billion years ago, while the remaining dust and gas
201 experienced a complex history of thermal processing and chemical mixing that led to the formation
202 of numerous additional solid phases (Rubin and Ma 2017, 2020).

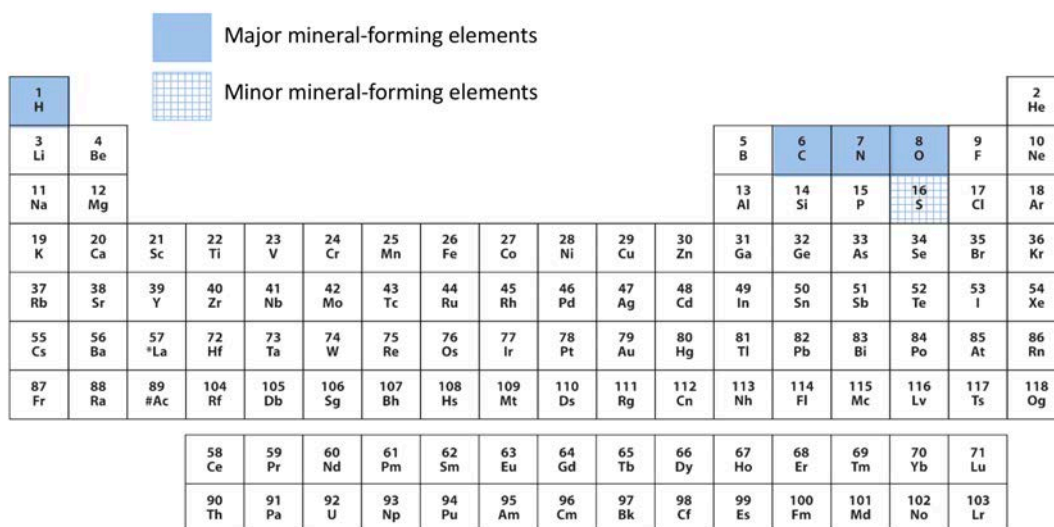
203 In this contribution we focus on presumed primary phases—those that are thought to have
204 formed by condensation directly from a gas phase, by subsequent solidification from a melt at
205 pressures less than 0.01 atm, and solid-state transformations (e.g., exsolution, annealing, or
206 ordering), as observed in calcium-aluminum-rich inclusions (CAIs), amoeboid olivine aggregates
207 (AOAs), and ultra-refractory inclusions (URIs) of chondrite meteorites (Figure 1). We also include
208 condensation of cubic ice (H₂O), the low-temperature crystalline polymorph of water ice (e.g.,
209 Gaffney and Matson 1980), as < 0.05 micron-thick crystalline mantles on oxide and silicate dust
210 particles in the cold, distant circumstellar regions of solar nebulae. It should be emphasized,
211 however, that most primary condensed interstellar and solar nebular phases were either lost
212 through sublimation or were eventually incorporated into larger bodies—asteroids, comets, and
213 planetesimals that experienced subsequent alteration by large-scale differentiation; fluid-rock
214 interactions; multiple thermal events, including heating by the decay of short-lived radioactive

215 isotopes, radiative heating, and conversion of gravitational potential energy; and high-energy
216 impacts. Thus, a continuum exists between pristine “primary” and altered “secondary” mineral
217 grains (e.g., Brearley and Jones 1998; MacPherson 2014; Rubin and Ma 2017). Primary mineral
218 phases preserved in chondrules, which formed by melt solidification and subsequent solid-state
219 reactions (Brearley and Jones 1998; Scott and Krot 2014; Connolly and Jones 2016), are the subject
220 of Part III of this series, whereas the rich variety of presumed secondary minerals, as processed in
221 the dynamic environments of growing planetesimals and preserved in the diverse meteorites that
222 fall to Earth, will be the focus of Parts IV and V.



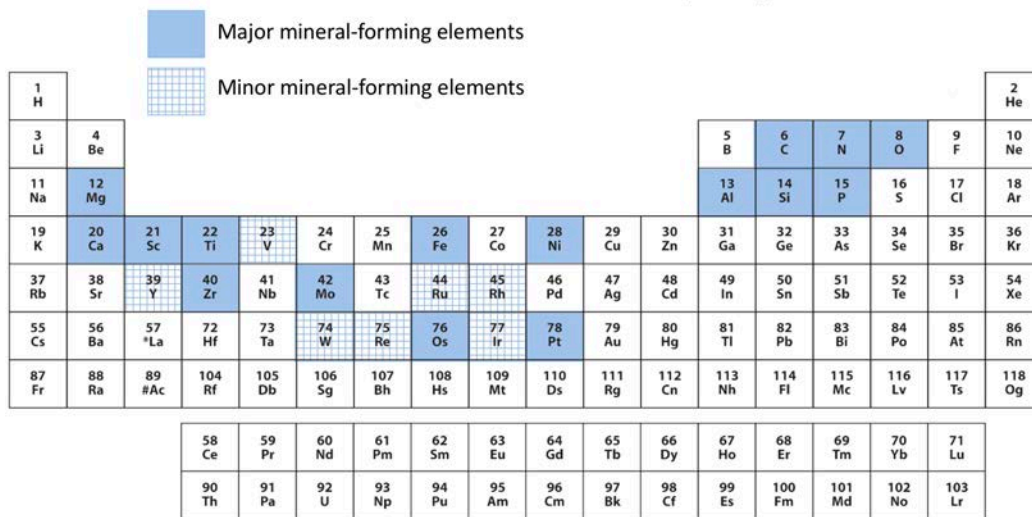
223 **A**

INTERSTELLAR MINERAL-FORMING ELEMENTS



224 **B**

MINERAL-FORMING ELEMENTS IN CAIs, URIs, and AOAs



225 **C**

226 **Figure 1.** The temperature, pressure, and compositional characteristics of primary interstellar and
 227 solar nebular condensates result in a distinctive second phase of the evolutionary system of
 228 mineralogy. **A.** These minerals formed at a wide range of temperatures via low-pressure ($P < 0.01$
 229 atm) condensation in interstellar and nebular environments. **B.** Interstellar minerals formed
 230 primarily from C, H, N, O, and probably S – five of the most abundant elements in the cosmos. **C.**
 231 Primary minerals in CAIs, URIs, and AOAs formed principally from 16 essential major elements,
 232 with important additional contributions from 7 minor elements.

233
234
235
236
237
238
239
240
241
242
243
244
245

THE MINERALOGY OF INTERSTELLAR MOLECULAR CLOUDS

Highly-evolved mineral-producing stars eject a significant fraction of their atmospheric dust and gas in energetic solar winds. Much of this ejected mass continues to be collected throughout the galaxy in a variety of molecular clouds, most of which are too warm and dispersed to form additional condensed phases (Greenberg 1991; Ferriere 2001). Only the so-called “cool, dense molecular clouds” have been the loci of a second significant pulse of cosmic condensation, albeit at significantly lower temperatures and pressures than their stellar precursors (Figure 2). These distinctive interstellar molecular clouds, typically composed of 99 percent gas, predominantly H in the form of H atoms and H₂ molecules (Wakelam et al. 2017) and atomic He, with important contributions by O-, C-, and N-bearing molecular species (Figure 1B), and ~1 weight percent (wt. %) mineral dust (primarily oxides, silicates, carbides, and carbon allotropes), are the nurseries of new star systems (e.g., Herbst 1995).



246
247
248
249
250
251
252

Figure 2. A 2015 Hubble Space Telescope image of a portion of the Eagle Nebula (NGC 6611 and IC 4703), dubbed “The Pillars of Creation,” displays a star-forming region of a dense molecular cloud. The core regions of this structure are cooler areas, dense molecular clouds where molecular solids condense. [image credit: NASA, ESA and the Hubble Heritage Team (STScI/AURA)].

253

254 *The environments of cool, dense molecular clouds*

255 “Cool, dense molecular clouds” might seem misnamed. They are relatively cold ($10 < T < 20$
256 K) regions of the interstellar medium that are characterized by the gradual condensation of a
257 variety of molecular solids (Kouchi and Yamamoto 1995; Allamandola et al. 1999; Ferriere 2001;
258 Gibb et al. 2004). Furthermore, “dense” in this context equates to approximately 10^2 to a maximum
259 of 10^6 molecules per cubic centimeter—i.e., orders of magnitude lower pressure than the 10^{10}
260 molecules per cm^3 in a typical laboratory “high vacuum,” though significantly greater than the
261 average galactic medium of fewer than one atom per cubic centimeter. Thus, the effective pressures
262 of condensation in cool, dense molecular clouds are thought to be less than 10^{-13} atm (Figure 1A).

263 Cool, dense molecular clouds are vast, sometimes exceeding 100 light years in diameter, and
264 they appear as dark irregular shapes in silhouette against the twinkling background of more distant
265 stars—a consequence of the cumulative effect of light-blocking dust (Ferriere 2001; Di Francesco
266 et al. 2006). Of note is the Taurus Molecular Cloud, which at a distance of ~430 light years is the
267 closest and among the best studied large star-forming regions (Luhman et al. 2010). In addition to
268 hundreds of relatively young stars, the Taurus Molecular Cloud hosts a diverse suite of molecular
269 species (Freeman and Millar 1983), some of which (though not all; e.g., Güstón et al. 2019)
270 condense into molecular crystals and amorphous solids.

271 Evidence for such interstellar condensed phases comes primarily from infrared absorption
272 measurements, as light from more distant stars passes through a molecular cloud, as well as by IR
273 and radio emission spectroscopy. Astronomical observations are interpreted using spectroscopic
274 data from laboratory experiments on small molecules under cold vacuum (e.g., Allamandola et al.

1999; Ehrenfreund and Cami 2010, and references therein). These interstellar solids are nanoscale in dimensions, volatile in subsequent warmer solar nebular environments, and inaccessible from Earth; consequently, they will never grace the collections of mineralogical museums. Nevertheless, these ephemeral, sub-microscopic condensed phases are among the largest molecular repositories in the cosmos; thus, they play a significant role in the origins and distribution of key volatile molecular species in planetary systems.

At 10 K, most molecular species have a “sticking coefficient” close to unity, meaning that almost all gaseous species except for H₂ and He adhere to cold surfaces. Under such conditions, gradual molecule-by-molecule condensation of the most abundant molecular species, including H₂O, CO, CO₂, CH₃OH, and CH₄, is thought to occur on the surfaces of dust grains. By contrast, condensed molecular phases are not thought to be present in the warmer diffuse interstellar medium ($50 < T < 100$ K; $< 10^3$ atoms/cm³; Ehrenfreund and Charnley 2000; Ferriere 2001).

The diversity and distribution of molecular components in interstellar solids reflect the initial gas phase composition, predominantly H and He with C, O, and N (Figure 1B), that has been significantly modified by several factors, including relative rates of condensation and sublimation at low temperatures, the nature of dust grain substrates, intermolecular chemical reactions, photochemical alteration by UV radiation and cosmic rays, and gradual annealing (Seki and Hasegawa 1983; Kouchi and Kuroda 1990; Jenniskens and Blake 1994, 1996; Kouchi et al. 1994; Ehrenfreund and Charnley 2000; Ehrenfreund and Fraser 2003; Gibb et al. 2004; Williams 2005; Hollenbach et al. 2009). For example, Allamandola et al. (1999) review the important role of hydrogen speciation, notably the ratio of H to H₂, in molecular clouds. In regions where monatomic hydrogen dominates, hydrogenation reactions lead to synthesis of H₂O, NH₃, and CH₄

297 as common condensed species. In H₂-rich environments, by contrast, O₂, N₂, CO, and CO₂ occur
298 more abundantly in condensates. Accordingly, Allamandola et al. (1999) conclude that condensed
299 molecular mantles on dust grains may fall into two principal populations distinguished by the
300 dominant local hydrogen species.

301

302 *Characterizing interstellar condensed phases*

303 The first interstellar molecular condensates to be identified were CO (Wilson et al. 1971) and
304 H₂O (Gillet and Forrest 1973), based on their strong absorption bands at 4.67 and 3.07 microns,
305 respectively. Subsequent discoveries of absorption and emission features point to hundreds of
306 molecular species, of which a few may condense and anneal in local concentrations that warrant
307 designation as an interstellar mineral. The most detailed picture of the nature and distribution of
308 these interstellar phases comes from orbiting telescopic measurements, for example as summarized
309 by Gibb et al. (2004), who review spectra in the 2.5- to 30-micron range measured by the Short-
310 Wavelength Spectrometer of the *Infrared Space Observatory (ISO)*. *ISO* spectra reveal diagnostic
311 absorption features from a range of molecular sources that point to more than a dozen forms of
312 interstellar condensed molecules, of which at least five—H₂O, CO, CO₂, CH₃OH, and CH₄—
313 occur as discrete nanoscale phases. **Table 2** lists several phases that condense in the extremely
314 cold, low-pressure environments of circumstellar and interstellar molecular clouds.

315 By far the most abundant interstellar molecular condensate is water in its low-density
316 amorphous form (Jenniskens and Blake 1994, 1996), comprising more than 60% of observable
317 molecular solids (Gibb et al. 2004). Water molecules are identified based on a characteristic O-H
318 stretching infrared absorption feature at 3.05 microns, coupled with bending and combination

319 absorption modes at 1.65, 4.5, and 6.0 microns (Whittet 2003; Hagen et al. 1981; Grundy and
320 Schmitt 1998; Newman et al. 2008). Importantly, interstellar water ice and other condensates were
321 the primary source of water and other volatiles on Earth (Alexander et al. 2018).

322 Four other common condensate species are CO (with a diagnostic C-O stretch mode at 4.67
323 microns), CO₂ (C-O stretch and O-C-O bending modes at 4.27 and 15.2 microns, respectively),
324 CH₃OH (four bands at 3.54, 3.95, 8.90, and 9.75 microns), and CH₄ (7.676 microns), all of which
325 have been confirmed to exist in the solid state. These molecular solids, which formed primarily by
326 heterogeneous condensation and/or photoreactions on dust grains (Seki and Hasegawa 1983; Lacy
327 et al. 1991; Kouchi and Yamamoto 1995; Gibb et al. 2004; Williams 2005), occur both as relatively
328 pure phases and as condensed molecular mixtures.

329 In addition to the five most abundant solid-forming molecules noted above, strong evidence
330 exists for other molecular species as generally minor, i.e., < 1 molecular percent (mol %) components of condensed phases, including N₂, O₂, OCS, H₂CO, HCOOH, XCN (where X may
331 be oxygen; Whittet et al. 2001), and NH₃, while the molecular ions OCN⁻, NH₄⁺, and CN⁻ may
332 also play a role in some condensed solids (Gibb et al. 2004).

334 Molecular clouds also reveal complex assemblages of organic species, the majority of which
335 accumulate in carbonaceous condensates analogous to soot and coal (Henning and Salama 1998;
336 Ehrenfreund and Charnley 2000; Pendleton and Allamandola 2002; Snow and McCall 2006;
337 Alexander et al. 2007; Tielens 2008). Ehrenfreund and Cami (2010) review carbon chemistry in
338 the interstellar medium, in which almost 800 molecular species have been identified in molecular
339 clouds (www.astrochemistry.net; accessed 12 August 2019), including significant quantities of
340 nitriles, ketones, and esters (Allamandola et al. 1999; Yan et al. 2005; Ehrenfreund and Cami

341 2010). Of special interest are polycyclic aromatic hydrocarbons, or “PAHs,” as well as a variety
342 of fullerenes, both of which form in the high-temperature circumstellar envelopes of carbon-rich
343 stars and have complex carbon chemistry analogous to soot formation in automobile exhaust or
344 wood-fire smoke (Henning et al. 2004; Snow and Witt 1995; Ehrendfreund and Cami 2010;
345 Salama et al. 2011).
346

347 **SYSTEMATIC EVOLUTIONARY MINERALOGY: PART IIA—INTERSTELLAR MINERALOGY**

348

349 From the mineralogical perspective, the nature of interstellar molecular solids presents
350 challenges when attempting to define discrete phases. At temperatures close to 10 K, almost all
351 molecular species will condense onto the cold surfaces of mineral grains immediately on contact
352 (Greenberg 1991; Gibb et al. 2004). The initial molecular distribution, therefore, is highly
353 disordered—a randomly condensed, amorphous molecular mixture rather than discrete, relatively
354 pure phases. Only the most abundant molecular species are likely to gradually anneal into
355 homogeneous nanoscale crystalline or amorphous volumes that might be justifiably characterized
356 as mineral kinds. Such phases may be as small as 1 to 2 nanometers in diameter; experimental and
357 theoretical experiments by Moberg et al. (2019) suggest that in the case of H₂O fewer than 100
358 molecules are required to form a discrete phase with the structural properties of ice.

359 Water ice, which accounts for 60 to 70% of molecular condensates in most observed molecular
360 clouds (Whittet 2003; Gibb et al. 2004), provides the least ambiguous case. Specific sharp infrared
361 emission features at 44 and 60 microns, as well as peak shapes and intensities of peaks at 1.65,
362 ~3.1, and 4.53 microns, point unambiguously to both crystalline and amorphous condensed regions
363 (Hagen et al. 1981; Moore and Hudson 1992; Grundy and Schmidt 1998; Newman et al. 2008).
364 As noted above, at the relatively cold temperatures of dense molecular clouds, cubic ice is the
365 expected crystalline form.

366 Carbon monoxide, often the second most abundant condensing molecular species at
367 concentrations up to 20 % (e.g., Gibb et al. 2004), presents an intriguing case with two spectral
368 types; the IR absorption spectra of solid CO differs significantly depending on its molecular
369 environment (Sandford et al. 1988; Elsila et al. 1997; Williams 2005). For matrices composed

370 predominantly of polar species (predominantly H₂O), the ~4.67-micron peak has a broad
371 component with a maximum at 4.682 microns. By contrast, a matrix of non-polar molecules (often
372 CO, itself) is characterized by a narrower peak at 4.673 microns (Chiar et al. 1995, 1998). In the
373 latter instance, a strong case can be made for discrete condensed amorphous CO as an interstellar
374 phase.

375 Interstellar methanol is characterized by differences in absorption peak profiles that are also
376 revealing, pointing to condensed regions of both relatively pure CH₃OH and methanol-water
377 mixtures (Pontopiddan et al. 2003). However, for other less abundant interstellar molecules, of
378 which hundreds have been catalogued (www.astrochemistry.net), the existence of discrete icy
379 phases is inferred primarily on their relative abundances, rather than on specific spectroscopic
380 characteristics.

381 Here we describe a few of the most abundant non-ionized interstellar molecules, including all
382 C₁ molecules (those with only one carbon atom per molecule) and other species that are estimated
383 to occur in some cool, dense molecular clouds at concentrations greater than 2 mol %. We catalog
384 and name 8 condensed phases as likely interstellar minerals, while an additional 10 molecular
385 species are labeled “unconfirmed as a discrete condensed phase” (Table 2).

386 Note that, with the exception of water ice, these 18 phases have not been identified in their
387 crystalline forms naturally on Earth and are thus not in the current list of official IMA mineral
388 species. Therefore, our nomenclature follows the conventions established by Hazen and Morrison
389 (2020). The name of the molecule is preceded by the modifier interstellar (i.e., “*interstellar*
390 *methane*”) to distinguish it from similar species that may condense in circumstellar, nebular (see
391 below), or planetary (Maynard-Casely et al. 2018; Hazen 2018) environments.

392

393 **NATIVE ELEMENTS**

394 *Interstellar hydrogen (H₂):* [unconfirmed as a discrete condensed phase] According to some
395 models of molecular condensation, a fraction of di-molecular hydrogen could condense at the
396 lowest temperatures (~10 K) in a cool dense molecular cloud. However, most hydrogen remains
397 in its gaseous form as H₂ or H atoms at T > 10 K.

398

399 *Interstellar nitrogen (N₂):* [unconfirmed as a discrete condensed phase] Molecular nitrogen
400 (N₂) is a relatively minor component of cool dense molecular clouds, but it should condense
401 heterogeneously with other molecules in environments with T < 20 K (Herbst and Klemperer 1973;
402 Womack et al. 1992; Knauth et al. 2004; Maret et al. 2006; Daranlot et al. 2012). In addition,
403 hydrogenation reactions of nitrogen play an important role in the formation of ammonia.

404

405 *Interstellar oxygen (O₂):* [unconfirmed as a discrete condensed phase] Oxygen is the third most
406 abundant element in most molecular clouds; nevertheless, molecular oxygen (O₂) is a minor
407 component of cool dense molecular clouds (Hollenbach et al. 2009; Wang et al. 2015). A
408 significant fraction of O₂ reacts with hydrogen to form water molecules.

409

410 **OXIDES**

411 *Interstellar cubic ice (H₂O):* Water (H₂O), both as an amorphous phase and crystalline ice, is
412 the most abundant interstellar condensed molecular species, comprising 60% or more of

413 condensates in cool dense molecular clouds (Whittet 2003; Gibb et al. 2004). The most familiar
414 crystalline structure of H₂O is the hexagonal form of snowflakes. However, below ~170 K the
415 stable crystalline form of ice condensed onto a cold substrate is “cubic ice” (Hobbs 1974). Because
416 water ice condenses at temperatures significantly higher than other common molecular solids (as
417 high as ~100 K), crystalline H₂O is also the only ice to commonly form mantles on silicate grains
418 as they are ejected from oxygen-rich stars (Kouchi and Yamamoto 1995), based on distinctive IR
419 absorption features (e.g., Whittet 2003).

420 “*Interstellar cubic ice (H₂O)*” in this evolutionary classification exclusively designates
421 crystalline H₂O, which is thought to account for significantly less than half of water condensates
422 in the interstellar medium. We retain the official IMA name, ice, for crystalline water, even though
423 the term “ice” is also commonly applied generically to other cold condensed molecular solids, both
424 crystalline and amorphous, in the cosmochemistry literature.

425
426 *Interstellar amorphous H₂O*: Amorphous H₂O is the most abundant interstellar mineral and is
427 a ubiquitous constituent of the icy mantles on presolar dust grains that form in cool dense molecular
428 clouds (Gibb et al. 2004). Amorphous H₂O may form by direct condensation at temperatures in a
429 molecular cloud, as well as by prolonged exposure of crystalline H₂O to ultraviolet or charged-
430 particle radiation (Kouchi and Kuroda 1990; Kouchi and Yamamoto 1995).

431 A complication is the possibility of multiple forms of amorphous H₂O (e.g., Kouchi 1987, 1990;
432 Sack and Baragiola 1993; Palumbo 2005), which depend on several factors, including the

433 temperature of condensation, the molecular/atomic flux density, exposure to ionizing radiation,
434 and the nature of the substrate.

435 The formation of amorphous versus crystalline H₂O is a balance between the temperature and
436 molecular/atomic flux. Crystalline water ices only form at relatively high temperature and low
437 molecular fluxes (e.g., < 10⁸ molecules per cm² per second at 50 K; Kouchi et al. 1994). At the
438 lower temperatures and higher fluxes of cool, dense molecular clouds there is insufficient time for
439 molecular order to occur, so amorphous phases prevail. Gradual annealing to crystalline H₂O can
440 occur, but the process is highly temperature dependent and is balanced by gradual sublimation at
441 higher temperatures.

442

443 *Interstellar amorphous carbon monoxide (CO)*: Interstellar carbon monoxide is a common
444 constituent of molecular clouds, identified by its prominent infrared absorption feature at 4.67
445 microns (Chiar et al. 1996; Elsila et al. 1997). Kouchi (1990) determined that CO condenses in
446 part as a separate amorphous phase and in part as an impurity up to a few percent in amorphous
447 H₂O (see also Collings et al. 2003). CO molecules can comprise a significant fraction (up to 25
448 mol %; Allamandola et al. 1999) of H₂O-dominated phases, with greater abundances in solids rich
449 in other nonpolar molecules, such as CO₂, O₂, and N₂ (Elsila et al 1997; Ehrenfreund et al. 1997).

450

451 *Interstellar carbon monoxide (CO)*: Crystalline interstellar carbon monoxide has been shown
452 to form when amorphous CO warms to 23 K and anneals (Kouchi 1990).

453

454 *Interstellar amorphous carbon dioxide (CO₂):* Interstellar carbon dioxide has been identified
455 by its characteristic infrared absorption features at 4.27 and 15.2 microns as a ubiquitous
456 condensed species (d'Hendecourt and de Muizon 1989; Chiar et al. 1998; Gerakines et al. 1999;
457 Nummelin et al. 2001; Boogert and Ehrenfreund 2004; Gibb et al. 2004; Pontoppidan et al. 2008).
458 While carbon dioxide is relatively rare in the interstellar gas phase, it can represent as much as 20
459 mol % of a condensed molecular mixture in both single-phase form and in heterogeneous
460 molecular mixtures. This situation has led several authors to suggest that CO₂ forms principally
461 by oxidation of condensed CO in the solid state (Allamandola et al. 1999; Roser et al. 2001;
462 Williams 2005).

463
464 *Interstellar sulfur dioxide (SO₂):* [unconfirmed as a discrete condensed phase] Condensed
465 interstellar sulfur dioxide is revealed by absorption at ~7.6 microns (Boogert et al. 1997; Zasowski
466 et al. 2009).

467

468 **ORGANIC MOLECULAR SOLIDS**

469

470 *Interstellar amorphous methanol (CH₃OH):* The presence of interstellar methanol at
471 abundances as high as 25 mol % is revealed by a distinctive suite of infrared absorption bands
472 (Grim et al. 1991; Gibb et al. 2004). Pontoppidan et al. (2003) analyzed absorption peak profiles
473 that indicate regions of relatively pure CH₃OH, as well as methanol-water mixtures. The measured
474 methanol abundance in the interstellar medium is often significantly greater than that predicted
475 from models of gas-phase chemistry, possibly as a result of solid-state hydrogenation reactions in

476 mixed-phase water-CO condensed phases to make methanol (Williams 2005; Qasim et al. 2018)—
477 further evidence that the molecular compositions of interstellar solids are not exclusively a
478 consequence of condensation (Öberg et al. 2008).

479

480 *Interstellar amorphous methane (CH₄):* Interstellar methane at concentrations from ~1 to 4 mol
481 % is revealed by a diagnostic 7.676-micron absorption band (Lacy et al. 1991; Boogert et al. 1996;
482 d’Hendecourt et al. 1996; Gibb et al 2004). Spectroscopic evidence for a much lower concentration
483 of gas-phase methane suggests that CH₄ forms in the solid state through hydrogenation of atomic
484 carbon (Boogert et al. 1998). An unknown fraction of condensed interstellar methane may occur
485 in the form of clathrate hydrates (Ghose et al. 2019).

486

487 *Interstellar cyanide (XCN):* [unconfirmed as a discrete condensed phase] The presence of a
488 weak absorption feature at 4.62 microns in the spectra of some dense molecular clouds points to
489 the C-N stretch feature of cyanide, which may constitute up to a few mol % of some objects.
490 Generally given as “XCN,” Whittet et al. (2001) suggest that X may be oxygen, though HCN is
491 likely present, as well (Snyder and Buhl 1971; Clark et al. 1974).

492

493 *Interstellar formaldehyde (H₂CO):* [unconfirmed as a discrete condensed phase] Diagnostic
494 microwave emissions at 4830 MHz (Snyder et al. 1969), as well as infrared features at 5.81 and
495 5.83 microns, point to molecular formaldehyde at abundances up to ~3 mol % (Grim et al. 1991;
496 Gibb et al. 2004).

497

498 *Interstellar formic acid (HCOOH)*: [unconfirmed as a discrete condensed phase] The presence
499 of formic acid at concentrations less than 2 mol % is revealed by radio emissions (Zuckerman et
500 al. 1971; Winnewisser and Churchwell 1975), as well as by infrared absorption bands at 5.85 and
501 7.243 microns (Gibb et al. 2004). Peak profiles of IR bands reveal formic acid molecules in both
502 gas and condensed states (Schutte et al. 1999; Bisschop et al. 2007).

503

504 *Interstellar acetaldehyde (CH₃HCO)*: [unconfirmed as a discrete condensed phase] An
505 absorption band at 7.414 microns suggests the presence of condensed acetaldehyde in significant
506 concentrations, perhaps as much as ~10 mol %, in many interstellar environments (Schutte et al.
507 1999; Gibb et al. 2004).

508

509 *Interstellar carbonyl sulfide (OCS)*: [unconfirmed as a discrete condensed phase] Characterized
510 by a distinctive absorption feature at 4.91 microns, OCS is present at typically < 1 mol % (Palumbo
511 et al. 1995, 1997; Gibb et al. 2004).

512

513 *Interstellar ammonia (NH₃)*: [unconfirmed as a discrete condensed phase] The presence of
514 interstellar ammonia is inferred from a minor absorption band at ~9 microns, close to the 9.3-
515 micron absorption of pure NH₃ (Smith et al. 1989; Chiar et al. 2000; Dartois et al. 2002). Note that
516 the position of the band shifts when the molecule is present in the polar environment of condensed
517 H₂O. This interpretation is reinforced by a band at 3.5 microns, which matches a broad feature
518 associated with ammonium hydrate (Gibb et al. 2004).

519

520 *Interstellar kerogen*: Laboratory studies of the effects of UV radiation on simple molecular
521 systems under high vacuum and low temperatures demonstrate the formation of complex insoluble
522 mixtures of non-volatile organic matter, not unlike the “kerogen” component that can be extracted
523 through acid dissolution of carbonaceous meteorites (Cronin and Pizzarello 1990; Greenberg et al.
524 1995; Widowiak et al. 1995; Ehrenfreund and Cami 2010). An absorption feature at ~3.47 microns
525 corresponds to the C-H stretch in hydrocarbons (Chiar et al. 1996), while several bands (3.3, 6.2,
526 8.6, and 11.3 microns) are consistent with polycyclic aromatic hydrocarbons – important carbon-
527 bearing components of carbonaceous meteorites (Grishko and Duley 2000). Kerridge (1983)
528 discovered isotopic heterogeneities in meteoritic kerogen consistent with low-temperature
529 interstellar origins. Ehrenfreund et al. (1991) demonstrated that distinctive features of the 3.4-
530 micron absorption band in the interstellar medium and in carbonaceous chondrites match closely.
531 Thus, it is likely that some, if not most, of the insoluble matter in the least altered (i.e., “3.0”)
532 carbon-rich meteorites represents relatively unaltered interstellar material.

533 Note that in spite of their comprehensive list of meteorite phases, Rubin and Ma (2017) do not
534 include condensed organic material, i.e., “kerogen.”

535 **PRIMARY CONDENSATION MINERALOGY OF THE SOLAR NEBULA**

536 Diverse and abundant chondrite meteorites provide an unparalleled view of the earliest stages
537 of our solar system's formation (Brearley and Jones 1998; Krot et al. 2014; MacPherson 2014;
538 Scott and Krot 2014; Connolly and Jones 2016). Data collected from these fascinating specimens,
539 coupled with experimental measurements and theoretical modeling of high-temperature mineral
540 condensation processes, provide an increasingly vivid picture of the first few million years of
541 nebular evolution (e.g., Hashimoto 1983, 1992; Mysen et al. 1985; Mysen and Kushiro 1988;
542 Davis et al. 1990; Nagahara et al. 1993; Wood and Hashimoto 1993; Ebel and Grossman 2000;
543 Richter et al. 2002, 2007; Lodders 2003; Ebel 2006; Ebel and Alexander 2011; Davis and Richter
544 2014; Saxena and Hrubciak 2014; Han et al. 2015; Wood et al. 2019). The most primitive nebular
545 phases survive in distinctive components of chondrite meteorites, including calcium-aluminum-
546 rich inclusions (MacPherson 2014), amoeboid olivine aggregates (Grossman and Steele 1976; Krot
547 et al. 2004), and ultra-refractory inclusions (El Goresy et al. 2002; Ma et al. 2014a). These ancient
548 quasi-spheroidal to irregularly-shaped objects, ranging in size from less than 1 millimeter to more
549 than a centimeter in diameter, have received extensive scrutiny and have been the subject of several
550 comprehensive reviews (Brearley and Jones 1998; Ebel 2006; MacPherson 2014; Scott and Krot
551 2014; Rubin and Ma 2017, 2020). What follows, therefore, summarizes and codifies information
552 that has been collated and reviewed by previous researchers.

553 Mineral evolution in the early solar nebula was driven by a succession of heating events,
554 initially associated with the pre-main-sequence life of the Sun (Desch et al. 2012; Connolly and
555 Jones 2016). Processes within this dynamic, evolving system are not fully understood, but include
556 radiative heating, FU Orionis-type flares (Bertout 1989), bipolar outflows (Sahai et al. 2003),
557 shock waves induced by infalling of gas (Iida et al. 2001), bow shocks from planetary embryos

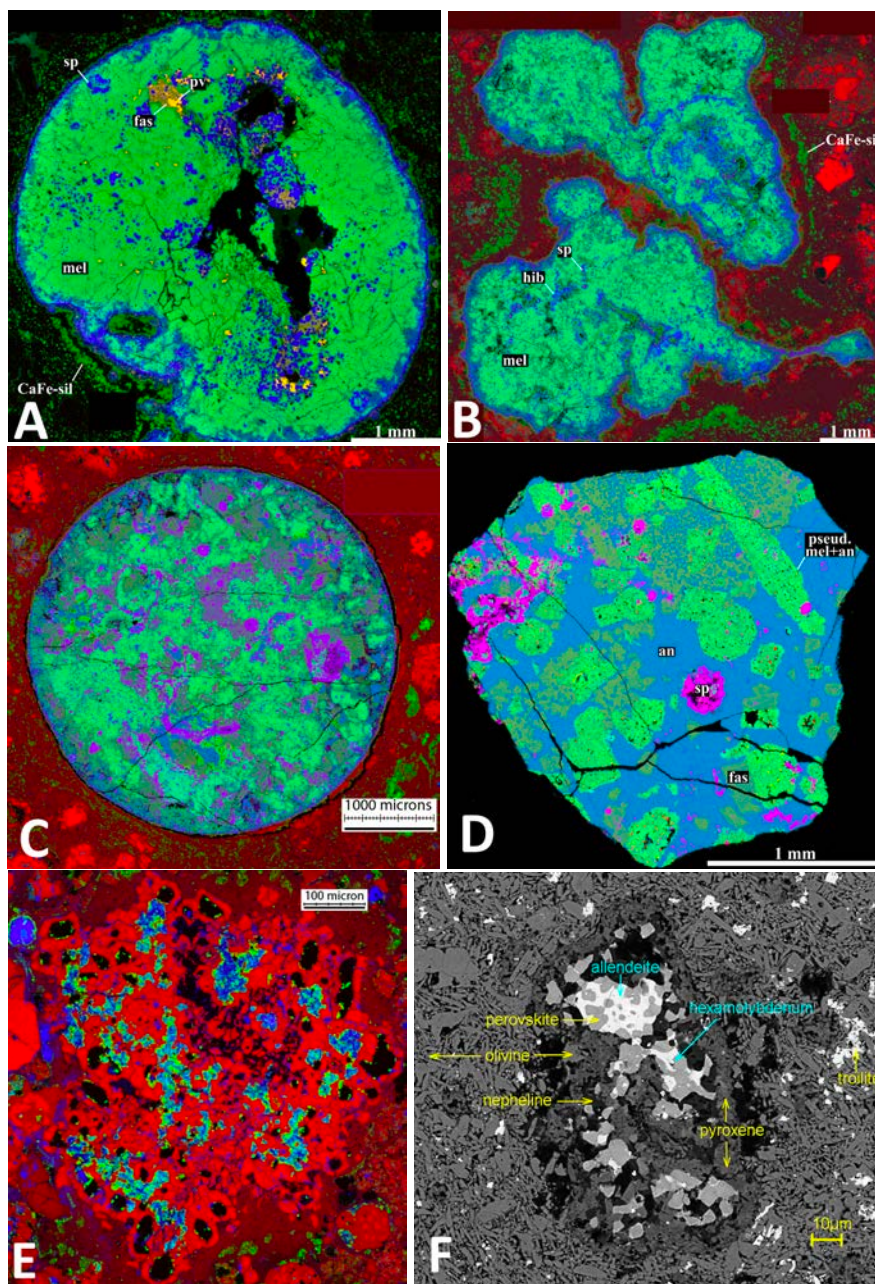
558 (Desch and Connolly 2002; Boss and Durisen 2005) and associated magnetic effects (Mann et al.
559 2016; Mai et al. 2018), current sheets (Joung et al. 2004; Hubbard et al. 2012), and nebular
560 lightning (Sorrell 1995; Desch and Cuzzi 2000), as well as cooling through thermal emission from
561 the nebula. As larger objects grew through gravitational accretion, impact processes and magma
562 formation increasingly played key roles. Therefore, primary mineralization in the early solar
563 nebula occurred through condensation from a vapor enriched in O, Si, Mg, Al, Ca, and Fe (Figure
564 1C), followed by melt crystallization, and solid-state reactions. The formation of these primary
565 nebular minerals has been the subject of extensive theoretical modeling (Urey 1955; Yoneda and
566 Grossman 1995; Ebel and Grossman 2000; Ebel 2006), as well as experimental research under
567 high-temperature, low-pressure conditions (Hashimoto 1983; Nagahara et al. 1993; Davis and
568 Richter 2014).

569 The following section reviews the three most primitive types of chondrite objects, all of which
570 contain primary condensation minerals of the early solar nebula: calcium-aluminum-rich
571 inclusions, amoeboid olivine aggregates, and ultra-refractory inclusions (Figure 3).

572 In Part III of this series we will consider primary minerals in chondrules, which are abundant
573 in many kinds of chondrite meteorites. Chondrules are igneous droplets thought to have formed
574 between 1.5 and 3 million years after CAIs (e.g., Connolly and Jones 2016). Note that additional
575 chondritic components, including opaque assemblages (also known as fremdlinge), dark
576 inclusions, and fine-grained matrices, often contain similar suites of primary phases, but their
577 histories are complicated by a succession of secondary processes associated with thermal, aqueous,
578 and impact alteration (Brearley 1986; Blum et al. 1988; Scott et al. 1988; Johnson et al. 1990;
579 Brearley and Jones 1998; MacPherson 2014; Rubin and Ma 2017). Thus, with the exception of

580 primary metal alloys, the mineralogy of these additional chondritic components will be considered
581 in Parts IV and V.

582



583

584

585 Figure 3. Components of primitive chondrite meteorites with primary mineral phases include:
586 calcium-aluminum-rich inclusions (CAIs), amoeboid olivine aggregates (AOAs), and ultra-
587 refractory inclusions (URIs). **A.** Compact type A CAI from the Adelaide meteorite with primarily
588 melilite and spinel and minor perovskite and fassaite (Ti = red; Ca = green; Al = blue); **B.** Fluffy
589 type A CAI from the Allende meteorite with melilite, spinel, fassaite, and anorthite (Mg = red; Ca
590 = green; Al = blue); **C.** Type B CAI from the Allende meteorite with melilite, fassaite, spinel, and
591 anorthite (Mg = red; Ca = green; Al = blue); **D.** Type C CAI with anorthite, melilite, spinel, and

592 fassaite (Mg = red; Ca = green; Al = blue); **E.** Forsterite-rich AOA from the Kainsaz meteorite
593 with dominant forsterite plus Fe-Ni metal alloys, fassaite, spinel, and anorthite (Mg = red; Ca =
594 green; Al = blue); **F.** URI in matrix from the Allende carbonaceous chondrite. [Image credits: A,
595 B, D, E courtesy of Alexander Krot, University of Hawaii; C courtesy of Denton Ebel, American
596 Museum of Natural History; F courtesy of Chi Ma, Caltech]

597
598 Calcium-aluminum-rich inclusions (CAIs): CAIs are the most ancient objects formed in the
599 solar nebula, with radiometric ages 4567.3 +/- 0.16 Ma (Amelin et al. 2002, 2010; Connelly et al.
600 2008, 2012; Krot 2019). These discrete components of primitive meteorites range in size from
601 approximately 100 microns to more than a centimeter in diameter, and they possess distinctive
602 suites of minerals reminiscent of ceramics—mineralogy that points to the earliest phase of solar
603 nebular cooling and condensation (Brearley and Jones 1998; MacPherson 2014). Collectively, the
604 refractory phases in CAIs represent the first ~5 percent of the solar nebula's condensable matter,
605 as reflected in primitive CI chondrite meteorites (Grossman 1972; Davis and Richter 2014).

606 Detailed observations of CAIs from diverse types of chondrite meteorites reveal significant
607 variations in bulk composition, mineralogy, and morphology—differences that reflect nebular
608 heterogeneities in space and time (Liu et al. 2009; Kööp et al. 2018; MacPherson 2014 and
609 references therein), as well as subsequent processing through re-melting, distillation, and a variety
610 of secondary processes (the subject of Parts IV and V of this series). Owing to their diversity, CAIs
611 have been divided into several groups according to size, shape, and mineralogy (Grossman 1975;
612 Wark 1987; Beckett and Stolper 1994; MacPherson 2014):

- 613 • *Compact Type A CAIs* are spheroidal objects, evidently a consequence of partial melting.
614 Melilite is often the dominant mineral with spinel, hibonite, perovskite, and other refractory
615 phases (Figure 3A).
- 616 • *Fluffy Type A CAIs* have similar mineralogy to compact type A CAIs but their shapes are
617 irregular, suggesting minimal melting (Figure 3B).

- 618 • *Type B CAIs* are spheroidal objects characterized by their relatively large size (up to several
619 centimeters) and mineralogy that commonly includes melilite, spinel, anorthite, forsterite, and
620 the Al-Ti-rich calcic clinopyroxene called fassaite (Figure 3C). Type B CAIs are further
621 divided into subcategories based on mineralogical details.
- 622 • *Type C CAIs* consist primarily of spinel, fassaite, and anorthite with textures characteristic of
623 igneous processes (Figure 3D).
- 624 • In addition to A-, B-, and C-type CAIs, researchers recognize other fine-grained (i.e., < 200
625 microns) objects with CAI affinities. *Spinel-hibonite-rich spherules* (sometimes abbreviated
626 SHIBs) are CAIs that contain a relatively unaltered assemblage of spinel, hibonite, and
627 perovskite, with associated melilite, fassaite, and anorthite (Ireland 1988; Kööp et al. 2016a).
- 628 • *Platy hibonite crystals*, known as PLACs, are CAIs that consist of lath-like crystals of
629 hibonite, sometimes surrounded by a silicate glass or fassaite, often with hibonite, grossite,
630 and melilite, but typically lacking spinel (Ireland 1988; Kööp et al. 2016b).
- 631 • A mineralogically curious type of CAI, dubbed “*FUN*” CAIs by Wasserburg et al. (1977),
632 displays “Fractionation and Unidentified Nuclear effects” – specifically, large mass-
633 dependent fractionations of Mg, Si, and O, as well as other isotopic anomalies. In terms of
634 primary mineralogy FUN CAIs are, for the most part, similar to type B CAIs. However, the
635 discovery of dmisteinbergite (CaAl₂Si₂O₈), a rare hexagonal high-temperature polymorph of
636 anorthite, points to an unusual formation environment close to the protosun with T > 1500 K
637 and P < 10⁻⁶ (i.e., significantly lower pressure than the ~10⁻⁴ atm modeled for most other
638 CAIs; Ma et al. 2013a).

639 In our review we focus on the primary mineralogy of CAIs and do not make distinctions among
640 these varieties of calcium-aluminum-rich inclusions. Note, however, that we do distinguish CAIs
641 from ultra-refractory inclusions, as the latter began to form later and are chemically and
642 mineralogically distinct from CAIs.

643 Isotopic evidence, including surprisingly uniform anomalous Mg and O isotopes across all
644 types of CAIs (McKeegan et al. 1998; MacPherson 2014 and references therein) and age
645 determinations by various methods (Connelly et al. 2012; see also, Amelin et al. 2002, 2010;
646 Connelly et al. 2008; Krot 2019), reveal that CAIs formed at $\sim 4567.3 \pm 0.16$ Ga over a span of
647 $\sim 200,000$ years. However, detailed chemical and isotopic investigations point to at least two stages
648 of CAI formation as a consequence of rapid protosun evolution during the earliest stages of the
649 solar system.

650 The earliest nebular condensates are represented by a relatively small population of platy
651 hibonite-bearing “PLAC” CAIs, which appear to have formed prior to an influx of ^{26}Al to the solar
652 nebula, as measured by diagnostic ^{26}Mg (Liu et al. 2009). Hibonite in these CAIs contains helium
653 and neon excesses that could only have formed under an intense flux of energetic particles, albeit
654 at a heliocentric distance significantly beyond the inner disk edge, where temperatures were cooler
655 (Kööp et al. 2018).

656 A second generation of CAIs of the spinel-hibonite-bearing “SHIB” type display at least three
657 important differences from PLAC CAIs: (1) they contain excess ^{10}B formed by the decay of short-
658 lived ^{10}Be , which points to condensation near the inner edge of the nebular disk in a single zone
659 close to the Sun (McKeegan et al. 2000; MacPherson et al. 2003; Krot 2019); (2) they incorporated
660 significant short-lived ^{26}Al (preserved as diagnostic ^{26}Mg), pointing to formation after PLAC

661 CAIs (Kööp et al. 2016a, 2016b); and (3) they lack the anomalous helium and neon contents of
662 PLAC hibonite (Kööp et al. 2018). According to current models, these CAIs were later dispersed
663 to beyond Jupiter's orbit by strong solar winds (Shu et al. 1996). Further studies of CAI isotopic
664 and mineralogical variations are likely to refine our understanding of the earliest stages of solar
665 system evolution.

666 CAIs rarely represent unaltered primordial nebular condensates. They typically have been
667 subjected to multiple stages of partial alteration from reheating, including annealing, melting, and
668 distillation; impact melting, volatilization, and metamorphism; and secondary alteration, including
669 oxidation, sulfidization, and hydration (MacPherson and Davis 1993; Beckett et al. 2000; Rubin
670 and Ma 2017). Here we focus exclusively on the so-called “primary” mineralization in the sense
671 of MacPherson (2014) – i.e., mineralization that results from “direct condensation, melt
672 solidification, or solid-state recrystallization.” Note that in this context solid-state recrystallization
673 includes only the first phase of reaction and replacement of earlier high-temperature phases by
674 exsolution, element ordering, or reversible phase transition, during equilibrium cooling of CAIs
675 below their initial condensation temperature and prior to their incorporation into larger bodies
676 (e.g., Yoneda and Grossman 1995; Ebel 2006). Chondrite mineralization through subsequent
677 secondary processes, including oxidation, sulfidation, aqueous and thermal alteration
678 (metamorphism), shock processes, and planetesimal differentiation, will be considered in Parts IV
679 and V of this series.

680 Only seven minerals, all of which occur in calculations of nebular condensation sequences
681 between ~1800 and 1100 K (e.g., Grossman 1972; Brearley and Jones 1988; Lodders 2006; Davis
682 and Richter 2014; MacPherson 2014, Table 1; Wood et al. 2019), are common primary minerals
683 in CAIs. In order of appearance, they are hibonite, perovskite, gehlenite/åkermanite (both members

684 of the melilite group), spinel, Al-Ti-rich calcic clinopyroxene (“fassaite”), forsterite, and anorthite.
685 Note that corundum is calculated to be the highest-temperature oxide condensate (Lattimer et al.
686 1978; Anders and Grevesse 1989; Lodders 2003; Wood et al. 2019), yet it is usually absent owing
687 to subsequent reactions with nebular vapor to hibonite, spinel, or melilite. Additional phases,
688 though less common, include the oxides grossite, krotite, panguite, and tistarite; the calcium-
689 titanium silicate rhönite; and alloys of Fe-Ni and platinum group elements (see [Table 3](#)).

690 An unresolved question related to CAIs is the paragenesis of ubiquitous thin outer layers, first
691 described by Wark and Lovering (1977) and now known as “Wark-Lovering rims” (MacPherson
692 et al. 1981; Ruzicka 1997; Wark and Boynton 2001). These layers are typically a few tens of
693 microns thick and consist of both refractory condensates, often spinel, melilite, and fassaite,
694 occasionally with hibonite, perovskite, anorthite, and forsterite, as well as such secondary minerals
695 as nepheline, Fe-rich spinel, hedenbergite, and andradite (MacPherson 2014, and references
696 therein). No new obviously primary minerals occur in these rims; therefore, for the purposes of
697 this review, even though they may represent a distinct timing and mode of mineral formation, we
698 do not consider Wark-Lovering rims as representing distinct natural kinds. Note, however, an
699 important feature of this evolutionary system of mineralogy is that specialists have the option of
700 splitting mineral natural kinds into finer and finer sub-categories, based on their distinctive modes
701 of origin, as reflected in diagnostic suites of physical and chemical attributes.

702
703 *Amoeboid olivine aggregates (AOAs)*: Amoeboid olivine aggregates (AOAs) represent a
704 second common refractory constituent of chondrite meteorites. Originally described from the
705 Allende CV chondrite by Grossman and Steele (1976) and subsequently identified from a wide
706 variety of carbonaceous meteorites (Grossman et al. 1979; Kornacki and Wood 1984; McPherson

707 et al. 1988; Aléon et al. 2002; Chizmadia et al. 2002; Krot et al. 2004; Rubin 2013), AOAs are
708 thought to have formed after CAIs, though before chondrules that were forming at $\sim 4565 \pm 0.5$
709 Ma (Connolly and Jones 2016), and at generally lower condensation temperatures and at pressures
710 consistent with 10^{-3} atm (Weisberg et al. 2004). They typically occur as irregularly-shaped
711 assemblages up to 0.5 millimeters in diameter, constituting a few percent of some carbonaceous
712 chondrites (Scott and Krot 2014; [Figure 3E](#)). AOAs consist of sintered accumulations of nebular
713 condensates, primarily forsterite (typically fine-grained, < 20 microns), with Fe-Ni metal alloys
714 and a refractory assemblage, commonly including fassaite, spinel, and anorthite, and occasionally
715 with perovskite and/or melilite. Models of AOA evolution suggest that other refractory phases,
716 including corundum, grossite, and hibonite, may have initially formed but were transformed to
717 melilite, clinopyroxene, spinel, and/or anorthite through continuous solid-state reactions of the
718 fine-grained constituents on cooling (Weisberg et al. 2004).

719 Many AOAs also hold a rich variety of secondary minerals, including phyllosilicates,
720 feldspathoids, sulfides, and other phases, which will be considered in Part V.

721
722 *Ultra-Refractory Inclusions (URIs)*: Ultra-refractory inclusions (URIs) are a scarce population of
723 mineralogically important pre-chondrule objects ([Figure 3F](#)), usually grouped with CAIs, that are
724 extremely enriched in Sc, Zr, Y, and other refractory elements by factors of as much as 10^3 (El
725 Goresy et al. 2002). A consequence of these enrichments is the appearance of more than a dozen
726 rare oxide and silicate minerals (Rubin and Ma 2017), including allendeite ($\text{Sc}_4\text{Zr}_3\text{O}_{12}$),
727 thortveitite ($\text{Sc}_2\text{Si}_2\text{O}_7$), and lakargite (CaZrO_3), as well as Sc- and Ti^{3+} -bearing clinopyroxenes
728 and garnets (Table 3). The unusual chemistry of URIs points to an early stage of nebular evolution

729 in regions that had already generated significant quantities of primary CAI minerals with Mg, Ca,
730 Al, and Ti. URIs are often found as inclusions in later chondrite objects, including AOAs,
731 chondrules, and fine-grained matrix (El Goresy et al. 2002; Ma et al. 2009a, 2014a).

732

733 *A note regarding opaque assemblages*

734 Some researchers have suggested that Fe-Ni-metal-rich opaque assemblages (also referred to
735 as “fremdlinge”), which are found associated with some CAIs (e.g., Brearley and Jones 1998;
736 MacPherson 2014), represent some of the earliest primary condensates of the solar nebula (El
737 Goresy et al. 1978; Armstrong et al. 1985, 1987). Others posit a later origin of these objects with
738 a complex history of alteration, for example by oxidation, sulfidation, and exsolution through
739 exposure to heterogeneous nebular environments (Wark and Lovering 1982a; Blum et al. 1988,
740 1989; MacPherson 2014). We include the primary metals of opaque assemblages – Fe-Ni and
741 platinum group element alloys – in the list of CAI minerals. However, the lower-temperature
742 mineral suites of opaque assemblage minerals, including fayalite, wollastonite, feldspathoids,
743 tungstate-molybdates, and varied sulfides and phosphates, will be considered in Parts IV and V.

744 **SYSTEMATIC EVOLUTIONARY MINERALOGY: PART IIB—PRIMARY NEBULAR MINERALOGY**

745 In the following section we outline the mineralogy of primary nebular phases, including
746 minerals in CAIs, AOAs, and URIs formed by condensation, melt crystallization, and their initial
747 solid-state reactions (see also Table 3). We tabulate 59 natural kinds of primary minerals,
748 corresponding to more than 40 IMA-approved species plus nebular silicate glass. We also include
749 one low-temperature solar nebular condensate, cubic H₂O ice, which has been observed through
750 telescopic observations in the cool (~ 100 K) outer regions of other stellar environments. Each
751 mineral natural kind is given a binomial designation: the first name indicates the paragenetic
752 context (e.g., *CAI*, *AOA*, or *URI*), whereas the second name for the most part conforms to approved
753 IMA mineral species' names. However, in several instances we deviate from IMA conventions:

- 754 • *Refractory metal alloys*: CAIs, URIs, and associated opaque assemblages often contain
755 micron-scale “nuggets” in which refractory metals such as Mo, Ir, Os, Ru, Rh, Re, Pt, W,
756 and Ru occur in hexagonal (*P6₃/mmc*) alloys with widely varied elemental proportions (e.g.,
757 Weber and Bischoff 1997; Berg et al. 2009; MacPherson 2014; Chi Ma, personal
758 communication). For example, Berg et al. (2009) report the compositions of 88 refractory
759 metal nuggets from the Murchison meteorite, most with significant concentrations of Mo,
760 Os, and Ru, with each of those elements dominant in some grains. IMA protocols require
761 naming each alloy based on the most abundant element; therefore, ruthenium, osmium,
762 molybdenum, and other metals have all been officially recognized as separate native
763 element mineral species. However, because these alloys form continuous solid solutions in
764 chondrite nuggets and they are all formed by the same paragenetic process of condensation
765 from a high-temperature nebular gas, we lump them together into platinum group element

766 (PGE) alloys. Similarly, we lump the cubic (*Fm3m*) iron-molybdenum alloys hexaferrum
767 (Fe,Os,Ir,Mo) and hexamolybdenum (Mo,Ru,Fe) into one natural kind: Fe-Mo alloys.

768 • *Anosovite*: The name “anosovite” for pseudobrookite-type Ti_3O_5 was discredited by
769 Bowles (1988), as it was only known as an anthropogenic phase in Ti-rich slags. However,
770 Zhang et al. (2015) have discovered this phase as a primary nebular condensate and we
771 resurrect the name anosovite, pending IMA’s decision on the naming of this mineral.

772 • *Melilite*: In the case of the melilite group, a complete solid solution exists between gehlenite
773 ($Ca_2Al_2SiO_7$) and åkermanite ($Ca_2MgSi_2O_7$), with primary meteoritic compositions
774 ranging from Åk₀₁ to Åk₁₀₀ (Brearley and Jones 1998). Individual grains, furthermore, may
775 be zoned such that cores are technically gehlenite and rims technically åkermanite. These
776 variations occur within a continuous solid solution and represent a single mode of
777 formation. Therefore, we classify melilite samples as “CAI melilite,” “AOA melilite,” or
778 “URI melilite.”

779 • *Fassaite*: A fourth deviation from standard IMA nomenclature relates to primary CAI,
780 AOA, and URI pyroxenes, typically a Ca-Mg-dominant, Fe-poor clinopyroxene with
781 significant Al and Ti (both Ti^{3+} and Ti^{4+}) in solid solution. The IMA-approved name for
782 most of these occurrences is diopside, because the closest compositional end-member is
783 $CaMgSi_2O_6$. However, the great majority of near-end-member diopside occurrences in
784 CAIs are of secondary origin (Brearley and Jones 1998), and thus should be distinguished
785 from the primary Al-Ti-bearing nebular calcic clinopyroxene phase,
786 $[Ca(Mg,Al,Ti^{3+},Ti^{4+})(Al,Si)SiO_6]$. This complex solid solution has long been called

787 “fassaite” in the meteoritics literature, based on its similarity to iron-poor calcic
788 clinopyroxenes from the Fassa Valley, Trento Province, Italy (Thompson 1818; Deer et al.
789 1963; Sack and Ghiorso 2017). The name fassaite was discredited during a reclassification
790 of pyroxene nomenclature (Morimoto et al. 1988; see also Hazen 1989), but it continues to
791 be used by many meteorite experts to describe the distinctive primary calcic clinopyroxenes
792 in chondrite meteorites (e.g., Brearley and Jones 1998; MacPherson 2014; Rubin and Ma
793 2017; Sack and Ghiorso 2017). Primary clinopyroxene from meteorites possesses a number
794 of diagnostic attributes, including extensive Al, Ti³⁺, Ti⁴⁺, and (less commonly) Sc and/or
795 V solid solution – compositional complexities that lead to a suite of distinctive optical
796 properties, including refractive indices, birefringence, extinction angle, optic axial angle,
797 and dispersion (e.g., Deer et al. 1963). Therefore, we retain the name fassaite for Al-Ti-
798 bearing clinopyroxene.

799 • *Rhönite*: Finally, we lump two rare primary CAI minerals of the sapphirine group, rhönite
800 [Ca₂(Mg,Al,Ti)₆(Si,Al)₆O₂₀] and addibischhoffite [Ca₂(Al,Mg,V,Ti)₆(Al,Si)₆O₂₀). These
801 similar phases represent a continuous solid solution and occur via the same paragenetic
802 mode.

803

804 **NATIVE ELEMENTS**

805 Iron-nickel alloys are common primary and secondary phases associated with CAIs, AOAs,
806 URIs, and associated opaque aggregates (Brearley and Jones 1998; Rubin and Ma 2020).
807 Chondrites also often incorporate micron-scale nuggets of highly refractory metal alloys, which
808 contain Ir, Os, Ru, Mo, and other siderophile elements (Sylvester et al. 1993; Berg et al. 2009). In

809 addition, refractory mineral assemblages occasionally incorporate metal grains with significant
810 amounts of both Fe and Mo (Ma et al. 2014a; Zhang et al. 2015; Rubin and Ma 2017).

811
812 **Platinum Group Element (PGE) Alloys (Os,Ir,Ru,Rh,Pt,W,Mo,Re):** CAIs often
813 incorporate micron-scale “refractory metal nuggets” (hexagonal, $P6_3/mmc$), containing elements
814 of the platinum group (Os, Ir, Ru, Rh, and Pt), as well as Mo, W, and Re (Palme et al. 1994;
815 Brearley and Jones 1998; MacPherson 2014), which condensed at temperatures between 1800 and
816 1300 K at 10^{-4} atm (Berg et al. 2009; Harries et al. 2012; Scott and Krot 2014). Some individual
817 sub-micron-scale grains are close to pure Pt, Ru, or Re, whereas others are multi-element alloys
818 with Os, Ir, Ru, or Pt as the most abundant metal (e.g., El Goresy et al. 1978; Wark and Lovering,
819 1978; Bischoff and Palme, 1987; Brearley and Jones 1998; Berg et al. 2009). Because these
820 elements form extensive solid solutions by the same nebular condensation mechanism, we lump
821 them together as “*PGE alloys*.”

822
823 *CAI PGE alloys:* Refractory metal nugget alloys of PGEs plus W, Mo, and Re are commonly
824 found as micron-scale grains, often as inclusions in oxides or silicates, in CAIs (e.g., El Goresy et
825 al. 1978, 1979, 1984; Wark and Lovering 1982b; Sylvester et al. 1993; Endress et al. 1994; Geiger
826 and Bischoff 1995; Weber and Bischoff 1997; Berg et al. 2009; MacPherson 2014).

827
828 *URI PGE alloys:* Micron-scale grains of Os-dominant PGE alloys are found in ultra-refractory
829 inclusions in association with typical CAI phases, including fassaite (often Sc- and Ti-rich),
830 perovskite, and spinel (Ma and Rossman 2008; Ma 2011; Ma et al. 2014a).

831

832 **Iron-Nickel Alloys:** Iron-nickel alloys condensed from the solar nebula at temperatures
833 estimated between 1350 and 1450 K (Campbell et al. 2005). Consequently, metal alloys with iron
834 dominant, typically incorporating significant Ni and at times with minor amounts of other
835 siderophile elements, are common as a minor phase in CAIs, AOAs, and URIs from many types
836 of chondrites. They occur as the minerals iron (also known as “kamacite”), taenite, and awaruite.

837 Here we accept iron and taenite as primary nebular condensates. Note that awaruite, an
838 isometric (*Pm3m*) Ni-dominant alloy of iron and nickel, is also a common minor metallic phase in
839 opaque aggregates associated with CAIs (Taylor et al. 1981; Rubin and Kallemeyn 1989; Ikeda
840 1992; Smith et al. 1993; Casanova and Simon 1994; Moggi-Cecchi et al. 2007). However, it
841 appears that most occurrences of awaruite in CAIs are of secondary origin (Brearley and Jones
842 1998; Rubin and Ma 2020).

843
844 **Iron (alpha-Fe):** Native iron, also known as kamacite (a discredited though often used mineral
845 name in the context of meteorites), is the most stable low-Ni alloy of Fe and Ni. This cubic (*Im3m*)
846 phase has nickel contents that are typically less than 10 wt. % Ni, while Co is less than 1 wt. %
847 (Brearley and Jones 1998). Native iron is common as an opaque phase associated with CAIs,
848 AOAs, and URIs (Bevan and Axon 1980; Zinner et al. 1991; Simon and Grossman 1992; Caillet
849 et al. 1993; Zhang et al. 1995; Shibata 1996; Ma and Rossman 2008).

850
851 **CAI iron:** Native iron has been reported as a primary phase (Campbell et al. 2005; Scott and
852 Krot 2014; Rubin and Ma 2017) in type A (MacPherson and Grossman 1984; Ulyanov et al. 1982),
853 type B (Blander and Fuchs 1975; Sylvester et al. 1992; Caillet et al. 1993), and rarely in type C
854 CAIs (Blander et al. 1980).

855

856 *AOA iron*: Iron-nickel alloys, typically with 5 to 7 wt. % Ni, are ubiquitous components of
857 amoeboid olivine aggregates (Weisberg et al. 1993, 2004; Chizmadia et al. 2002; Krot et al. 2004).
858 They occur as blebs up to 10 microns in diameter, often as inclusions in refractory oxides and
859 silicates.

860

861 *URI iron*: Ma and Rossman (2008) recorded sub-micron grains of Fe-Ni alloy associated with
862 zirconolite, tazheranite, and PGE alloys in an ultra-refractory inclusion from the Allende chondrite.

863

864 **Taenite [gamma-(Fe,Ni)]**: Taenite is an isometric (*Pm3m*) alloy of gamma-iron, typically with
865 10 to more than 50 wt. % Ni (Affatalab and Wasson 1980; Nagahara 1982). Taenite often occurs
866 in CAIs and opaque assemblages as a minor phase, typically in close association with kamacite
867 (Zinner et al. 1991; Simon and Grossman 1992; Sylvester et al. 1992; Caillet et al. 1993; Brearley
868 and Jones 1998), in some instances as exsolution lamellae in kamacite (Noguchi 1994; Ichikawa
869 and Ikeda 1995). Taenite and kamacite are also associated in fine-grained mixtures known as
870 “plessite” (Massalski et al. 1966; Scott and Rajan 1979).

871

872 *CAI taenite*: Taenite commonly occurs, both as isolated grains and as exsolution lamellae in
873 kamacite, in types A and B CAIs (MacPherson and Davis 1993; Ichikawa and Ikeda 1995;
874 Campbell et al. 2005; Rubin and Ma 2017).

875

876 **Iron-Molybdenum Alloys (Fe,Mo)**: Iron and molybdenum, in combination with refractory
877 metals, notably Ir, Os, and Ru, occasionally form micron-scale nuggets of hexagonal (*P6₃/mmc*)

878 alloys, which must have condensed or solidified at temperatures intermediate between the ultra-
879 refractory platinum group alloys and the lower-temperature Fe-Ni alloys described above. At least
880 two IMA-approved species have been identified from CAIs in the Allende meteorite – hexaferrum
881 [(Fe,Os,Ir,Mo); Ma 2012; Zhang et al. 2015] and hexamolybdenum [(Mo,Ru,Fe); Ma et al. 2011b,
882 2014a]. Ma et al. (2014a) provide a review of this “continuum of meteoritic refractory alloys with
883 the $P6_3/mmc$ structure.”

884

885 *CAI Fe-Mo alloys:* Ma et al. (2011a) and Ma (2012) described micron-scale nuggets of
886 hexagonal alloys with varying proportions of Fe, Mo, Ru, and other metals from CAIs in the
887 Allende and NWA 1934 meteorites.

888

889 *URI Fe-Mo alloys:* Ma et al. (2014a) found hexamolybdenum in association with allendeite in
890 an ultra-refractory inclusion, while Zhang et al. (2015) report hexaferrum.

891

892 **CARBIDES**

893 Khamrabaevite (TiC) is the only confirmed refractory carbide with characteristics of primary
894 nebular phases (Ma and Rossman 2009a). Iron carbide minerals, including cohenite [(Fe,Ni)₃C],
895 edscottite (Fe₅C₂), and haxonite [(Fe,Ni)₂₃C₆], are known from highly reduced chondrules in
896 carbonaceous chondrites and enstatite chondrites (e.g.,; MacPherson 2014; Rubin and Ma 2017;
897 Ma and Rubin 2019), but they have not been documented as primary phases in CAIs, AOAs, or
898 URIs. Consequently, they are considered in Part III of this series.

899

900 *URI khamrabaevite*: Titanium carbide (TiC) was identified by Ma and Rossman (2009c) as a
901 10-micron diameter grain associated with corundum and tistarite from the Allende carbonaceous
902 chondrite.

903

904 **NITRIDES**

905 Nitrides are rare in meteorites. Nierite (Si₃N₄) is known as a stellar mineral (Hazen and
906 Morrison 2020), but has not to our knowledge been reported in CAIs, AOAs, or URIs. Sinoite
907 (Si₂N₂O) is known as both a primary chondrule mineral and as an impact product in enstatite
908 chondrites (Lin et al. 2011; El Goresy et al. 2011; see Parts III and IV).

909 The only known candidate for a primary nebular condensate mineral is osbornite (TiN), which
910 is known from chondrules of enstatite chondrites (e.g., El Goresy et al. 2011), as well as from
911 CAIs in several carbonaceous chondrites (Weisberg et al. 1988; Grokhovsky 2006; Krot et al.
912 2006; MacPherson 2014). Note that osbornite is also known as a secondary mineral in enstatite
913 chondrite impact melts (Rubin and Ma 2020).

914

915 *CAI osbornite*: Osbornite (TiN) was identified in CAIs from the Isheyevo (Grokhovsky 2006;
916 Krot et al. 2006) and Allan Hills 85085 (Weisberg et al. 1988) carbonaceous chondrites. Osbornite
917 was also found in Stardust samples that were presumed to be CAI fragments (Weisberg et al.
918 2006).

919

920 **SILICIDES**

921 The silicide perryite $[(\text{Ni},\text{Fe})_5(\text{Si},\text{P})_2]$ is a refractory phase with characteristics of primary
922 condensates (MacPherson 2014; Rubin and Ma 2017). However, perryite is found principally in
923 the highly reduced mineral assemblages of enstatite chondrite chondrules and will be described in
924 Part III of this series.

925

926 **PHOSPHIDES**

927 At least two phosphides, monipite (MoNiP) and schreibersite $[(\text{Fe},\text{Ni})_3\text{P}]$, have been described
928 as primary phases in chondrite meteorites. The exact mode of formation of these grains is
929 uncertain; plausible hypotheses include reaction of a P-bearing nebular gas-phase with an Fe-Ni
930 alloy (Schaefer and Fegley 2010), crystallization from a P-rich immiscible melt that exsolved from
931 Fe-Ni melt, or exsolution from a solidified Fe-Ni alloy (Ma et al. 2014b). In this tabulation we list
932 only monipite, which was discovered in a CAI. Schreibersite is known principally from highly
933 reduced assemblages in enstatite chondrite chondrules and will be considered in Part III.

934

935 *CAI monipite:* Monipite with composition $[(\text{Mo}_{0.84}\text{Fe}_{0.06}\text{Co}_{0.04}\text{Rh}_{0.03})(\text{Ni}_{0.89}\text{Ru}_{0.09})\text{P}]$ was
936 described by Ma et al. (2014b) from a 1- x 2-micron crystal in a type B CAI from the Allende
937 meteorite. It occurs in association with primary phases melilite, fassaite, and spinel, as well as
938 probable alteration minerals, including awaruite, the rare oxides kamiokite ($\text{Fe}_2\text{Mo}_3\text{O}_8$),
939 tugarinovite (MoO_2), and an unnamed Nb-rich oxide $[(\text{Nb},\text{V},\text{Fe})\text{O}_2]$.

940

941 **SULFIDES**

942 A number of sulfide minerals, including niningerite (MgS), oldhamite (CaS), pentlandite
943 [(Fe,Ni)₉S₈], and troilite (FeS), probably formed early in the history of the solar nebula (Rubin
944 and Ma 2017, 2020). However, all of these phases, as well as numerous subsequent sulfides, either
945 formed by igneous processes in chondrules (e.g., Rubin et al. 1999; MacPherson 2014; see Part
946 III), by sulfidation of earlier phases through reaction with an S-rich vapor, or by solid-state
947 reactions (Rubin and Ma 2017). Therefore, we do not list any sulfide minerals as primary nebular
948 condensates in Part II.

949 Troilite represents a difficult case. In some instances, it appears to be a primary chondrule
950 mineral (e.g., Rubin et al. 1999; El Goresy et al. 2011) and thus will be included in Part III of this
951 series. However, many occurrences in meteorites, including in CAIs of enstatite chondrites, appear
952 to represent secondary mineralization by sulfidation (Fagan et al. 2000; Guan et al. 2000;
953 MacPherson 2014). Therefore, in spite of instances where troilite in CAIs is associated with
954 primary oxide and silicate phases and a primary origin for the sulfide cannot be ruled out (Fagan
955 et al. 2001), we do not list any sulfides as primary nebular condensates in CAIs, AOAs, or URIs.

956

957 **OXIDES**

958 Oxygen is the most abundant element in the solar nebula after hydrogen and helium, and it
959 played a dominant role in the condensation of primary refractory phases in CAIs, AOAs, and URIs.
960 The most common primary nebular oxides in CAIs, AOAs, and URIs contain Mg, Ca, Al, and/or
961 Ti, with rare minor oxides of Mo, Sc, V, and Zr. We also include ice (cubic H₂O) as the only
962 molecular crystal likely to have condensed in the cool (~ 100K) outer regions of the solar nebula.

963 Note that more than two dozen other refractory oxides are recorded as primary minerals from
964 chondrules (MacPherson 2014; Rubin and Ma 2017). The distinction between primary condensates

965 in CAIs, AOAs, and URIs (the subject of this contribution) versus primary igneous phases in
966 chondrules (which will be summarized in Part III) is important. The limited number of confirmed
967 CAI, AOA, and URI oxide phases listed below are thought to have formed by condensation via
968 cooling of high-temperature, low-pressure vapor or their subsequent solid-state reactions in the
969 earliest solar nebula at ~ 4.567 Ga. Subsequent primary phases in chondrules were formed by
970 partial melting of nebular materials at least 1.5 million years later – a time when planetesimal
971 formation and nebular heterogeneities had become well established (e.g., Gilmour and Saxton
972 2001; Connolly and Jones 2016). Primary chondrule minerals thus crystallized at a later time by a
973 different combination of processes; i.e., at generally lower temperatures, during relatively short
974 heating events, and on nebular material that had already undergone a preliminary stage of chemical
975 and isotopic fractionation.

976 Confusion can arise as to what constitutes a primary CAI, AOA, or URI phase. For example,
977 the rare mineral tistarite (Ti_2O_3) was described from a single 1- x 2-micron grain in a chondrule
978 from the Allende carbonaceous chondrite (Ma and Rossman 2009c). Because of its presumed
979 primordial character, MacPherson (2014, Table 1) listed tistarite as one of only 15 CAI primary
980 minerals. However, coexisting rutile (TiO_2) is not included in this tabulation of the earliest primary
981 nebular minerals, because it appears to represent a later stage of nebular mineralization (Ma 2019).
982 Numerous other meteoritic oxide minerals will be considered in Parts III, IV, and V of this series.

983

984 **Ice (H_2O):** Primary solar nebular mineralogy consists almost exclusively of high-temperature
985 ($T > 1100$ K) refractory phases that form by condensation from a vapor phase or melt
986 crystallization in close proximity to the central star. However, infrared telescopic observations

987 reveal the presence of crystalline H₂O, presumably condensed as thin mantles (< 0.05 microns
988 thick) on oxide and silicate dust grains in the cold circumstellar regions of some oxygen-rich stars
989 (Omont et al. 1990). We therefore include ice as a primary nebular condensate.

990 The distinction between crystalline and amorphous condensed H₂O in the context of
991 circumstellar environments is important. Crystalline water, which is revealed by sharp IR emission
992 features at 44 and 60 microns, can only condense directly at temperatures > 50 K under relatively
993 low molecular fluxes (estimated at $\sim 10^4$ molecules per cm² per second in circumstellar
994 environments; Kouchi and Yamamoto 1995). By contrast, at the significantly lower temperatures
995 and greater molecular fluxes of interstellar clouds, amorphous H₂O with diagnostic broad emission
996 peaks (notably at 3.1 microns) is more likely to form.

997 Water that initially condenses in the amorphous form will not crystallize to cubic ice unless T
998 rises above 110 K and it has sufficient time to anneal. However, 110 K is close to the sublimation
999 temperature, while the sublimation rate of amorphous H₂O may be an order of magnitude greater
1000 than that of crystalline H₂O (Léger et al. 1983). Therefore, condensed H₂O phases may disappear
1001 (Kouchi et al. 1994). Indeed, one line of evidence for amorphous H₂O (as opposed to a crystalline
1002 form) in comets is the anomalously high sublimation rate of some comets (Mukai 1986).

1003 Laboratory experiments on ice formation under low-pressure, cryogenic conditions suggest that
1004 the stable crystalline form of H₂O under circumstellar conditions is “cubic ice” (Gaffney and
1005 Matson 1980; Bartels-Rausch et al. 2012; Fuentes-Landete et al. 2015; Salzmann 2018). Note that
1006 fewer than 100 H₂O molecules are required to form a localized phase with the structural properties

1007 of crystalline ice (Moberg et al. 2019; Jordan 2019). We recognize one likely circumstellar, low-
1008 temperature condensate, designated “*Circumstellar ice*.”

1009
1010 *Circumstellar ice*: Occurring as < 0.05-micron-thick mantles on oxide and silicate dust grains,
1011 circumstellar cubic ice (H₂O) condenses in relatively cool (50 < T < 150 K) toroidal volumes
1012 surrounding some solar nebulas and O-rich stars (Omont et al. 1990).

1013
1014 **Corundum (Al₂O₃)**: Corundum is thought to be the highest temperature oxide condensate at
1015 T ~ 1770 K (Grossman 1972; Davis and Richter 2014; Wood et al. 2019). However, because
1016 corundum reacts with the cooling gas to form other oxides such as hibonite or melilite it is a
1017 relatively rare mineral in CAIs.

1018
1019 *CAI corundum*: End-member Al₂O₃ with minor Mg and Fe is a rare mineral in CAIs. Sub-
1020 micron grains have been recorded in CAI cores, as inclusions in spinel or hibonite, or enclosing a
1021 central core of hibonite (Bar-Matthews et al. 1982; MacPherson et al. 1984; Wark 1986; Greshake
1022 et al. 1996).

1023
1024 *URI corundum*: Ma and Rossman (2009c) reported corundum associated with khamrabaevite
1025 and tistarite in an ultra-refractory inclusion from the Allende meteorite.

1026
1027 **Tistarite (Ti₂O₃)**: The refractory mineral tistarite (Ti³⁺₂O₃), a member of the corundum group,
1028 is known from a single 5- x 7-micron subhedral grain from a chondrule in the Allende

1029 carbonaceous chondrite (Ma and Rossman 2009c; Ma et al. 2009a). It occurs in association with
1030 the primary phases corundum, khamrabaevite (TiC), and kaitianite ($\text{Ti}^{3+}_2\text{Ti}^{4+}\text{O}_5$), as well as rutile
1031 (TiO_2).

1032
1033 *URI tistarite*: Tistarite has been found as a single grain in an ultra-refractory inclusion
1034 contained within a chondrule from the Allende carbonaceous chondrite (Ma and Rossman 2009c).

1035
1036 **Kaitianite ($\text{Ti}^{3+}_2\text{Ti}^{4+}\text{O}_5$)**: Two crystals of the mixed-valence titanium oxide mineral,
1037 kaitianite, were discovered by Ma (2019) in association with the primary phases corundum,
1038 tistarite, and khamrabaevite (TiC), as well as rutile (TiO_2). Micron-scale kaitianite crystals have
1039 the monoclinic (*C2/c*) oxyvanite (V_3O_5) structure.

1040
1041 *URI kaitianite*: Kaitianite has been found as two grains in an ultra-refractory inclusion; the
1042 observed composition is $(\text{Ti}^{3+}_{1.75}\text{Al}_{0.05}\text{Ti}^{4+}_{0.10}\text{Mg}_{0.08}\text{Fe}_{0.02})\text{Ti}^{4+}\text{O}_5$ (Ma 2019).

1043
1044 **Rutile (TiO_2)**: Rutile has been reported in association with tistarite and kaitianite by Ma and
1045 coworkers (Ma and Rossman 2009c; Ma et al. 2009a; Ma 2019), who suggest it is a primary phase
1046 in some URIs.

1047
1048 *URI rutile*: Occurs as micron-scale grains in an ultra-refractory inclusion from the Allende
1049 meteorite (Ma 2019).

1050

1051 **Baddeleyite (ZrO₂):** Presumably primary baddeleyite was described from meteorite MAC
1052 88107, while grains of ZrO₂ (lacking structural details) have also been reported from Murchison
1053 and Allende chondrites (Krot et al. 2019). It occurs in association with allendeite and zirkelite.

1054

1055 *URI baddeleyite:* Occurs as micron-scale grains in URIs (Krot et al. 2019).

1056

1057 **Anosovite [(Ti⁴⁺,Ti³⁺,Mg,Sc,Al)₃O₅]:** A second polymorph of Ti₃O₅ (in addition to kaitianite)
1058 was reported by Zhang et al. (2015) from an ultra-refractory inclusion in the Sayh al Uhaymir 290
1059 (CH3) carbonaceous chondrite. This Sc-bearing phase has the orthorhombic (*Cmcm*)
1060 pseudobrookite structure and thus is equivalent to the discredited mineral “anosovite,” which was
1061 originally identified in Ti-rich slags (Bowles 1988). It occurs as micron-scale grains in association
1062 with fassaite, spinel, anorthite, perovskite, panguite, davisite, and Fe-Ir-Mo-Os alloy nuggets.

1063

1064 *URI anosovite:* Two grains of ultra-refractory anosovite with the average composition of
1065 (Ti⁴⁺_{1.36}Ti³⁺_{0.59}Mg_{0.34}Sc_{0.20}Al_{0.20}V_{0.05}Ca_{0.05}Si_{0.03}Fe_{0.03}Cr_{0.03}Zr_{0.03})O₅ were reported by
1066 Zhang et al. (2015).

1067

1068 **Spinel (MgAl₂O₄):** Spinel is perhaps the most ubiquitous primary mineralogical component of
1069 CAIs in most chondrite types except CI (MacPherson 2014), as well as a common phase in Wark-
1070 Lovering rims. Fe-rich varieties of spinel group minerals, including chromite and hercynite, have

1071 also been described from CAIs (e.g., Brearley and Jones 1998), but they are always of secondary
1072 origins.

1073

1074 *CAI spinel*: Most CAIs incorporate near end-member MgAl_2O_4 spinel, though with a wide
1075 range of observed trace and minor elements – notably Fe, Ti, V, Cr, and Zn (Brearley and Jones
1076 1998). Spinel occurs in a variety of habits, including euhedral octahedral crystal inclusions in
1077 melilite, fassaite, or anorthite (Grossman 1980); as framboidal aggregates (El Goresy et al. 1979);
1078 surrounding a hibonite core (Steele 1995); as spinel-hibonite or spinel-perovskite spherules
1079 (Macdougall 1981); as spherical shells, or “palisades,” of spinel enclosing melilite, fassaite, and/or
1080 anorthite, within larger CAIs (Wark and Lovering 1982b; Simon and Grossman 1997); in
1081 association with grossite-bearing inclusions (Brearley and Jones 1998); and as a common layer in
1082 Wark-Lovering rims (Wark and Lovering 1977).

1083

1084 *AOA spinel*: Spinel, typically in sub-micron grains, occurs as a primary phase associated with
1085 perovskite, fassaite, and anorthite in amoeboid olivine aggregates (Krot et al. 2004; Weisberg et
1086 al. 2004).

1087

1088 *URI spinel*: Spinel occurs in ultra-refractory inclusions in association with Sc-rich fassaite,
1089 REE-enriched perovskite, and other distinctive Sc, Zr, Ti, and REE phases (e.g., Ma and Rossman
1090 2009b; Ma et al. 2013b, 2014a).

1091

1092 **Hibonite ($\text{CaAl}_{12}\text{O}_{19}$)**: Hibonite, nominally $\text{CaAl}_{12}\text{O}_{19}$ but commonly incorporating
1093 significant $\text{Mg}+\text{Ti}^{4+} \leftrightarrow 2\text{Al}$ (up to ~4.5 and 9 wt. % MgO and TiO_2 , respectively) as well as

1094 minor V, Fe, Si, Cr, and Sc, is an important mineralogical component of CAIs in most types of
1095 chondrite meteorites (Keil and Fuchs 1971; Brearley and Jones 1998; MacPherson 2014). As much
1096 as a quarter of hibonite Ti may be present as Ti^{3+} - an indication of the highly reducing formation
1097 conditions of some CAIs (Ihinger and Stolper 1986; Beckett et al. 1988).

1098 Hibonite is thought to form initially by reaction of the gas phase with corundum at $T > 1700$ K.
1099 Because of its high temperature of condensation (Davis and Richter 2014; Wood et al. 2019),
1100 hibonite is often the earliest preserved mineral in a CAI. As a consequence, hibonite petrology,
1101 major and trace element composition, and stable isotopes have been extensively studied to provide
1102 clues regarding primitive stellar environments (Hinton et al. 1988; Ireland 1988; Ireland et al.
1103 1988; Brearley and Jones 1998; MacPherson 2014 and references therein; Kööp et al. 2016a,
1104 2016b, 2018).

1105
1106 *CAI hibonite:* CAI hibonite occurs in a variety of contexts and morphologies (Ireland 1988),
1107 including acicular crystals associated with spinel, melilite, and perovskite in compact type A
1108 inclusions (Grossman 1975; Sylvester et al. 1993); as a common constituent of fluffy type A CAIs
1109 (Grossman 1975; Kornacki and Wood 1984); as 1- to 25-micron laths near the exterior of type B
1110 CAIs in the Allende CV chondrite (Blander and Fuchs 1975); in fine-grained spinel-rich inclusions
1111 (Kornicki and Wood 1985); as up to 1-millimeter diameter grains in CAI cores (Allen et al. 1980;
1112 Armstrong et al. 1982; MacPherson et al. 1983); in clusters of tabular crystals surrounded by spinel
1113 in a CAI core (Steele 1995); as inclusions in spinel, fassaite, melilite, and grossite CAI cores (Wark
1114 and Lovering 1977; Kornacki and Wood 1985; Mao et al. 1990; Weber and Bischoff 1994); in
1115 association with corundum (MacPherson et al. 1984; Hinton et al. 1988); as isolated crystal
1116 fragments (MacPherson et al. 1983; Ireland 1988); in spinel-hibonite spherules as 5- to 20-micron

1117 bladed crystals (Macdougall 1981) and rims (MacPherson et al. 1984); and as layers in Wark-
1118 Lovering rims.

1119

1120 **Perovskite (CaTiO₃):** Near-stoichiometric calcium titanate perovskite, albeit with trace or
1121 minor Mg, Al, Si, Cr, Sc, V, Fe, Y, Zr, Nb, REE, Th, and U, is an important mineralogical
1122 component of CAIs in most chondrite types (Kornacki and Wood 1985; Weber and Bischoff 1994;
1123 Brearley and Jones 1998; MacPherson 2014). Twinning in perovskite crystallites suggest that they
1124 were heated above the cubic-orthorhombic transition at 1573 K.

1125

1126 *CAI perovskite:* Near end-member perovskite is a common phase in CAIs (Brearley and Jones
1127 1998). Perovskite generally occurs as very fine-grained (< 15 microns) inclusions in melilite,
1128 spinel, and fassaite, and less commonly hibonite and grossite (Macdougall 1981; Fahey et al. 1994;
1129 Kojima et al. 1995; Steele 1995; Weber et al. 1995). It is also a common component in Wark-
1130 Lovering rims (Weisberg et al. 1993; Keller and Buseck 1994).

1131

1132 *AOA perovskite:* Perovskite, often as sub-micron grains in association with spinel, is a common
1133 primary phase in amoeboid olivine aggregates (Weisberg et al. 2004).

1134

1135 *URI perovskite:* Perovskite enriched in REE occurs in ultra-refractory inclusions, for example
1136 from the Allende carbonaceous chondrite in association with Sc-rich fassaite, spinel, and kangite
1137 (Ma and Rossman 2009b; Ma 2011; Ma et al. 2013b, 2014a, 2015).

1138

1139 **Lakargiite (CaZrO₃):** Ma (2011) identified sub-micron grains of a Zr-dominant perovskite in
1140 an ultra-refractory inclusion from the Acfer 094 carbonaceous chondrite. Lakargiite
1141 [Ca_{0.95}(Zr_{0.87}Ti_{0.16})O₃] is found as inclusions in hibonite and in association with perovskite
1142 [Ca_{0.94}(Ti_{0.98}Zr_{0.06})O₃], tazheranite, an Os-dominant alloy, and other refractory phases (Krot et
1143 al. 2019).

1144

1145 *URI lakargiite:* Ma (2011) identified Zr-rich perovskite from an ultra-refractory inclusion in
1146 Acfer 094.

1147

1148 **Grossite (CaAl₄O₇):** Grossite is one of several high-temperature calcium aluminate minerals
1149 that forms in CAIs, presumably in environments with low Mg and Si shortly after the condensation
1150 of corundum and hibonite (Michel-Lévy et al. 1982; Weber and Bischoff 1994; Aléon et al. 2002).
1151 Samples are near stoichiometric, though they commonly incorporate minor Mg, Si, Ti, and Fe.

1152

1153 *CAI grossite:* Grossite typically occurs as 5- to 10-micron diameter crystallites, often as
1154 inclusions in association with melilite, perovskite, spinel, hibonite, fassaite, and anorthite
1155 (Greenwood et al. 1992; Simon et al. 1994).

1156

1157 **Krotite (CaAl₂O₄):** Krotite is one of several refractory calcium aluminates that occur as
1158 primary condensates in CAIs with low Mg and Si (Ivanova et al. 2002; Ma et al. 2011b). Mikouchi

1159 et al. (2009) identified a second polymorph of CaAl_2O_4 , dmitryivanovite, which is thought to be a
1160 high-pressure form that results from impact transformation (see Part IV of this series).

1161

1162 *CAI krotite*: The single known occurrence of krotite was found as aggregates of crystals from
1163 10- to 350-microns diameter in the central and mantle portions of a CAI from the NWA 1934 CV3
1164 carbonaceous chondrite (Ivanova et al. 2002; Ma et al. 2011b). It is found in association with
1165 perovskite, melilite, grossite, hibonite, and spinel.

1166

1167 **Machiite ($\text{Al}_2\text{Ti}_3\text{O}_9$)**: Krot et al. (2020) identified machiite, a new ultra-refractory oxide
1168 mineral from the Murchison carbonaceous chondrite that probably formed by direct condensation
1169 from a gas phase or by crystallization from a Ca-Al-rich melt in CAI-forming nebular regions. The
1170 ideal composition is $\text{Al}_2\text{Ti}_3\text{O}_9$ but, as is typical with ultra-refractory oxide phases, machiite
1171 incorporates significant Sc, Y, and Zr, as well. It was found as a single 4.4-micron diameter
1172 euhedral grain in association with euhedral corundum. Electron diffraction studies suggest a
1173 monoclinic ($C2/c$) schreyerite-type structure.

1174

1175 *URI machiite*: Krot et al. (2020) describe a single 4.4-micron diameter crystallite with empirical
1176 composition $(\text{Al}_{1.17}\text{Sc}_{0.56}\text{Y}_{0.10}\text{Ti}^{4+}_{0.08}\text{Fe}_{0.06}\text{Ca}_{0.03}\text{Mg}_{0.01})(\text{Ti}^{4+}_{2.71}\text{Zr}_{0.28}\text{Si}_{0.01})\text{O}_9$.

1177

1178 **Zirkelite [(Ti,Ca,Zr)O_{2-x}]**: Krot et al. (2019) record a possible grain of zirkelite, a complex
1179 Ti-Ca-Zr oxide with a defect cubic fluorite structure, as a micron-scale phase in an ultra-refractory
1180 inclusion from meteorite MAC 88107.

1181
1182 *URI zirkelite*: Zirkelite was identified as a micron-scale grain from MAC 88107 (Krot et al.
1183 2019).

1184
1185 **Kangite [(Sc,Ti,Al,Zr,Mg,Ca)_{1.8}O₃] and Panguite [(Ti⁴⁺,Sc,Al,Mg,Zr,Ca)_{1.8}O₃]**: Ma and
1186 coworkers described two closely-related Ti-Sc oxides – Sc-dominant kangite (Ma et al. 2013b)
1187 and Ti-dominant panguite (Ma et al. 2012) from ultra-refractory inclusions in the Allende
1188 carbonaceous chondrite, as well as an occurrence of panguite from the Murchison chondrite (Ma
1189 et al. 2011a). Both minerals occur as micron-scale grains in association with Sc-rich davisite,
1190 perovskite, and spinel, and both have cation-deficient bixbyite structures. Thus, kangite and
1191 panguite might be lumped into a single natural kind; however, kangite is reported to be cubic
1192 $Ia\bar{3}$, whereas the panguite structure occurs in the orthorhombic subgroup *Pbca*. Therefore,
1193 we list two different natural kinds, subject to further structural and compositional details. Note that
1194 Ma et al. (2012) also report several Zr-rich grains of panguite.

1195
1196 *URI kangite*: Sc-dominant kangite was described from an ultra-refractory inclusion in the
1197 Allende carbonaceous chondrite (Ma et al. 2013b).

1198
1199 *URI panguite*: Micron-scale crystallites of Ti-dominant panguite are associated with fassaite in
1200 ultra-refractory inclusions (Ma et al. 2012; Krot et al. 2019). The most complete description is
1201 from a 20- x 30-micron amoeboid olivine aggregate in the Allende carbonaceous chondrite, while
1202 additional occurrences have been reported from the Allende, Murchison, and Sayh al Uhaymir 290
1203 meteorites (Ma et al. 2012; Zhang et al. 2015).

1204

1205 **Zirconolite (CaZrTi₂O₇):** Ma and Rossman (2008) reported zirconolite in an ultra-refractory
1206 inclusion in an amoeboid olivine aggregate from the Allende carbonaceous chondrite. It is
1207 associated with micron-scale inclusions of cubic zirconia (tazheranite) and Fe-Ni and PGE alloys.

1208

1209 *URI zirconolite:* Zirconolite from the Allende meteorite was recorded by Ma and Rossman
1210 (2008).

1211

1212 **Tazheranite [(Zr,Sc,Ca,Y,Ti)O_{1.75}]:** Ma and Rossman (2008) described natural Sc-Ti-rich
1213 cubic zirconia as crystals up to 1.2-micron diameter from ultra-refractory inclusions within an
1214 AOA in the Allende meteorite. Tazheranite occurs as inclusions in zirconolite; associated minerals
1215 include fassaite and Fe-Ni and PGE alloys. A second occurrence from an Allende URI in fine-
1216 grained matrix (Ma et al. 2014a) is associated with allendeite, spinel, fassaite, and perovskite.

1217

1218 *URI tazheranite:* Tazheranite is a rare mineral from ultra-refractory inclusions from the Allende
1219 meteorite (Ma and Rossman 2008; Ma et al. 2014a; Krot et al. 2019).

1220

1221 **Allendeite (Sc₄Zr₃O₁₂):** Allendeite was described by Ma et al. (2014a), who examined grains
1222 up to 25-microns diameter in an ultra-refractory inclusion in the Allende carbonaceous carbonate.
1223 It contains inclusions of spinel and hexamolybdenum, and is closely associated with fassaite,
1224 perovskite, tazheranite, and Os-dominant PGE alloys.

1225

1226 *URI allendeite*: Allendeite was discovered in an ultra-refractory inclusion from the Allende
1227 meteorite (Ma et al. 2014a; Krot et al. 2019).

1228

1229 **SILICATES**

1230 Refractory silicates are major components of CAIs, AOAs, and URIs. Several major rock-
1231 forming mineral groups, including olivine, garnet, pyroxene, and feldspar, are represented, as well
1232 as rare ultra-refractory Ti, Sc, and Zr silicates.

1233

1234 **Quartz (SiO₂)**: Komatsu et al. (2018) reported an unusual occurrence of silica condensation
1235 within the solar nebula in a region with low Mg/Si – an example of nebular element fractionation
1236 in the period following CAI formation. Quartz occurs as grains up to 20-microns diameter in
1237 association with fassaite, anorthite, and spinel in an amoeboid olivine aggregate from the Yamato-
1238 793261 carbonaceous chondrite.

1239

1240 *AOA quartz*: Quartz occurs as primary grains associated with fassaite, forsterite, anorthite, and
1241 spinel in an AOA (Komatsu et al. 2018).

1242

1243 **Olivine group [(Mg,Fe,Ca,Mn)₂SiO₄]**: Nebular olivine represents a solid solution among four
1244 principal end members, forsterite (Mg), fayalite (Fe), monticellite (Ca), and tephroite (Mn).
1245 Primary olivine that formed by direct condensation or melt solidification in CAIs and AOAs is
1246 typically close to end-member forsterite (Brearley and Jones 1998). Davis et al. (1991) describe
1247 rare instances where CAI forsterite (replaced by akermanite) and fassaite (replaced by gehlenite
1248 and perovskite) have been partially evaporated, resulting in a different mode of mineral formation

1249 due to a reheating event (and loss of Si and Mg) to at least 1700 K, possibly by remixing close to
1250 the Sun (Davis and Richter 2014).

1251
1252 *CAI forsterite*: Forsteritic olivine is a minor primary phase in CAIs. It occurs, for example, as
1253 < 5-micron diameter grains associated with spinel and fassaite, as well as in Wark-Lovering rims,
1254 in a variety of carbonaceous chondrites (Greenwood et al. 1994; MacPherson and Davis 1994),
1255 and as an interstitial phase with anorthite and melilite in a CAI from PCA91082 (Birjukov and
1256 Ulyanov 1996).

1257
1258 *AOA forsterite*: Mg-rich olivine (Fo > 98), in some cases with rims enriched in Mn (Mn > Fe),
1259 is the principal constituent of AOA's (Krot et al. 2004; Weisberg et al. 2004). Micron-scale crystals
1260 (<10 microns) occur in irregular-shaped aggregates up to 1 millimeter in diameter. Klöck et al.
1261 (1989) suggest that the Mn enrichment arose from condensation of a tephroite component directly
1262 from the solar nebular at temperatures close to 1100 K, compared to the ~1440 K condensation of
1263 pure forsterite, and far above the ~500 K reaction of Fe metal with forsterite to form fayalite.

1264
1265 **Garnet group** [$\text{Ca}_3(\text{Al}, \text{Ti}^{3+}, \text{V}, \text{Sc})_2\text{Si}_3\text{O}_{12}$]: Ca-Al garnet with significant Ti^{3+} and/or Sc is a
1266 scarce primary phase in the earliest nebular condensates. Garnet with composition close to the
1267 grossular end-member (ideally $\text{Ca}_3\text{Al}_2\text{Si}_3\text{O}_{12}$) is known almost exclusively as a secondary phase
1268 in chondrites (Fuchs 1974; Wark et al. 1987; Brearley and Jones 1998; Rubin and Ma 2017). In
1269 addition, Simon and Grossman (1992) reported goldmanite [$\text{Ca}_3(\text{V}, \text{Al}, \text{Fe}, \text{Ti})_2\text{Si}_3\text{O}_{12}$] in a
1270 Fremdlinge from the Leoville chondrite (see Part III). However, Ma and coworkers have

1271 discovered two rare primary garnets with the general formula $\text{Ca}_3(\text{Ti}^{3+}, \text{Sc}, \text{Mg}, \text{Y})\text{Si}_3\text{O}_{12}$ in
1272 chondrite meteorites (Ma 2012; Ma et al. 2017a), including the end-members eringaite
1273 ($\text{Ca}_3\text{Sc}_2\text{Si}_3\text{O}_{12}$) and rubinite ($\text{Ca}_3\text{Ti}^{3+}_2\text{Si}_3\text{O}_{12}$). These compositional extremes reveal fascinating
1274 heterogeneities in the early solar nebula.

1275 Eringaite (Ma 2012), the Sc-dominant, Al-poor garnet $\text{Ca}_3(\text{Sc}, \text{Y}, \text{Ti})_2\text{Si}_3\text{O}_{12}$, was discovered
1276 with rubinite in an ultra-refractory inclusion within an AOA from the Vigarano carbonaceous
1277 chondrite. It occurs as micron-scale crystals within davisite and in association with spinel,
1278 tazheranite, and hexaferrum.

1279 The Ti^{3+} end-member, dubbed rubinite by Ma et al. (2017a), was discovered as crystals up to
1280 20-microns diameter in both type A CAIs from the Allende and Efremovka carbonaceous
1281 chondrites, where it occurs with the major primary CAI minerals, as well as eringaite and Ti^{3+} -
1282 dominant fassaite (grossmanite). Rubinite significantly enriched in Y, Sc, and Zr was found in an
1283 ultra-refractory inclusion in the Vigarano meteorite with spinel, panguite, fassaite, and davisite,
1284 which is enclosed in an AOA.

1285
1286 *CAI rubinite:* Rubinite occurs in type A CAIs from the Allende and Efremovka carbonaceous
1287 chondrites (Ma 2012).

1288
1289 *URI rubinite:* Rubinite occurs with eringaite in an ultra-refractory inclusion in the Vigarano
1290 chondrite (Ma et al. 2017a); significantly enriched in Y, Sc, and Zr.

1291

1292 *URI eringaite*: Eringaite occurs with rubinite in an ultra-refractory inclusion in the Vigarano
1293 chondrite (Ma et al. 2017a).

1294

1295 **Melilite group [gehlenite ($\text{Ca}_2\text{Al}_2\text{SiO}_7$) to åkermanite ($\text{Ca}_2\text{MgSi}_2\text{O}_7$)]:** The calcium silicates
1296 of the melilite group, which feature complete solid solution between Al_2 (gehlenite) and MgSi
1297 (åkermanite) end members, are major mineralogical constituents of CAIs. Unlike many igneous
1298 examples, CAI melilite contains minimal Fe and Na. Wood et al. (2019), in revised calculations
1299 of condensation temperatures that take trace elements into account, suggest that gehlenite-
1300 dominant melilite condenses first, between 1550 and 1600 K, following the appearance of
1301 corundum and hibonite. As condensation temperatures fall, melilite crystals typically develop
1302 zoning from gehlenite-rich cores to åkermanite-dominant rims. Because melilite in CAIs spans the
1303 complete compositional range from Al_2 to MgSi end-members, we lump CAI gehlenite and
1304 åkermanite into a single natural kind. Melilite is common in most types of CAIs, as well as in
1305 AOAs.

1306

1307 *CAI melilite*: Melilite is among the commonest primary condensed phases in CAIs, ranging in
1308 composition from Åk_{01} to Åk_{100} (Grossman 1975, 1980; Wark et al. 1987; Davis et al. 1991;
1309 Podosek et al. 1991), often with zoning from more gehlenite-rich cores to more åkermanite-rich
1310 rims. It occurs as coarse-grained (2 to 3 millimeter) crystals in the cores of many CAIs (e.g.,
1311 MacPherson 2014); as rims on spinel (Holmberg and Hashimoto 1992); in nodular aggregates with
1312 spinel and fassaite (Weisberg et al. 1993); as a component of hibonite-, spinel-, and grossite-

1313 bearing inclusions (J.N. Grossman et al. 1988; Weber et al. 1995); and as layers in Wark-Lovering
1314 rims (Wark and Lovering 1977).

1315

1316 *AOA melilite*: Gehlenite-rich melilite (Ge_{80-85}) is an occasional primary phase in AOAs,
1317 typically associated with anorthite and spinel (Krot et al. 2004). Weisberg et al. (2004) suggest
1318 that some AOA melilite underwent solid-state reactions on cooling to form anorthite.

1319

1320 *URI melilite*: Ma et al. (2015) reported gehlenitic melilite in a Sc-rich ultra-refractory inclusion
1321 in the Vigarano carbonaceous chondrite, associated with warkite, davisite, perovskite, and spinel.

1322

1323 **Clinopyroxene Group** $[\text{Ca}(\text{Mg},\text{Al},\text{Ti}^{3+},\text{Ti}^{4+},\text{Sc},\text{V})(\text{Al},\text{Si})\text{SiO}_6]$: Fassaite and related calcic
1324 clinopyroxenes are abundant primary phases in CAIs, AOAs, and URIs (Brearley and Jones 1998;
1325 Davis and Richter 2014; MacPherson 2014; Sack and Ghiorso 2017). Ca-Mg-dominant, Fe-poor
1326 clinopyroxene with significant Al and Ti (both Ti^{3+} and Ti^{4+}), and occasionally Sc or V, is closest
1327 compositionally to the IMA-approved species diopside ($\text{CaMgSi}_2\text{O}_6$), though end-member
1328 diopside has not been confirmed as a primary nebular condensate (Brearley and Jones 1998). The
1329 discredited name “fassaite” (Morimoto et al. 1988) is still widely used by the meteoritics
1330 community and the name is retained here.

1331 The crystal chemistry of fassaite can be modeled with four dominant ideal end-members (Sack
1332 and Ghiorso 1994a, 1994b, 1994c, 2017). In addition to diopside, rare Al-rich grains are closer to
1333 ($\text{CaAl}_2\text{SiO}_6$), the IMA-approved end-member kushiroite (Kimura et al. 2009), though long called
1334 the “calcium Tschermak’s pyroxene” (e.g., Ma et al. 2009b). Other examples are closer in

1335 composition to grossmanite ($\text{CaTi}^{3+}\text{AlSiO}_6$; Ma and Rossman 2009a), while Sack and Ghiorso
1336 (1994a, 1994c, 2017) also recognize “alumino-buffonite” ($\text{CaMg}_{0.5}\text{Ti}^{4+}_{0.5}\text{AlSiO}_6$) as an important
1337 additional end-member with the maximum possible octahedral Ti^{4+} content. Phase equilibria in
1338 this four-component fassaite system are complex; Sack and Ghiorso (2017) suggest as many as
1339 four miscibility gaps, based on both thermodynamic modeling and observed coexistence of fassaite
1340 rims and cores of different compositions that appear to be in equilibrium (Wark and Lovering
1341 1982). Additional complexity arises from the occurrence of rare micron-scale grains of burnettite
1342 ($\text{CaV}^{3+}\text{AlSiO}_6$; Ma and Beckett 2016) and davisite ($\text{CaSc}^{3+}\text{AlSiO}_6$; Simon et al. 1996; Ma and
1343 Rossman 2009b).

1344 How many natural kinds of primary nebular clinopyroxene should be recognized remains an
1345 open question. Evidence for fassaite miscibility gaps points to the need for multiple natural kinds;
1346 however, until more analyses and other diagnostic attributes are available for cluster analysis, we
1347 lump primary nebular clinopyroxenes from the quadrilateral defined by diopside, kushiroite,
1348 grossmanite, and “alumino-buffonite” into one natural kind, “fassaite”
1349 $[\text{Ca}(\text{Mg},\text{Al},\text{Ti}^{3+},\text{Ti}^{4+})(\text{Al},\text{Si})\text{SiO}_6]$.

1350 The fassaite phase region may extend to Sc- and/or V-rich compositions; however, only two
1351 examples of these extremes have been reported and both appear idiosyncratic. Burnettite is an
1352 oddity, with octahedral M2 site composition $[(\text{V}^{3+}_{0.29}\text{Sc}_{0.24}\text{Ti}^{3+}_{0.13}\text{Al}_{0.09})\text{Ti}^{4+}_{0.12}\text{Mg}_{0.08}]$ (Ma
1353 and Beckett 2016); thus, V, Sc, and Ti are present in roughly equal amounts and no cation is present
1354 at greater than 29 mol % M2 occupancy. Burnettite is therefore far from any ideal end-member

1355 composition. We designate the only known occurrence, from an unusual V-rich fluffy type A CAI,
1356 as “*CAI burnettite*.”

1357 Davisite [Ca(Sc,Ti³⁺,Ti⁴⁺,Mg,Zr)AlSiO₆], is a minor phase that occurs occasionally in ultra-
1358 refractory inclusions (Ma and Rossman 2009b). Common associations include fassaite (with
1359 significantly less Sc than in coexisting davisite), as well as perovskite, spinel, and a host of rare
1360 Sc-bearing minerals, including eringaite, kangite, panguite, rubinite, thortveitite, and warkite (Ma
1361 et al. 2011a, 2012, 2013b, 2015, 2017a; Ma 2012; Krot et al. 2019).

1362
1363 *CAI fassaite*: Ca-rich, Fe-poor pyroxenes are, in combination with spinel, the most common
1364 CAI phases, occurring in types A, B, and C CAIs and URIs (Grossman 1980; Wark 1987; Wark
1365 et al. 1987; Podosek et al. 1991; Brearley and Jones 1998), as well as layers in Wark-Lovering
1366 rings (Wark and Lovering 1977). Primary fassaite commonly occurs with anorthite, melilite,
1367 forsterite, and spinel as CAI cores, mantles, and rims (Macdougall 1979, 1981; Doukhan et al.
1368 1991; Kimura et al. 1993; Kojima et al. 1995; Simon et al. 1996). Of special note regarding CAI
1369 fassaite is the occurrence of both trivalent and tetravalent Ti—a consequence of the extremely
1370 reducing conditions of its formation (Beckett 1986), perhaps dominated by hot H₂ gas, as well as
1371 conditions in which C/O > 0.5.

1372
1373 *AOA fassaite*: Al-Ti-rich calcic clinopyroxene with Al and Ti as high as 20 and 13 wt. %,
1374 respectively, is a common primary phase in AOAs, especially in Al-rich refractory inclusions
1375 where it occurs in close association with forsterite and anorthite, as well as melilite, spinel, and
1376 perovskite (Hashimoto and Grossman 1987; Krot et al. 2004; Weisberg et al. 2004; Ma et al. 2012).

1377

1378 *URI fassaite*: Fassaite enriched in Sc, Ti³⁺, and/or V³⁺ occurs as sub-millimeter grains in ultra-
1379 refractory inclusions in association with davisite, spinel, perovskite, melilite, and a variety of rare
1380 oxides and silicates (Ma and Rossman 2009a, 2009b; Ma et al. 2013b, 2014a, 2015).

1381
1382 *CAI burnettite*: V-dominant, Sc- and Ti-rich calcic clinopyroxene was identified by Ma and
1383 Beckett (2016) from one fluffy type A CAI in the Allende meteorite.

1384
1385 *URI davisite*: Davisite is a Sc-dominant calcic clinopyroxene that occurs in association with
1386 fassaite, perovskite, spinel, and rare Sc-bearing phases in ultra-refractory inclusions (Ma and
1387 Rossman 2009b).

1388
1389 **Feldspar Group [(Na,Ca)(Al,Si)₄O₈]**

1390 **Anorthite (Ca₂Al₂SiO₈)**: End-member (i.e., Na-free) anorthite is common as both a primary
1391 and secondary mineral, notably in type B and type C CAIs (Podosek et al. 1991; Caillet et al. 1993;
1392 Brearley and Jones 1998). Condensing initially at ~1410 K (Davis and Richter 2014), anorthite is
1393 the last of the common CAI primary phases to appear; it crystallizes from a melt and is often found
1394 in close association with melilite or spinel (MacPherson and Davis 1993; Kojima et al. 1995). Note
1395 that plagioclase feldspar, typically with a significant albitic component (NaAlSi₃O₈), is a common
1396 secondary phase in chondrite meteorites, including as a fine-grained alteration phase in CAIs and
1397 their Wark-Lovering rims, as a common minor phase in AOAs, and in chondrules (see Part III).

1398

1399 *CAI anorthite*: The last major primary phase to condense from the solar nebula, anorthite is
1400 commonly found as coarse-grained laths in CAIs (Brearley and Jones 1998).

1401
1402 *AOA anorthite*: Near end-member Ca plagioclase is a common, if volumetrically minor,
1403 constituent of AOAs (Weisberg et al. 2004).

1404
1405 **Dmisteinbergite (CaAl₂Si₂O₈)**: Rare individual crystals of dmisteinbergite, a hexagonal high-
1406 temperature polymorph of anorthite, have been documented from a type B FUN CAI in the Allende
1407 carbonaceous chondrite (Ma et al. 2013a). This phase points to an origin environment with T >
1408 1500 K and P < 10⁻⁶ atm (Abe et al. 1991; Mendybaev et al. 2009), likely close to the protosun,
1409 where it crystallized directly from a silicate vapor or melt phase. Ma et al. (2013a) also note a Ba-
1410 rich grain of dmisteinbergite with up to 27 atom percent Ba substituting for Ca.

1411
1412 *CAI dmisteinbergite*: Dmisteinbergite occurs as 100- to 600-micron diameter crystals in
1413 association with melilite, fassaite, and spinel (Ma et al. 2013a).

1414
1415 **Baghdadite [Ca₃(Zr,Ti)Si₂O₉]**: Ma (2018) reported the first extraterrestrial occurrence of
1416 baghdadite, a CAI silicate mineral from the Allende carbonaceous chondrite that may be one of
1417 the earliest primary silicate condensates. A single 0.8-micron diameter euhedral grain is associated
1418 with primary spinel, perovskite, hibonite, fassaite, refractory metal nuggets, and the rare phases
1419 burnettite and paqueite as inclusions in melilite. The baghdadite structure is monoclinic (*P2₁/a*).

1420

1421 CAI *baghdadite*: Ma (2018) reported a single baghdadite grain with composition
1422 $(\text{Ca}_{2.77}\text{Mg}_{0.08})(\text{Zr}_{0.55}\text{Ti}_{0.35}\text{Nb}_{0.02})(\text{Si}_{1.89}\text{Al}_{0.35})\text{O}_9$.

1423
1424 **Rhönite** $[\text{Ca}_2(\text{Mg},\text{Al},\text{Ti})_6(\text{Si},\text{Al})_6\text{O}_{20}]$, **Addibischoffite** $[\text{Ca}_2(\text{Al},\text{Mg},\text{V},\text{Ti})_6(\text{Al},\text{Si})_6\text{O}_{20}]$, and

1425 **Warkite** $[\text{Ca}_2(\text{Sc},\text{Ti},\text{Al},\text{Mg},\text{Zr})_6\text{Al}_6\text{O}_{20}]$: Rhönite, a rare refractory member of the sapphirine
1426 group (triclinic, $P\{\bar{1}\}$), was first reported by Fuchs (1971), and was subsequently identified in
1427 both type A and type B CAIs in association with melilite, spinel, fassaite, and perovskite (Fuchs
1428 1978; Grossman 1980; Podosek et al. 1991; Jambon and Boudouma 2011). Ma and colleagues
1429 subsequently identified two closely-related Ca-Al oxides/silicates, also with the $P\{\bar{1}\}$
1430 sapphirine structure. Addibischoffite, with the general formula $[\text{Ca}_2(\text{Al},\text{Mg},\text{V},\text{Ti})_6(\text{Al},\text{Si})_6\text{O}_{20}]$,
1431 was discovered as a 9-micron diameter crystal in a CAI from the Acfer 214 carbonaceous
1432 chondrite. Like rhönite, it occurs in association with typical CAI phases – Al-dominant fassaite
1433 (kushiroite), hibonite, spinel, melilite, perovskite, anorthite, and Fe-Ni alloy (Ma et al. 2017b). We
1434 conclude that rhönite and addibischoffite are part of a continuous solid solution and form in similar
1435 environments. Therefore, we combine these minerals into one natural kind: “CAI *rhönite*.”

1436 Warkite was identified by Ma et al. (2015) from ultra-refractory inclusions in the Murchison
1437 and Vigarano carbonaceous chondrites. Warkite, general formula $[\text{Ca}_2(\text{Sc},\text{Ti},\text{Al},\text{Mg},\text{Zr})_6\text{Al}_6\text{O}_{20}]$,
1438 occurs as aggregates of crystals up to 4-microns diameter in association with perovskite, davisite,
1439 spinel (in Murchison), and melilite (in Vigarano). Warkite may well form a continuous solid-
1440 solution with rhönite and addibischoffite; however, because it forms in a different mineralogical
1441 environment and appears to be Si-poor, we recognize “URI warkite” as a distinct natural kind.

1442

1443 *CAI rhönite*: Rhönite has been identified in both A and B type CAIs from several carbonaceous
1444 chondrites (Fuchs 1971; Ma et al. 2017b).

1445
1446 *URI warkite*: Warkite was described by Ma et al. (2015) from ultra-refractory inclusions in the
1447 Murchison and Vigarano meteorites (see also, Krot et al. 2019).

1448
1449 **Paqueite** [$\text{Ca}_3\text{TiSi}_2(\text{Al,Ti,Si})_3\text{O}_{14}$]: Ma and Beckett (2016) identified a new Ca-Ti silicate
1450 from a fluffy type A CAI in the Allende carbonaceous chondrite. It occurs as micron-scale euhedral
1451 crystals in association with melilite, spinel, V-rich perovskite, fassaite, hibonite, and refractory
1452 metal grains.

1453
1454 *CAI paqueite*: Paqueite was discovered by Ma and Beckett (2016) in a V-rich fluffy type A
1455 CAI.

1456
1457 **Thortveitite** ($\text{Sc}_2\text{Si}_2\text{O}_7$): Ma et al. (2011a) and Ma (2012) report the occurrence of thortveitite
1458 in an ultra-refractory inclusion from the Murchison meteorite. It occurs with fassaite, davisite,
1459 panguite, and spinel as subhedral crystals up to 9-microns maximum dimension.

1460
1461 *URI thortveitite*: Thortveitite occurs in an ultra-refractory inclusion in the Murchison chondrite
1462 (Ma et al. 2011a; Krot et al. 2019).

1463
1464 **Silicate Glass** (Ca,Mg,Al,Si,O): A glass of aluminous pyroxene composition is a significant
1465 component of hibonite-silicate spherules, a type of CAI less than 200-microns in diameter (Kimura

1466 et al. 1993; Beckett and Stolper 1994; Russell et al. 1998; MacPherson 2014). Silicate glass occurs
1467 with fassaite and hibonite, often in association with perovskite, melilite, and grossite. These
1468 spherules contain primary phases that crystallized from a melt or, in the case of hibonite, may
1469 represent unmelted relict crystals. Note that we distinguish nebular silicate glass, which formed
1470 from a melt, from stellar amorphous silicate, which condenses from the gas phase (Hazen and
1471 Morrison 2020).

1472

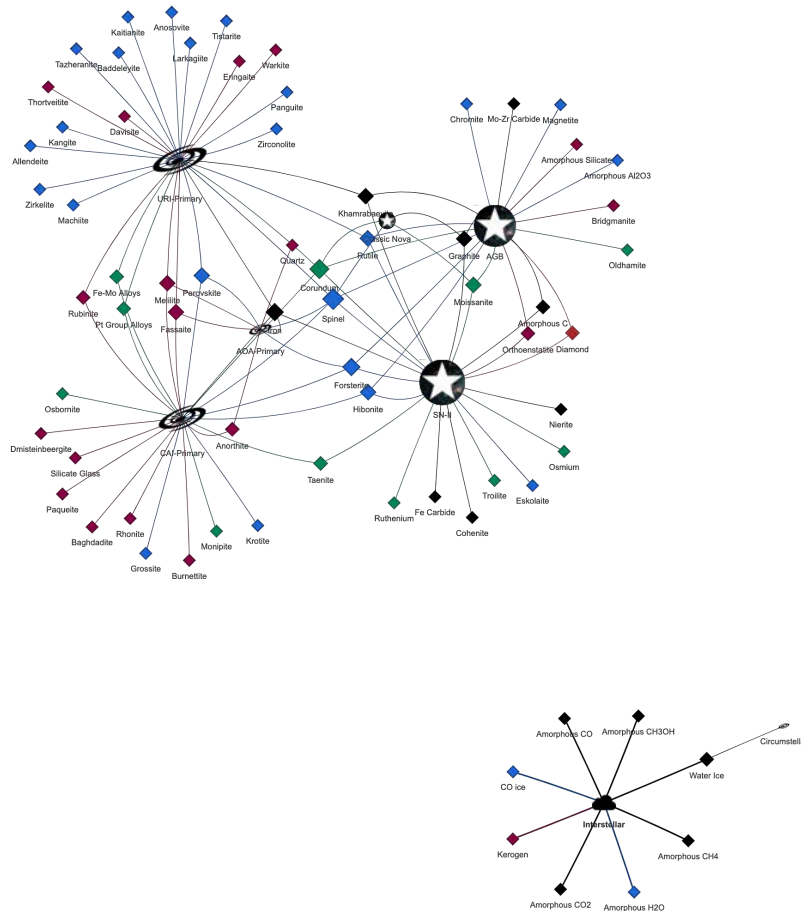
1473 *CAI silicate glass*: Silicate glass is a significant component of hibonite-silicate spherules
1474 (MacPherson 2014).

1475 **NETWORK GRAPH OF STELLAR AND PRIMARY NEBULAR MINERALS**

1476 The evolutionary system of mineralogy is illustrated using bipartite mineral network graphs
1477 (Fruchterman and Reingold 1991; Asratian et al. 1998; Morrison et al. 2017), which display
1478 relationships among mineral phases and their attributes, in this instance their paragenetic modes
1479 (Hazen et al. 2019; Hazen and Morrison 2020; Morrison et al. 2020). **Figure 4** displays a bipartite
1480 force-directed network graph of primary stellar, interstellar, and nebular minerals formed prior to
1481 ~4,565 Ma, in which 69 different phases, including 10 amorphous condensed phases, are
1482 represented by diamond-shaped nodes. Each of these mineral nodes is linked to one or more node
1483 representing a paragenetic mode of formation. Three different star-shaped nodes (AGB, SN-II, and
1484 CNova) represent stellar environments that impart distinctive isotopic signatures to minerals. A
1485 cloud-shaped node indicates interstellar dense molecular clouds (DMC), whereas four flattened
1486 disk icons represent different primary mineral-forming nebular environments (Circumstellar, CAI,
1487 AOA, and URI).

1488 Node size, shape, and color convey information. Mineral compositions are indicated by the
1489 color of diamond-shaped mineral nodes: black (C-bearing), green (lacking C or O), blue (contains
1490 O, but not C or Si), and red (contains Si + O). The sizes of mineral nodes correspond to the numbers
1491 of paragenetic modes to which they are linked. Similarly, the sizes of the star-, cloud-, and disk-
1492 shaped symbols indicate the numbers of different minerals to which they are associated.

1493 At this early stage of mineral evolution, 8 different low-temperature interstellar and nebular
1494 condensed molecular phases ($T < 100$ K) form a separate network from 56 high-temperature stellar
1495 and nebular condensates ($T > 1100$ K). In future parts of this series, phases formed at intermediate
1496 temperatures in planetary surface environments will provide links between these two mineral-
1497 forming environments.



1498

1499 **Figure 4.** Bipartite force-directed network graph (Morrison et al. 2017) of primary stellar, interstellar, and
 1500 nebular minerals linked to their modes of paragenesis. Diamond-shaped nodes represent condensed
 1501 crystalline and amorphous phases [black (C-bearing), green (not C or O), blue (contains O, but not C or Si),
 1502 and red (contains Si + O)]. Star-shaped nodes represent three types of host stars— asymptotic giant branch
 1503 stars (AGB), Type II supernovae (SN-II), and classical novae (CNova); the cloud-shaped node represents
 1504 dense molecular clouds (DMC); and four disk-shaped nodes indicate circumstellar environments, CAIs,
 1505 AOs, and URIs. The sizes of nodes correspond to the numbers of links to other nodes. Note that 8 low-
 1506 temperature phases of the interstellar medium are not linked to 61 high-temperature primary phases of
 1507 stellar and nebular environments.

1508

1509 This bipartite network of mineral evolution is a visual representation of all confirmed stellar,
 1510 interstellar, and primary nebular minerals described in Parts I and II of the evolutionary system of
 1511 mineralogy. As new parts are introduced, and new nodes for minerals and paragenetic processes

1512 are added, this information-rich graphical approach will provide a dynamic, expanding, interactive
1513 view of the entire sweep of mineral evolution.

1514

1538 planetesimal environments – minerals as preserved in altered chondrite and achondrite meteorites
1539 – will provide the focus of Parts IV and V.

1540

1541 **ACKNOWLEDGMENTS**

1542 We thank Anirudh Prabhu, who developed the bipartite network representation of stellar,
1543 interstellar, and nebular mineralogy. We are grateful to Denton Ebel for providing images of
1544 refractory inclusions. Denton Ebel, Chi Ma, Alan Rubin, and B. J. Tkalcec contributed invaluable
1545 detailed reviews of the manuscript. The sections on nebular condensate mineralogy, in particular,
1546 benefitted from the advice of Rubin and Ma, who provided access to highly relevant work in press,
1547 including a draft of their forthcoming book, *Meteorite Mineralogy*. We are grateful to Conel O.
1548 M'D. Alexander, Asmaa Boujibar, Carol Cleland, Robert T. Downs, Olivier Gagné, Sergey
1549 Krivovichev, Glenn MacPherson, Michael Walter, and Shuang Zhang for thoughtful discussions
1550 and comments.

1551

1552 **FUNDING**

1553 This publication is a contribution to the Deep Carbon Observatory. Studies of mineral
1554 evolution and mineral ecology have been supported by the Deep Carbon Observatory, the Alfred
1555 P. Sloan Foundation, the W. M. Keck Foundation, the John Templeton Foundation, the NASA
1556 Astrobiology Institute ENIGMA team, a private foundation, and the Carnegie Institution for
1557 Science. Any opinions, findings, or recommendations expressed herein are those of the authors
1558 and do not necessarily reflect the views of the National Aeronautics and Space Administration.

1559

1560 **REFERENCES**

- 1561 Abe, T., Tsukamoto, K., and Sunagawa, I. (1991) Nucleation, growth and stability of $\text{CaAl}_2\text{Si}_2\text{O}_8$
1562 polymorphs. *Physics and Chemistry of Minerals*, 17, 257-281.
- 1563 Affiatalab, F., and Wasson, J.T. (1980) Composition of the metal phases in ordinary chondrites:
1564 Implications regarding classification and metamorphism. *Geochimica et Cosmochimica Acta*,
1565 44, 431-446.
- 1566 Aléon, J., Krot, A.N., and McKeegan, K.D. (2002) Calcium–aluminum-rich inclusions and
1567 amoeboid olivine aggregates from the CR carbonaceous chondrites. *Meteoritics & Planetary*
1568 *Science*, 37, 1729–1755.
- 1569 Alexander, C.M.O’D., Fogel, M., Yabuta, H., and Cody, G.D. (2007) The origin and evolution of
1570 chondrites recorded in the elemental and isotopic compositions of their macromolecular organic
1571 matter. *Geochimica et Cosmochimica Acta*, 71, 4380–4403.
- 1572 Alexander, C.M.O’D., McKeegan, K.D., and Altwegg, K. (2018) Water reservoirs in small
1573 planetary bodies: meteorites, asteroids, and comets. *Space Science Reviews*, 214, 36-83. Doi:
1574 10.1007/s11214-018-0474-9
- 1575 Allamandola, L.J., Bernstein, M.P., Sandford, S.A., and Walker, R.L. (1999) Evolution of
1576 interstellar ices. *Space Science Reviews*, 90, 219-232.
- 1577 Allen, J.M., Grossman, L., Lee, T., and Wasserburg, G.J. (1980) Mineralogy and petrography of
1578 HAL, an isotopically unusual Allende inclusion. *Geochimica et Cosmochimica Acta*, 44, 685-
1579 699.
- 1580 Amelin, Y., Krot, A.N., Hutcheon, I.D., and Ulyanov, A.A. (2002) Lead isotopic ages of
1581 chondrules and calcium–aluminum-rich inclusions. *Science*, 297, 1678–1683.

- 1582 Amelin, Y., Kaltenbach, A., Iizuka, T., Stirling, C.H., Ireland, T.R., Petaev, M., and Jacobsen, S.B.
1583 (2010) U–Pb chronology of the Solar System’s oldest solids with variable $^{238}\text{U}/^{235}\text{U}$. Earth and
1584 Planetary Science Letters, 300, 343–350.
- 1585 Anders, E., and Grevesse, N. (1989) Abundances of the elements: Meteoritic and solar.
1586 Geochimica et Cosmochimica Acta, 53, 197-214.
- 1587 Armstrong, J.T., Meeker, G.P., Huneke, J.C., and Wasserburg, G.J. (1982) The Blue Angel: I.
1588 mineralogy and petrogenesis of a hibonite inclusion from the Murchison meteorite. Geochimica
1589 et Cosmochimica Acta, 46, 575-595.
- 1590 Armstrong, J.T., El Goresy, A., and Wasserburg, G.J. (1985) Willy: A prize noble Ur-Fremdling
1591 – its history and implications for the formation of Fremdlinge and CAI. Geochimica et
1592 Cosmochimica Acta, 49, 1001-1022.
- 1593 Armstrong, J.T., Hutcheon, I.D., and Wasserburg, G.J. (1987) Zelda and company: Petrogenesis
1594 of sulfide-rich fremdlinge and constraints on solar nebula processes. Geochimica et
1595 Cosmochimica Acta, 51, 3155-3173.
- 1596 Asratian, A.S., Denley, T.M.J., and Häggkvist, R. (1998) Bipartite Graphs and their Applications.
1597 Cambridge University Press.
- 1598 Bar-Matthews, M., Hutcheon, I.D., MacPherson, G.J., and Grossman, L. (1982) A corundum-rich
1599 inclusion in the Murchison carbonaceous chondrite. Geochimica et Cosmochimica Acta, 46,
1600 31–41.
- 1601 Bartels-Rausch, T., Bergeron, V., Cartwright, J.H.E., Escibano, R., Finney, J.L., Grothe, H,
1602 Gutierrez, P.J., Haapala, J., Kuhs, W.F., Pettersson, J.B.C., Price, D.C, Sainz-Daz, C.I., Stokes,
1603 D.J., Strazzulla, G., Thomson, E.S., Trinks, H., and Uras-Aytemiz, N. (2012) Ice structures,
1604 patterns, and processes: A view across the icefields. Reviews of Modern Physics, 84, 885-944.

- 1605 Beckett, J.R. (1986) The origin of calcium-, aluminum-rich inclusions from carbonaceous
1606 chondrites: An experimental study. Ph.D. Dissertation, University of Chicago, Chicago,
1607 Illinois.
- 1608 Beckett, J.R. and Stolper, E. (1994) The stability of hibonite, melilite and other aluminous phases
1609 in silicate melts: Implications for the origin of hibonite-bearing inclusions from carbonaceous
1610 chondrites. *Meteoritics*, 29, 41–65.
- 1611 Beckett, J.R., Live, D., Tsay, F.-D., Grossman, L., and Stolper, E. (1988) Ti^{3+} in meteoritic and
1612 synthetic hibonite. *Geochimica et Cosmochimica Acta*, 52, 1479-1495.
- 1613 Beckett, J.R., Simon, S.B., and Stolper, E. (2000) The partitioning of Na between melilite and
1614 liquid: Part II. Applications to Type B inclusions from carbonaceous chondrites. *Geochimica*
1615 *et Cosmochimica Acta*, 64, 2519–2534.
- 1616 Berg, T., Maul, J., Schönhense, G., Marosits, E., Hoppe, P., Ott, U., and Palme, H. (2009) Direct
1617 evidence for condensation in the early solar system and implications for nebular cooling rates.
1618 *The Astrophysical Journal*, 702, L172-L176.
- 1619 Bertout, C. (1989) T Tauri stars—wild as dust. *Annual Reviews of Astronomy and*
1620 *Astrophysics*, 27, 351-395.
- 1621 Bevan, A.W.R., and Axon, H.J. (1980) Metallography and thermal history of the Tieschitz
1622 unequilibrated meteorite – metallic chondrules and the origin of polycrystalline taenite. *Earth*
1623 *and Planetary Science Letters*, 47, 353-360.
- 1624 Birjukov, V., and Ulyanov, V. (1996) Petrology and classification of new Antarctic carbonaceous
1625 chondrites PCA91082, TIL91722, and WIS91600. *Proceedings of the NIPR Symposium on*
1626 *Antarctic Meteorites*, 9, 8-19.

- 1627 Bischoff, A., and Palme, H. (1987) Composition and mineralogy of refractory-metal-rich
1628 assemblages from a Ca,Al-rich inclusion in the Allende meteorite. *Geochimica et*
1629 *Cosmochimica Acta*, 51, 2733-2748.
- 1630 Bisschop, S.E., Fuchs, G.W., Boogert, A.C.A., van Dishoeck, E.F., and Linnartz, H. (2007)
1631 Infrared spectroscopy of HCOOH in interstellar ice analogues. *Astronomy & Astrophysics*,
1632 470, 749-759.
- 1633 Blander, L., and Fuchs, L.H. (1975) Calcium-aluminum-rich inclusions in the Allende meteorite:
1634 Evidence for a liquid origin. *Geochimica et Cosmochimica Acta*, 39, 1605-1619.
- 1635 Blander, L., Fuchs, L.H., Horowitz, C., and Land, R. (1980) Primordial refractory metal particles
1636 in the Allende meteorite. *Geochimica et Cosmochimica Acta*, 44, 217-223.
- 1637 Blum, J.D., Wasserburg, G.J., Hutcheon, I.D., Beckett, J.R., and Stolper, E.M. (1988) “Domestic”
1638 origin of opaque assemblages in refractory inclusions in meteorites. *Nature*, 331, 405-409.
- 1639 Blum, J.D., Wasserburg, G.J., Hutcheon, I.D., Beckett, J.R., and Stolper, E.M. (1989) Origin of
1640 opaque assemblages in CV3 meteorites: Implications for nebular and planetary processes.
1641 *Geochimica et Cosmochimica Acta*, 53, 543-556.
- 1642 Boogert, A.C.A., and Ehrenfreund, P. (2004) Interstellar ices. In: A.N. Witt, G.C. Clayton, and
1643 B.T. Draine, Eds., *Astrophysics of Dust*. ASP Conference Series, 309, 547-573.
- 1644 Boogert, A.C.C., Schutte, W.A., Tielens, A.G.G.M., Whittet, D.C.B., Helmich, F.P., Ehrenfreund,
1645 P., Wesseliuss, P.R., de Graauw, T., and Prusti, T. (1996) Solid methane toward deeply
1646 embedded protostars. *Astronomy & Astrophysics*, 315, L377-L380.
- 1647 Boogert, A.C.C., Schutte, W.A., Helmich, F.P., Tielens, A.G.G.M., and Wooden, D.H. (1997)
1648 Infrared observations and laboratory simulations of interstellar CH₄ and SO₂. *Astronomy &*
1649 *Astrophysics*, 317, 929-941.

- 1650 Boogert, A.C.C., Helmich, F.P., van Dishoeck, E.F., Schutte, W.A., Tielens, A.G.G.M., and
1651 Whittet, D.C.B. (1998) The gas/solid methane abundance ratio toward deeply embedded
1652 protostars. *Astronomy & Astrophysics*, 336, 352-358.
- 1653 Boss, A.J., and Durisen, R.H. (2005) Sources of shock waves in the protoplanetary disk. ASP
1654 Conference Series, 341, 821-838.
- 1655 Bowles, J.F.W. (1988) Definition and range of composition of naturally occurring minerals with
1656 the pseudobrookite structure. *American Mineralogist*, 73, 1377-1383.
- 1657 Brearley, A.J., and Jones, R.H. (1998) Chondritic meteorites. *Reviews in Mineralogy*, 36, 3.01-
1658 3.398.
- 1659 Burke, E.A.J. (2006) The end of CNMMN and CCM—Long live the CNMNC! *Elements*, 2, 388.
- 1660 Caillet, C., Zinner, E.K., and MacPherson, G.J. (1993) Petrologic and Al–Mg isotopic clues to the
1661 accretion of two refractory inclusions onto the Leoville parent body: One was hot, the other
1662 wasn't. *Geochimica et Cosmochimica Acta*, 57, 4725–4743.
- 1663 Campbell, A.J., Zanda, B., Perron, C., Meiborn, A., and Petaev, M.I. (2005) Origin and thermal
1664 history of Fe-Ni metal in primitive chondrites. In A.N. Krot, E.R.D. Scott, and B. Reipurth,
1665 Eds., *Chondrites and the Protoplanetary Disk*. Astronomical Society of the Pacific Conference
1666 Series, 341, 407-431.
- 1667 Casanova, I., and Simon, S.B. (1994) Opaque minerals in CAIs, and classification of the Axtell
1668 (CV3) chondrite. *Meteoritics*, 29, 454-455.
- 1669 Chiar, J.E., Adamson, A.J., Kerr, T.H., and Whittet, D.C.B. (1995) High-resolution studies of solid
1670 CO in the Taurus Dark Cloud: Characterizing the ices in quiescent clouds. *The Astrophysical*
1671 *Journal*, 455, 234-243.

- 1672 Chiar, J.E., Adamson, A.J., and Whittet, D.C.B. (1996) Three micron hydrocarbon and methanol
1673 absorption in Taurus. *The Astrophysical Journal*, 472, 665-472.
- 1674 Chiar, J.E., Adamson, A.J., and Whittet, D.C.B. (1998) Detection of abundant CO₂ ice in the
1675 quiescent dark cloud medium toward Elias 16. *The Astrophysical Journal*, 498, L159-L163.
- 1676 Chiar, J.E., Tielens, A.G.G.M., Whittet, D.C.B., Schutte, W.A., Boogert, A.C.A., Lutz, D., van
1677 Dishoeck, E.F., and Bernstein, M.P. (2000) The composition and distribution of dust along the
1678 line of sight toward the galactic center. *The Astrophysical Journal*, 537, 749-762.
- 1679 Chizmadia, L.J., Rubin, A.E., and Wasson, J.T. (2002) Mineralogy and petrology of amoeboid
1680 olivine inclusions in CO₃ chondrites: relationship to parent-body aqueous alteration.
1681 *Meteoritics & Planetary Sciences*, 37, 1781–1796.
- 1682 Clark, F.O., Buhl, D., and Snyder L.E. (1974) Observational evidence for the excitation of HCN
1683 and H₂O in protostellar molecular clouds. *The Astrophysical Journal*, 190, 545-556.
- 1684 Cleland, C.E. (2011) Prediction and explanation in historical natural science. *British Journal of the*
1685 *Philosophy of Science*, 62, 551-582.
- 1686 Cleland, C.E. (2013) Common cause explanation and the search for the smoking gun. *The*
1687 *Geological Society of America Special Paper*, 502, 1-9. doi: 10.1130/2013.2502(01)
- 1688 Collings, M.P., Dever, J.W., Fraser, H.J., McCoustra, M.R.S., and Williams, D.A. (2003) Carbon
1689 monoxide entrapment in interstellar ice analogs. *The Astrophysical Journal*, 583, 1058-1062.
- 1690 Connelly, J.N., Amelin, Y., Krot, A.N., and Bizzarro, M. (2008) Chronology of the solar system's
1691 oldest solids. *The Astrophysical Journal*, 67, L121–L124.
- 1692 Connelly, J.N., Bizzarro, M., Krot, A.N., Nordlund, Å., Wielandt, D., and Ivanova, M.A. (2012)
1693 The absolute chronology and thermal processing of solids in the solar protoplanetary disk.
1694 *Science*, 338, 651–655.

- 1695 Connolly, H.C. Jr., and Jones, R.H. (2016) Chondrules: The canonical and noncanonical views.
1696 *Journal of Geophysical Research: Planets*, 121, 1885-1899.
- 1697 Cronin, J.R., and Pizzarello, S. (1990) Aliphatic hydrocarbons of the Murchison meteorite.
1698 *Geochimica et Cosmochimica Acta*, 54, 2859-2868.
- 1699 Dana, J.D. (1850) A System of Mineralogy, Comprising the Most Recent Discoveries, Including
1700 Full Descriptions of Species and their Localities, Chemical Analyses and Formulas, Tables for
1701 the Determination of Minerals, and a Treatise on Mathematical Crystallography and the
1702 Drafting of Figures of Crystals. Third Edition, Rewritten, Rearranged, and Enlarged. George P.
1703 Putnam.
- 1704 Daranlot, J., Hincelin, U., Bergeat, A., Costes, M., Loison, J.-C., Wakelam, V., and Hickson, K.M.
1705 (2012) Elemental nitrogen partitioning in dense interstellar clouds. *Proceedings of the National*
1706 *Academy of Sciences USA*, 109, 10233-10238. doi: 10.1073/pnas.1200017109.
- 1707 Dartois, E., d'Hendecourt, L., Thi, W., Pontoppidan, K.M., and van Dishoeck, E.F. (2002)
1708 Combined VLT ISAAC/ISO SWS spectroscopy of two protostellar sources. *Astronomy &*
1709 *Astrophysics*, 394, 1057-1068.
- 1710 Davis, A.M., and Richter, F.M. (2014) Condensation and evaporation of solar system materials.
1711 In *Treatise on Geochemistry, Vol. 1: Meteorites, Comets, and Planets, Second Edition*. A.M.
1712 Davis, H.D.Holland, and K.K.Turekian, Eds., pp.335-360. Elsevier-Pergamon.
- 1713 Davis, A.M., Hashimoto, A., Clayton, R.N., and Mayeda, T.K. (1990) Isotope mass fractionation
1714 during evaporation of forsterite (Mg₂SiO₄). *Nature*, 347, 655-658.
- 1715 Davis, A.M., MacPherson, G.J., Clayton, R.N., Mayeda, T.K., Sylvester, P.J., Grossman, L.,
1716 Hinton, R.W., and Laughlin, J.R. (1991) Melt solidification and late-stage evaporation in the

- 1717 evolution of a FUN inclusion from the Vigarano C3V condrite. *Geochimica et Cosmochimica*
1718 *Acta*, 55, 621-637.
- 1719 Deer, W.A., Howie, R.A., and Zussman, J. (1963) *Rock-Forming Minerals, Vol. 2, Chain Silicates*,
1720 pp. 161-166. John Wiley and Sons.
- 1721 Desch S.J., and Connolly H.C., Jr. (2002) A model for the thermal processing of particles in solar
1722 nebula shocks: Application to the cooling rates of chondrules. *Meteoritics & Planetary Science*,
1723 37, 183–207.
- 1724 Desch, S.J., and Cuzzi, J.N. (2000) The generation of lightning in the solar nebula. *Icarus*, 143,
1725 87-105.
- 1726 Desch, S.J., Morris, M.A., Connolly, H.C. Jr., and Boss, A.P. (2012) The importance of
1727 experiments: Constraints on chondrule formation models. *Meteoritics & Planetary Science*, 47,
1728 1139-1156.
- 1729 d’Hendecourt, L.B., and de Muizon, M.J. (1989) The discovery of interstellar carbon dioxide.
1730 *Astronomy & Astrophysics*, 223, L5-L8.
- 1731 d’Hendecourt, L., Jourdain de Muizon, M., Dartois, E., Breittellner, M., Ehrenfreund, P., Benit,
1732 J., Boulanger, F., Puget, J.L., and Habing, H.J. (1996) ISO-SWS observations of solid state
1733 features towards RAFGL 7009S. *Astronomy & Astrophysics*, 315, L365-L368.
- 1734 Di Francesco, J., Evans, N.J. II, Caselli, P., Myers, P.C., Shirley, Y., Aikawa, Y., and Tafalla, M.
1735 (2006) An observational perspective of low-mass dense cores I: Internal physics and chemical
1736 properties. *Protostars and Planets V*, pp. 18-32. University of Arizona Press, Tucson.
- 1737 Doukhan, N., Doukhan, J.C., and Poirier, J.P. (1991) Transmission electron microscopy of a
1738 refractory inclusion from the Allende meteorite: Anatomy of a pyroxene. *Meteoritics*, 26, 105-
1739 109.

- 1740 Ebel, D.S. (2006) Condensation of rocky materials in astrophysical environments. In D.S. Lauretta
1741 and H.Y. McSween Jr., Eds., *Meteorites and the Early Solar System II*, pp. 253-277. University
1742 of Arizona Press, Tucson.
- 1743 Ebel, D.S., and Alexander, C.M.O'D. (2011) Equilibrium condensation from chondritic porous
1744 IDP enriched vapor: Implications for Mercury and enstatite chondrite origins. *Planetary and*
1745 *Space Science*, 59, 1888-1894.
- 1746 Ebel, D.S., and Grossman, L. (2000) Condensation in dust-rich systems. *Geochimica et*
1747 *Cosmochimica Acta*, 65, 469-477.
- 1748 Ehrenfreund, P., and Cami, J. (2010) Cosmic carbon chemistry: From the interstellar medium to
1749 early Earth. In D. Deamer and J.W. Szostak, Eds., *Perspectives on the Origins of Life*, pp. 1-
1750 14. Cold Spring Harbor Press.
- 1751 Ehrenfreund, P., and Charnley, S.B. (2000) Organic molecules in the interstellar medium, comets,
1752 and meteorites: A voyage from dark clouds to the early Earth. *Annual Reviews in Astronomy*
1753 *and Astrophysics*, 38, 427-483.
- 1754 Ehrenfreund, P., and Fraser, H. (2003) Ice chemistry in space. In V. Pirronello, K. Krelowski, and
1755 G. Manico, Eds., *Solid State Astrochemistry*, pp. 317-356. Kluwer Academic Publishers,
1756 Dordrecht.
- 1757 Ehrenfreund, P., Robert, F., d'Hendecourt, L., and Behar, F. (1991) Comparison of interstellar and
1758 meteoritic organic matter at 3.4 microns. *Astronomy & Astrophysics*, 252, 712-717.
- 1759 Ehrenfreund, P., Boogert, A.C.A., Gerakines, P.A., Tielens, A.G.G.M., and van Dishoek, E.F.
1760 (1997) Infrared spectroscopy of interstellar apolar ice analogs. *Astronomy & Astrophysics*, 328,
1761 649-669.

- 1762 El Goresy, A., Nagel, K., and Ramdohr, P. (1978) Fremdlinges and their noble relatives.
1763 Proceedings of the Lunar and Planetary Science Conference, 9, 1279-1303.
- 1764 El Goresy, A., Nagel, K., and Ramdohr, P. (1979) Spinel framboids and Fremdlinge in Allende
1765 inclusions: Possible sequential markers in the early history of the solar system. Proceedings of
1766 the Lunar and Planetary Science Conference, 10, 833-850.
- 1767 El Goresy, A., Palme, H., Yabuki, H., Nagel, K., Herrwerth, I., and Ramdohr, P. (1984) A calcium-
1768 aluminum inclusion from Essebi (CM2) chondrite: Evidence for captured spinel-hibonite
1769 spherules and for an ultra-refractory rimming sequence. *Geochimica et Cosmochimica Acta*,
1770 48, 2283-2298.
- 1771 El Goresy, A., Zinner, E., Matsunami, S., Palme, H., Spettel, B., Lin, Y., and Nazarov, M. (2002)
1772 Efremovka 101.1: A CAI with ultra-refractory REE patterns and enormous enrichments of Sc,
1773 Zr, and Y in fassaite and perovskite. *Geochimica et Cosmochimica Acta*, 66, 1459–1491.
- 1774 El Goresy, A., Boyer, M., and Miyahara, M. (2011) Almahata Sita MS-17 EL-3 chondrite
1775 fragment: contrasting oldhamite assemblages in chondrules and matrix and significant
1776 oldhamite REE-patterns. *Meteoritics & Planetary Sciences*, 46, Abstract #5079.
- 1777 Elsila, J., Allamandola, L.J., and Sandford, S.A. (1997) The 2140 cm^{-1} (4.673 microns) solid CO
1778 band: The case for interstellar O₂ and N₂ and the photochemistry of nonpolar interstellar ice
1779 analogs. *The Astrophysical Journal*, 479, 818-838.
- 1780 Endress, M., Keil, K., Bischoff, A., Spettel, B., Clayton, R.N., and Mayeda, T.K. (1994) On the
1781 origin of dark clasts in Acfer 059/El Djouf 001 CR2 chondrite. *Meteoritics*, 29, 26-40.
- 1782 Fagan, T.J., Krot, A.N., and Keil, K. (2000) Calcium–aluminum-rich inclusions in enstatite
1783 chondrites: I. Mineralogy and textures. *Meteoritics & Planetary Science*, 35, 771–781.

- 1784 Fagan, T.J., McKeegan, K.D., Krot, A.N., and Keil, K. (2001) Calcium–aluminum-rich inclusions
1785 in enstatite chondrites: II. Oxygen isotopes. *Meteoritics & Planetary Science*, 36, 223–230.
- 1786 Fahey, A.J., Zinner, E., Kurat, K., and Kracher, A. (1994) Hibonite-hercynite inclusions HH-1
1787 from the Lance (CO3) meteorite: The history of an ultra-refractory inclusion CAI. *Geochimica
1788 et Cosmochimica Acta*, 58, 4779-4793.
- 1789 Ferriere, D. (2001) The interstellar environment of our galaxy. *Reviews of Modern Physics*, 73,
1790 1031-1066.
- 1791 Freeman, A., and Millar, T.J. (1983) Formation of complex molecules in TMC-1. *Nature*, 301,
1792 402-404.
- 1793 Fruchterman, T.M.J., and Reingold, E.M. (1991) Graph drawing by force-directed placement.
1794 *Software: Practice and Experience*, 21, 1129-1164.
- 1795 Fuchs, L.H. (1971) Occurrence of wollastonite, rhönite and andradite in the Allende meteorite.
1796 *American Mineralogist*, 56, 2053-2068.
- 1797 Fuchs, F.H. (1974) Grossular in the Allende (Type III carbonaceous) meteorite. *Meteoritics*, 13,
1798 73-88.
- 1799 Fuchs, L.H. (1978) The mineralogy of a rhönite-bearing calcium aluminum rich in the Allende
1800 meteorite. *Meteoritics*, 13, 73-88.
- 1801 Fuentes-Landete, V., Mitterdorfer, C., Handle, P.H., Ruiz, G.N., Bernard, J., Bogdan, A., Seidl,
1802 M., Amann-Winkel, K., Stern, J., Fuhrmann, S., and Loerting, T. (2015) Crystalline and
1803 amorphous ices. *Proceedings of the International School of Physics*, 187. Doi: 10.3254/978-1-
1804 61499-507-4-173
- 1805 Gaffney, E.S., and Matson, D.L. (1980) Water ice polymorphs and their significance on planetary
1806 surfaces. *Icarus*, 44, 511-519.

- 1807 Geiger, T., and Bischoff, A. (1995) Formation of opaque minerals in CK chondrites. *Planetary &*
1808 *Space Science*, 43, 485-498.
- 1809 Gerakines, P.A., Whittet, D.C.B., Ehrenfreund, P., Boogert, A.C.A., Tielens, A.G.G.M., Schutte,
1810 W.A., Chiar, J.E., van Dishoeck, E.F., Prusti, T., Helmich, F.P., and de Graauw, T. (1999) ISO-
1811 SWS observations of solid carbon dioxide in molecular clouds. *The Astrophysical Journal*, 522,
1812 357-377.
- 1813 Ghose, J., Methikkalam, R.R.J., Bhui, R.G., Ragupathy, G., Choudhary, N., Kumar, R., and
1814 Pradeep, T. (2019) Clathrate hydrates in interstellar environment. *Proceedings of the National*
1815 *Academy of Sciences USA*, 116, 1526-1531.
- 1816 Gibb, E.L., Whittet, D.C.B., Boogert, A.C.A., and Tielens, A.G.G.M. (2004) Interstellar ice: The
1817 Infrared Space Observatory legacy. *The Astrophysical Journal Supplement Series*, 151, 35-73.
- 1818 Gillet, F.C., and Forrest, W.J. (1973) Spectra of the Becklin-Neugebauer point source and the
1819 Kleinmann-Low nebula from 2.8 to 13.5 microns. *The Astrophysical Journal*, 179, 483-491.
- 1820 Gimour, J.D., and Saxton, J.M. (2001) A time-scale of formation of the first solids. *Philosophical*
1821 *Transactions of the Royal Society London*, A359, 2037-2048.
- 1822 Greenberg, J.M. (1991) Interstellar dust-gas relationships. In M.M. Shapiro, R. Silberberg, and
1823 J.P. Wefel, Eds., *Cosmic Rays, Supernovae, and the Interstellar Medium*. NATO ASI Series:
1824 *Mathematical and Physical Sciences*, 120, 57-68.
- 1825 Greenberg, J.M., Li, A., Mendoza-Gomez, C.X., Schutte, W.A., Gerakines, P.A., and de Groot,
1826 M. (1995) Approaching the interstellar grain organic refractory component. *The Astrophysical*
1827 *Journal Letters*, 455, L177-L180.
- 1828 Greenwood, R.C., Hutchison, R., Huss, G.R., and Hutcheon, I.D. (1992) CAIs in CO₃ meteorites:
1829 Parent body or nebular alteration? *Meteoritics*, 27, 229.

- 1830 Greenwood, R.C., Lee, M.R., Hutchison, R., and Barber, D.J. (1994) Formation and alteration of
1831 CAIs in Cold Bokkeveld (CM2). *Geochimica et Cosmochimica Acta*, 58, 1913-1935.
- 1832 Greshake, A., Bischoff, A., Putnis, A., and Palme, H. (1996) Corundum, rutile, periclase, and CaO
1833 in Ca,Al-rich inclusions from carbonaceous chondrites. *Science*, 272, 1316-1318.
- 1834 Grim, R.J.A., Bass, F., Geballe, T.R., Greenberg, J.M., and Schutte, W.A. (1991) Detection of
1835 solid methanol toward W33A. *Astronomy & Astrophysics*, 243, 473-477.
- 1836 Grishko, V.I., and Duley, W.W. (2000) Detection of new infrared spectral features in hydrogenated
1837 amorphous carbon. *The Astrophysical Journal*, 543, L85-L88.
- 1838 Grokhovsky, V.I. (2006) Osbornite in CB/CH-like carbonaceous chondrite Isheyev. *Meteoritics*
1839 *& Planetary Science*, 41, A68.
- 1840 Grossman, J.N., Rubin, A.E., and MacPherson, G.J. (1988) ALH 85085: A unique volatile-poor
1841 carbonaceous chondrite with implications for nebular fractionation practices. *Earth and*
1842 *Planetary Science Letters*, 91, 33-54.
- 1843 Grossman, L. (1972) Condensation in the primitive solar nebula. *Geochimica et Cosmochimica*
1844 *Acta*, 36, 597-619.
- 1845 Grossman, L. (1975) Petrography and mineral chemistry of Ca-rich inclusions in the Allende
1846 meteorite. *Geochimica et Cosmochimica Acta*, 39, 433-453.
- 1847 Grossman, L. (1980) Refractory inclusions in the Allende meteorite. *Annual Reviews of Earth and*
1848 *Planetary Sciences*, 8, 559-608.
- 1849 Grossman, L., and Steele, I.M. (1976) Amoeboid olivine aggregates in the Allende meteorite.
1850 *Geochimica et Cosmochimica Acta*, 40, 149-155.
- 1851 Grossman, L., Ganapathy, R., Methot, R.L., and Davis, A.M. (1979) Trace elements in the Allende
1852 meteorite amoeboid olivine aggregates. *Geochimica et Cosmochimica Acta*, 43, 817-829.

- 1853 Grundy, W.M., and Schmitt, B. (1998) The temperature-dependent near-infrared absorption
1854 spectrum of hexagonal H₂O ice. *Journal of Geophysical Research*, 103, 25809.
- 1855 Guan, Y., Huss, G.R., MacPherson, G.J., and Wasserburg, G.J. (2000) Calcium–aluminum-rich
1856 inclusions from enstatite chondrites: Indigenous or foreign? *Science*, 289, 1330–1333.
- 1857 Güsten, R., Wiesemeyer, H., Neufeld, D., Menten, K.M., Graf, U.U., Jacobs, K., Klein, B., Ricken,
1858 O., Risacher, C., and Stutzki, J. (2019) Astrophysical detection of the helium hydride ion HeH⁺.
1859 *Nature*, 568, 357-360.
- 1860 Hagen, W., Tielens, A.G.G.M., and Greenberg, J.M. (1981) The infrared spectra of amorphous
1861 solid water and ice between 10 and 140 K. *Chemical Physics*, 56, 367-379.
- 1862 Han, J., Brearley, A.J., and Keller, L.P. (2015) Microstructural evidence for a disequilibrium
1863 condensation origin for hibonite-spinel inclusions in the ALHA77307 CO3.0 chondrite.
1864 *Meteoritics & Planetary Science*, 50, 2121-2136.
- 1865 Harries, D., Berg, T., Langenhorst, F, and Palme, H. (2012) Structural clues to the origin of
1866 refractory metal alloys as condensates of the solar nebula. *Meteoritics & Planetary Sciences*,
1867 47, 2148-2159.
- 1868 Hashimoto, A. (1983) Evaporation metamorphism in the early solar nebula—evaporation
1869 experiments on the melt FeO-MgO-SiO₂-CaO-Al₂O₃ and chemical fractionations of primitive
1870 materials. *Geochemical Journal*, 17, 111-145.
- 1871 Hashimoto, A. (1992) The effect of H₂O gas on volatilities of planet-forming major elements: I.
1872 Experimental determination of thermodynamic properties of C-, Al-, and Si-hydroxide gas
1873 molecules, and its application to the solar nebula. *Geochimica et Cosmochimica Acta*, 56, 511-
1874 532.

- 1875 Hashimoto, A., and Grossman, L. (1987) Alteration of Al-rich inclusions inside amoeboid olivine
1876 aggregates in the Allende meteorite. *Geochimica et Cosmochimica Acta*, 51, 1685-1704.
- 1877 Hazen, R.M. (1989) A farewell to obsolete pyroxenes. *The Lattice*, February 1989, 6-7.
- 1878 Hazen, R.M. (2018) Titan mineralogy: A window on organic mineral evolution. *American*
1879 *Mineralogist*, 103, 341-342.
- 1880 Hazen, R.M. (2019) An evolutionary system of mineralogy: Proposal for a classification based on
1881 natural kind clustering. *American Mineralogist*, 104, 810-816.
- 1882 Hazen, R.M., and Ferry, J.M. (2010) Mineral evolution: Mineralogy in the fourth dimension.
1883 *Elements*, 6, #1, 9-12.
- 1884 Hazen, R.M., and Morrison, S.M. (2020) An evolutionary system of mineralogy, part I: stellar
1885 mineralogy (>13 to 4.6 Ga). *American Mineralogist*, 105, in press.
- 1886 Hazen, R.M., Papineau, D., Bleeker, W., Downs, R.T., Ferry, J.M., McCoy, T.L., Sverjensky,
1887 D.A., and Yang, H. (2008) Mineral evolution. *American Mineralogist*, **93**, 1693-1720.
- 1888 Hazen, R.M., Sverjensky, D.A., Azzolini, D., Bish, D.L., Elmore, S.C., Hinnov, L., and Milliken,
1889 R.E. (2013) Clay mineral evolution. *American Mineralogist*, 98, 2007-2029.
- 1890 Hazen, R.M., Downs, R.T., Elesish, A., Fox, P., Gagné, O., Golden, J.J., Grew, E.S., Hummer,
1891 D.R., Hystad, G., Krivovichev, S.V., Li, C., Liu, C., Ma, X., Morrison, S.M., Pan, F., Pires,
1892 A.J., Prabhu, A., Ralph, J., Runyon, S.E., and Zhong, H. (2019) Data-driven discovery in
1893 mineralogy: Recent advances in data resources, analysis, and visualization. *China Engineering*,
1894 5, 397-405.
- 1895 Henning, T., Jager, C., and Mutschke, H. (2004) Laboratory studies on carbonaceous dust. In A.N.
1896 Witt, G.C. Clayton, and B.T. Draine [Editors], *Astrophysics of Dust*. ASP Conference Series,
1897 309, 603-628.

- 1898 Henning, T., and Salama, E. (1998) Carbon in the universe. *Science*, 282, 2204-2210.
- 1899 Herbst, E. (1995) Chemistry in the interstellar medium. *Annual Review of Physical Chemistry*,
1900 46, 27-54.
- 1901 Herbst, E., and Klemperer, W. (1973) The formation and depletion of molecules in dense
1902 interstellar clouds. *The Astrophysical Journal*, 185, 505–533.
- 1903 Hinton, R.W., Davis, A.M., Scalena-Wachel, D.E., Grossman, L., and Draus, R.J. (1988) A
1904 chemical and isotopic study of hibonite-rich refractory inclusions in primitive meteorites.
1905 *Geochimica et Cosmochimica Acta*, 52, 2573-2598.
- 1906 Hobbs, P.V. (1974) *Ice Physics*. Oxford University Press.
- 1907 Hollenbach, D., Kaufman, M.J., Bergin, E.A., and Melnick, G.J. (2009) Water, O₂, and ice in
1908 molecular clouds. *The Astrophysical Journal*, 690, 1497-1521.
- 1909 Holmberg, A.A., and Hashimoto, H. (1992) A unique (almost) unaltered spinel-rich fine-grained
1910 inclusion in Kainsaz. *Meteoritics*, 27, 149-153.
- 1911 Hubbard, A., McNally, C.P., and Mac Low, M.-M. (2012) Short circuits in thermally ionized
1912 plasmas: A mechanism for intermittent heating of protoplanetary disks. *The Astrophysical*
1913 *Journal*, 761, 58-67.
- 1914 Ichikawa, O., and Ikeda, Y. (1995) Petrology of the Yamato-8559 CR chondrite. *Proceedings of*
1915 *the NIPR Symposium on Antarctic Meteorites*, 8, 63-78.
- 1916 Ihinger, P.D., and Stolper, E. (1986) The color of meteoritic hibonite: An indicator of oxygen
1917 fugacity. *Earth and Planetary Science Letters*, 78, 67–79.
- 1918 Iida, A., Nakamoto, T., Susa, H, and Nakagawa, Y. (2001) A shock model for chondrule formation
1919 in a protoplanetary disk. *Icarus*, 153, 430-450.

- 1920 Ikeda, Y. (1992) An overview of the research consortium, “Antarctic carbonaceous chondrites
1921 with CI affinities,” Yamato-86720, Yamato-82162, and Belgica-7904. Proceedings of the NIPR
1922 Symposium on Antarctic Meteorites, 5, 49-73.
- 1923 Ireland, T.R. (1988) Correlated morphological, chemical, and isotopic characteristics of hibonites
1924 from the Murchison carbonaceous chondrite. *Geochimica et Cosmochimica Acta*, 52, 2827–
1925 2839.
- 1926 Ireland, T.R., Fahey, A.J., and Zinner, E.K. (1988) Trace element abundances in hibonites from
1927 the Murchison carbonaceous chondrite: Constraints on high-temperature processes in the solar
1928 nebula. *Geochimica et Cosmochimica Acta*, 52, 2841–2854.
- 1929 Ivanova, M.A., Petaev, M.I., MacPherson, G.J., Nazarov, M.A., Taylor, L.A., and Wood, J.A.
1930 (2002) The first known natural occurrence of CaAl_2O_4 , in a Ca–Al-rich inclusion from the CH
1931 chondrite NWA470. *Meteoritics & Planetary Science*, 37, 1337–1344.
- 1932 Jambon, A., and Boudouma, O. (2011) Evidence for rhönite in angrites D'Orbigny and Sahara
1933 99555. 74th Annual Meeting of the Meteoritical Society, *Meteoritics & Planetary Science*
1934 Supplement, id.5167 (Sept 2011).
- 1935 Jeans, J.H. (1902) The stability of a spherical nebula. *Philosophical Transactions of the Royal*
1936 *Society A*, 199, 1-53.
- 1937 Jenniskens, P., and Blake, D.F. (1994) Structural transitions in amorphous water ice and
1938 astrophysical implications. *Science*, 265, 753-756.
- 1939 Jenniskens, P., and Blake, D.F. (1996) Crystallization of amorphous water ice in the solar system.
1940 *The Astrophysical Journal*, 473, 1104-1113.
- 1941 Jordan, K.D. (2019) Smallest water clusters supporting the ice I structure. Proceedings of the
1942 National Academy of Sciences USA, 116, 24383-24385.

- 1943 Joung, R.M.K., MacLow, M.M., and Ebel, D.S. (2004) Chondrule formation and protoplanetary
1944 disk heating by current sheets in nonideal magnetohydrodynamic turbulence. *The Astrophysical*
1945 *Journal*, 606, 532–541.
- 1946 Keil, K., and Fuchs, L.H. (1971) Hibonite from the Leoville and Allende chondritic meteorites.
1947 *Earth and Planetary Science Letters*, 12, 184-190.
- 1948 Keller, L.P., and Buseck, P.R. (1994) Twinning in meteoritic and synthetic perovskite. *American*
1949 *Mineralogist*, 79, 73-79.
- 1950 Kerridge, J.F. (1983) Isotopic composition of carbonaceous-chondrite kerogen: Evidence for an
1951 interstellar origin of organic matter in meteorites. *Earth and Planetary Science Letters*, 64, 186-
1952 200.
- 1953 Kimura, M., El Goresy, A., Palme, H., and Zinner, E. (1993) Ca-Al-rich inclusions in the unique
1954 chondrite ALH85085: Petrology, chemistry, and isotopic compositions. *Geochimica et*
1955 *Cosmochimica Acta*, 57, 2329-2359.
- 1956 Kimura, M., Mikouchi, T., Suzuki, A., Miyahara, M., Ohtani, E., and El Goresy, A. (2009)
1957 Kushiroite, CaAlAlSiO₆: A new mineral of the pyroxene group from the ALH 85085 CH
1958 chondrite, and its genetic significance in refractory inclusions. *American Mineralogist*, 94,
1959 1479–1482.
- 1960 Klöck, W., Thomas, K.L., McKay, D.S., and Palme, H. (1989) Unusual olivine and pyroxene
1961 compositions in interplanetary dust and unequilibrated ordinary chondrites. *Nature*, 339,126–
1962 128.
- 1963 Knauth, D.C., Andersson, B.-G., McCandliss, S.R., and Moos, H.W. (2004) The interstellar N₂
1964 abundance towards HD 124314 from far-ultraviolet observations. *Nature*, 429, 636–638.

- 1965 Kojima, T., Yada, S., and Tomeoka, K. (1995) Ca-Al-rich inclusion in three Antarctic CO₃
1966 chondrites, Y-81020, Yamato-82050 and Yamato-790992: Record of low temperature
1967 alteration processes. Proceedings of the NIPR Symposium on Antarctic Meteorites, 8, 79-86.
- 1968 Komatsu, M., Fagan, T.J., Krot, A.N., Nagashima, K., Petaev, M.I., Kimura, M., and Yamaguchi,
1969 A. (2018) First evidence for silica condensation within the solar protoplanetary disk.
1970 Proceedings of the National Academy of Sciences, 115, 7497-7502.
- 1971 Kööp, L., Nakashima, D., Heck, P.R., Kita, N.T., Tenner, T.J., Krot, A.N., Nagashima, K., Park,
1972 C., and Davis, A.M. (2016a) New constraints on the relationship between ²⁶Al and oxygen,
1973 calcium, and titanium isotopic variation in the early solar system from a multielement isotopic
1974 study of spinel-hibonite inclusions. *Geochimica et Cosmochimica Acta*, 184, 151-172.
- 1975 Kööp, L., Davis, A.M., Nakashima, D., Park, C., Krot, A.N., Nagashima, K., Temmer, T.J., Heck,
1976 P.R., and Kita, N.T. (2016b) A link between oxygen, calcium and titanium isotopes in ²⁶Al-
1977 poor hibonite-rich CAIs from Murchison and implications for the heterogeneity of dust
1978 reservoirs in the solar nebula. *Geochimica et Cosmochimica Acta*, 189, 70-95.
- 1979 Kööp, L., Heck, P.R., Busemann, H., Davis, A.M., Greer, J., Maden, C., Meier, M.M.M., and
1980 Wieler, R. (2018) High early solar activity inferred from helium and neon excess in the oldest
1981 meteorite inclusions. *Nature Astronomy*, 2, 709-713.
- 1982 Kornacki, A.S., and Wood, J.A. (1984) Petrography and classification of Ca,Al-rich and olivine-
1983 rich inclusions in the Allende CV3 chondrite. Proceedings of the Lunar and Planetary Science
1984 Conference, 14, B573-B587.
- 1985 Kornacki, A.S., and Wood, J.A. (1985) The identification of Group II inclusions in carbonaceous
1986 chondrites by electron microprobe analysis of perovskite. *Earth and Planetary Science Letters*,
1987 72, 74-86.

- 1988 Kouchi, A. (1987) Vapour pressure of amorphous H₂O ice and its astrophysical implications.
1989 Nature, 330, 550-552.
- 1990 Kouchi, A. (1990) Evaporation of H₂O-CO ice and its astrophysical implications. Journal of
1991 Crystal Growth, 99, 1220-1226.
- 1992 Kouchi, A., and Kuroda, T. (1990) Amorphization of cubic ice by ultraviolet irradiation. Nature,
1993 344, 134-135.
- 1994 Kouchi, A., and Yamamoto, T. (1995) Cosmoglaciology: Evolution of ice in interstellar space and
1995 the early solar system. Progress in Crystal Growth and Characterization of Materials, 30, 83-
1996 107.
- 1997 Kouchi, A., Yamamoto, T., Kozasa, T., Kuroda, T., and Greenberg, J.M. (1994) Conditions for
1998 condensation and preservation of amorphous water ice and crystallinity of astrophysical ices.
1999 Astronomy & Astrophysics, 290, 1009-1018.
- 2000 Krivovichev, S.V. (2012) Topological complexity of crystal structures: quantitative approach.
2001 Acta Crystallographica, A68, 393-398.
- 2002 Krivovichev, S.V. (2013) Structural complexity of minerals: information storage and processing
2003 in the mineral world. Mineralogical Magazine, 77, 275-326.
- 2004 Krot, A.N. (2019) Refractory inclusions in carbonaceous chondrites: Records of early solar
2005 systems processes. Meteoritics & Planetary Science, 54, 1647-1691.
- 2006 Krot, A.N., Petaev, M.I., Russell, S.S., Itoh, S., Fagan, T.J., Yurimoto, H., Chizmadia, L.,
2007 Weisberg, M.K., Komatsu, M., Ulyanov, A.A., and Keil, K. (2004) Amoeboid olivine
2008 aggregates and related objects in carbonaceous chondrites: records of nebular and asteroid
2009 processes. Chemie der Erde Geochemistry, 64, 185-239.

- 2010 Krot, A.N., Ulyanov, A.A., and Ivanova, M.A. (2006) Refractory inclusions and aluminum-rich
2011 chondrules in the CB/CH-like carbonaceous chondrite Isheyev. Proceedings of the Lunar and
2012 Planetary Science Conference, 37, 1226.
- 2013 Krot, A.N., Keil, K., Scott, E.R.D., Goodrich, C.A., and Weisberg, M.K. (2014) Classification of
2014 meteorites and their genetic relationships. In: A.M. Davis, Ed., Treatise on Geochemistry
2015 (Second Edition), Volume 1, pp. 1-63. Elsevier.
- 2016 Krot, A.N., Ma, C., Nagashima, K., Davis, A.M., Beckett, J.R., Simon, S.B., Komatsu, M., Fagan,
2017 T.J., Brenker, F., Ivanova, M.A., and Bischoff, A. (2019) Mineralogy, petrology, and oxygen
2018 isotopic compositions of ultra-refractory inclusions from carbonaceous chondrites.
2019 *Geochemistry*, 79, 125519 (29 pp.).
- 2020 Krot, A.N., Nagashima, K., and Rossman, G.R. (2020) Machiite, $\text{Al}_2\text{Ti}_3\text{O}_9$, a new oxide mineral
2021 from the Murchison carbonaceous chondrite: A new ultra-refractory phase from the solar
2022 nebula. *American Mineralogist*, 105, in press.
- 2023 Lacy, J.H., Carr, J.S., Evans, N.J. II, Baas, F., Achtermann, J.M., and Arens, J.F. (1991) Discovery
2024 of interstellar methane: Observations of gaseous and solid CH_4 absorption toward young stars
2025 in molecular clouds. *The Astrophysical Journal*, 376, 556-560.
- 2026 Lattimer, J.M., Schramm, D.N., and Grossman, L. (1978) Condensation in supernova ejecta and
2027 isotopic anomalies in meteorites. *The Astrophysical Journal*, 219, 230-249.
- 2028 Léger, A., Gauthier, S. Defourneau, D., and Rouan, D. (1983) Properties of amorphous H_2O ice
2029 and origin of the 3.1 micron absorption. *Astronomy & Astrophysics*, 117, 164-169.
- 2030 Lin, Y., El Goresy, A., Boyer, M., Feng, L., Zhang, J. and Hao, J. (2011) Earliest solid condensates
2031 consisting of the assemblage oldhamite, sinoite, graphite and excess ^{36}S in lawrencite from

- 2032 Almahata Sitta MS-17 EL3 chondrite. Workshop on Formation of the First Solids in the Solar
2033 System, Abstract #9040.
- 2034 Liu, M.-C., McKeegan, K.D., Goswami, J.N., Marhas, K.K., Sahijpal, S., Ireland, T.R., and Davis,
2035 A.M. (2009) Isotopic records in CM hibonites: Implications for timescales of mixing of isotope
2036 reservoirs in the solar nebula. *Geochimica et Cosmochimica Acta*, 73, 5051-5079.
- 2037 Lodders, K. (2003) Solar system abundances and condensation temperatures of the elements. *The*
2038 *Astrophysical Journal*, 591, 1220-1247.
- 2039 Longair, M.S. (2008) *Galaxy Formation, Second Edition*. Springer.
- 2040 Luhman, K.L., Allen, P.R., Espaillat, C., Hartmann, L., and Calvet, N. (2010) The disk population
2041 of the Taurus star-forming region. *The Astrophysical Journal Supplement Series*, 186, 111-174.
- 2042 Ma, C. (2011) Discovery of meteoritic lakargiite (CaZrO_3), a new ultra-refractory mineral from
2043 the Acfer 094 carbonaceous chondrite. *Proceedings of the Annual Meeting of the Meteoritical*
2044 *Society*, 74, 5169.
- 2045 Ma, C. (2012) Discovery of meteoritic eringaite, $\text{Ca}_3(\text{Sc,Y,Ti})_2\text{Si}_3\text{O}_{12}$, the first solar garnet?
2046 *Meteoritics & Planetary Science*, 47, A256.
- 2047 Ma, C. (2018) Discovery of meteoritic baghdadite, $\text{Ca}_3(\text{Zr,Ti})\text{Si}_2\text{O}_9$, in Allende: The first solar
2048 silicate with structurally essential zirconium? *Meteoritics & Planetary Science*, 53 (S1),
2049 Abstract No. 6358.
- 2050 Ma, C. (2019) Discovery of kaitianite, $\text{Ti}^{3+}_2\text{Ti}^{4+}\text{O}_5$, in Allende: A new refractory mineral from
2051 the solar nebula. *Proceedings of the Annual Meeting of the Meteoritical Society*, 82, 6098.

- 2052 Ma, C., and Beckett, J.R. (2016) Burnettite, CaVAISiO_6 , and Paqueite, $\text{Ca}_3\text{TiSi}_2(\text{Al}_2\text{Ti})\text{O}_{14}$, two
2053 new minerals from Allende: Clues to the evolution of a V-rich Ca-Al-inclusion. Proceedings of
2054 the Lunar and Planetary Science Conference, 47, 1595.
- 2055 Ma, C., and Rossman, G.R. (2008) Discovery of tazheranite (cubic zirconia) in the Allende
2056 meteorite. *Geochimica et Cosmochimica Acta*, 72, A577.
- 2057 Ma, C., and Rossman, G.R. (2009a) Grossmanite, $\text{CaTi}^{3+}\text{AlSiO}_6$, a new pyroxene from the
2058 Allende meteorite. *American Mineralogist*, 94, 1491–1494.
- 2059 Ma, C., and Rossman, G.R. (2009b) Davisite, CaScAlSiO_6 , a new pyroxene from the Allende
2060 meteorite. *American Mineralogist*, 94, 845–848.
- 2061 Ma, C., and Rossman, G.R. (2009c) Tistarite, Ti_2O_3 , a new refractory mineral from the Allende
2062 meteorite. *American Mineralogist*, 94, 841–844.
- 2063 Ma, C., and Rubin, A.E. (2019) Edscottite, Fe_5C_2 , a new iron carbide mineral from the Ni-rich
2064 Wedderburn IAB iron meteorite. *American Mineralogist*, 104, 1351-1355.
- 2065 Ma, C., Beckett, J.R., Rossman, G.R., Connolly, H.C.Jr., Guan, Y., Eiler, J.M., and Hofmann, A.E.
2066 (2009a) In-situ discovery of a cluster of refractory grains in an Allende ferromagnesian
2067 chondrule. Proceedings of the Lunar and Planetary Science Conference, 40, 2138.
- 2068 Ma, C., Simon, S.B., Rossman, G.R., and Grossman, L. (2009b) Calcium Tschermak's pyroxene,
2069 CaAlAlSiO_6 , from the Allende and Murray meteorites: EBSD and micro-Raman
2070 characterizations. *American Mineralogist*, 94, 1483-1486.
- 2071 Ma, C., Beckett, J.R., Tschauer, O., and Rossman, G.R. (2011a) Thortveitite ($\text{Sc}_2\text{Si}_2\text{O}_7$), the first
2072 solar silicate? Proceedings of the Annual Meeting of the Meteoritical Society, 74, 5171.

- 2073 Ma, C., Kampf, A.R., Connolly, H.C. Jr., Beckett, J.R., Rossman, G.R., Sweeney Smith, S.A., and
2074 Schrader, D.L. (2011b) Krotite, CaAl_2O_4 , a new refractory mineral from the NWA 1934
2075 meteorite. *American Mineralogist*, 96, 709–715.
- 2076 Ma, C., Tschauner, O., Beckett, J.R., Rossman, G.R., and Liu, W. (2012) Panguite, $(\text{Ti}^{4+},$
2077 $\text{Sc,Al,Mg,Zr,Ca})_{1.8}\text{O}_3$, a new ultra-refractory titania mineral from the Allende meteorite:
2078 synchrotron micro-diffraction and EBSD. *American Mineralogist*, 97, 1219–1225.
- 2079 Ma, C., Krot, A.N., and Bizzarro, M. (2013a) Discovery of dmisteinbergite (hexagonal
2080 $\text{CaAl}_2\text{Si}_2\text{O}_8$) in the Allende meteorite: A new member of refractory silicates formed in the solar
2081 nebula. *American Mineralogist*, 98, 1368-1371.
- 2082 Ma, C., Tschauner, O., Beckett, J.R., Rossmann, G.R., and Liu, W. (2013b) Kangite,
2083 $(\text{Sc,Ti,Al,Zr,Mg,Ca},\square)_2\text{O}_3$, a new ultra-refractory scandia mineral from the Allende meteorite:
2084 Synchrotron micro-Laue diffraction and electron backscatter diffraction. *American*
2085 *Mineralogist*, 98, 870-878.
- 2086 Ma, C., Beckett, J.R., and Rossman, G.R. (2014a) Allendeite ($\text{Sc}_4\text{Zr}_3\text{O}_{12}$) and hexamolybdenum
2087 (Mo,Ru,Fe) , two new minerals from an ultra-refractory inclusion from the Allende meteorite.
2088 *American Mineralogist*, 99, 654-666.
- 2089 Ma, C., Beckett, J.R., and Rossman, G.R. (2014b) Monipite, MoNiP , a new phosphide mineral in
2090 a Ca-Al-rich inclusion from the Allende meteorite. *American Mineralogist*, 99, 198-205.
- 2091 Ma, C., Krot, A.N., Beckett, J.R., Nagashima, K., and Tschauner, O. (2015) Discovery of warkite,
2092 $\text{Ca}_2\text{Sc}_6\text{Al}_6\text{O}_{20}$, a new Sc-rich ultra-refractory mineral in Murchison and Vigarano. *Proceedings*
2093 *of the Annual Meeting of the Meteoritical Society*, 78, 5025.

- 2094 Ma, C., Yoshizaki, T., Krot, A.N., Beckett, J.R., Nakamura, T., Nagashima, K., Muto, J., Ivanova,
2095 M.A. (2017a) Discovery of rubinite, $\text{Ca}_3\text{Ti}^{3+}_2\text{Si}_3\text{O}_{12}$, a new garnet mineral in refractory
2096 inclusions from carbonaceous chondrites. Proceedings of the Annual Meeting of the
2097 Meteoritical Society, 80, 6023.
- 2098 Ma, C., Krot, A.N., and Nagashima, K. (2017b) Addibischhoffite, $\text{Ca}_2\text{Al}_6\text{Al}_6\text{O}_{20}$, a new calcium
2099 aluminate mineral from the Acfer 214 CH carbonaceous chondrite: A new refractory phase
2100 from the solar nebula. American Mineralogist, 102, 1556-1560.
- 2101 Macdougall, J.D. (1979) Refractory-element-rich inclusions in C2 meteorites. Earth and Planetary
2102 Science Letters, 42, 1-6.
- 2103 Macdougall, J.D. (1981) Refractory spherules in the Murchison meteorite: Are they chondrules?
2104 Geophysical Research Letters, 8, 966-969.
- 2105 MacPherson, G.J. (2014) Calcium-aluminum-rich inclusions in chondritic meteorites. In Treatise
2106 on Geochemistry, Vol. 1: Meteorites, Comets, and Planets, Second Edition. A.M. Davis,
2107 H.D.Holland, and K.K.Turekian, Eds., pp.139-179. Elsevier-Pergamon.
- 2108 MacPherson, G.J., and Davis, A.M. (1993) A petrologic and ion microprobe study of a Vigarano
2109 Type B2 refractory inclusion: Evolution by multiple stages of melting and alteration.
2110 Geochimica et Cosmochimica Acta, 57, 231–243.
- 2111 MacPherson, G.J., and Davis, A.M. (1994) Refractory inclusions in the prototypical CM chondrite,
2112 Mighei. Geochimica et Cosmochimica Acta, 58, 5599–5625.
- 2113 MacPherson, G.J., and Grossman, L. (1984) Fluffy Type-A inclusions in the Allende meteorite.
2114 Geochimica et Cosmochimica Acta, 48, 29–46.

- 2115 MacPherson, G.J., Grossman, L., Allen, J.M., and Beckett, J.R. (1981) Origin of rims on coarse-
2116 grained inclusions in the Allende meteorite. *Proceedings of the Lunar and Planetary Science*
2117 *Conference*, 12, 1079–1091.
- 2118 MacPherson, G.J., Bar-Matthews, M., Tanaka, T., Olsen, E., and Grossman, L. (1983) Refractory
2119 inclusions in the Murchison meteorite. *Geochimica et Cosmochimica Acta*, 47, 823–839.
- 2120 MacPherson, G.J., Paque, J.M., Stolper, E., and Grossman, L. (1984) The origin and significance
2121 of reverse zoning in melilite from Allende Type B inclusions. *Journal of Geology*, 92, 289–305.
- 2122 MacPherson, G.J., Wark, D.A., and Armstrong, J.T. (1988) Primitive material surviving in
2123 chondrites: refractory inclusions. In: J.F. Kerridge and M.S. Matthews, M.S., Eds., *Meteorites*
2124 *and the Early Solar System*, pp. 746-807. University of Arizona Press.
- 2125 MacPherson, G.J., Huss, G.R., and Davis, A.M. (2003) Extinct ^{10}Be in Type A CAIs from CV
2126 chondrites. *Geochimica et Cosmochimica Acta*, 67, 3165–3179.
- 2127 Mai, C, Desch, S.J., and Boley, A.C., and Weiss, B.P. (2018) Magnetic fields recorded by
2128 chondrules formed in nebular shocks. *The Astrophysical Journal*, 857, 96 (13 pp.).
- 2129 Mann, C.R., Boley, A.C., and Morris, M.A. (2016) Planetary embryo bow shocks as a mechanism
2130 for chondrule formation. *The Astrophysical Journal*, 818, 103-123.
- 2131 Mao, X.Y., Ward, B.J., Grossman, L., and MacPherson, G.J. (1990) Chemical compositions of
2132 refractory inclusions from the Vigarano and Leoville carbonaceous chondrites. *Geochimica et*
2133 *Cosmochimica Acta*, 54, 2121–2132.
- 2134 Maret, S., Bergin, E.A., and Lada, C.J. (2006) A low fraction of nitrogen in molecular form in a
2135 dark cloud. *Nature*, 442, 425–427.
- 2136 Massalkski, T.B., Park, F.R., and Vassalmillet, L.F. (1966) Speculations about plessite.
2137 *Geochimica et Cosmochimica Acta*, 30, 649-662.

- 2138 Maynard-Casely, H.E., Cable, M.L., Malaska, M.J., Vu, T.H., Choukroun, M., and Hodyss, R.
2139 (2018) Prospects for mineralogy on Titan. *American Mineralogist*, 103, 343-349.
- 2140 McKeegan, K.D., Leshin, L.A., Russell, S.S., and MacPherson, G.J. (1998) Oxygen isotope
2141 abundances in calcium-aluminum-rich inclusions from ordinary chondrites: implications for
2142 nebular heterogeneity. *Science*, 280, 414-418.
- 2143 McKeegan, K.D., Chaussidon, M., and Robert, F. (2000) Incorporation of short-lived ^{10}Be in a
2144 calcium-aluminum-rich inclusion from the Allende meteorite. *Science*, 289, 1334-1337.
- 2145 Mendybaev, R.A., Richter, F.M., Georg, R.B., and Davis, A.M. (2009) Evaporation kinetics of
2146 forsterite-rich melts and thermal histories of FUN CAIs. *Proceedings of the Lunar and Planetary
2147 Science Conference*, 40, #2461.
- 2148 Michel-Lévy, M.C., Kurat, G., and Brandstätter, F. (1982) A new calcium aluminate from a
2149 refractory inclusion in the Leoville carbonaceous chondrite. *Earth and Planetary Science
2150 Letters*, 61, 13-22.
- 2151 Mikouchi, T., Zolensky, M., Ivanova, M., Tachikawa, O., Komatsu, M., Le, L., and Gounelle, M.
2152 (2009) Dmitryivanovite: A new high-pressure calcium aluminate from the Northwest Africa
2153 470 CH3 chondrite characterized using electron backscatter diffraction analysis. *American
2154 Mineralogist*. 94, 746–750.
- 2155 Mills, S.J., Hatert, F., Nickel, E.H., and Ferrais, G. (2009) The standardization of mineral group
2156 hierarchies: Application to recent nomenclature proposals. *European Journal of Mineralogy*,
2157 21, 1073-1080.
- 2158 Mizuno, A., Onishi, T., Hayashi, M., Ohashi, N., Sunada, K., Hasegawa, T., and Fukui, Y. (1994)
2159 Molecular cloud condensation as a tracer of low-mass star formation. *Nature*, 368, 719-721.

- 2160 Moberg, D.R., Becker, D., Dierking, C.W., Zurheide, F., Bandow, B., Buck, U., Hudait, A.,
2161 Molinero, V., Paesani, F., and Zeuch, T. (2019) The end of ice I. Proceedings of the National
2162 Academy of Sciences USA, 116, 24413-24419.
- 2163 Moggi-Cecchi, V., Pratesi, G., Salvadori, A., Franchi, I.A., and Greenwood, R.C. (2007) Textural
2164 and minerochemical features of NWA 1807 and 2180, two new CV3 chondrites from Northwest
2165 Africa. Lunar and Planetary Science Conference, 38, 2338.
- 2166 Moore, M.H., and Hudson, R.L. (1992) Far-infrared spectral studies of phase changes in water ice
2167 induced by proton radiation. The Astrophysical Journal, 401, 353.
- 2168 Morimoto, N., Fabries, J., Ferguson, A.K., Ginzburg, I.V., Ross, M., Seifert, F.A., Zussman, J.,
2169 Aoki, K., and Gottardi, G. (1988) Nomenclature of pyroxenes. American Mineralogist, 73,
2170 1123–1133.
- 2171 Morrison, S.M., Liu, C., Eleish, A., Prabhu, A., Li, C., Ralph, J., Downs, R.T., Golden, J.J., Fox,
2172 P., Hummer, D.R., Meyer, M.B., and Hazen, R.M. (2017) Network analysis of mineralogical
2173 systems. American Mineralogist, 102, 1588-1596.
- 2174 Morrison, S.M., Downs, R.T., Eleish, A., Fox, P., Hummer, D.R., Hystad, G., Golden, J.J., Liu,
2175 C., Prabhu, A., Zahirovic, S., and Hazen, R.M. (2020) Visualizing carbon minerals: Recent
2176 advances in C mineral evolution, mineral ecology, and network analysis. Frontiers in Earth
2177 Sciences, in press.
- 2178 Mukai, T. (1986) Analysis of a dirty water-ice model for cometary dust. Astronomy &
2179 Astrophysics, 164, 397-407.
- 2180 Mysen, B.O., and Kushiro, I. (1988) Composition, evaporation, melting and crystallization in the
2181 primitive solar nebula: Experimental data in the system MgO - SiO₂ - H₂ to 1.0 x 10⁻⁹ bar and
2182 1870^o C with variable oxygen fugacity. American Mineralogist, 73, 1-19.

- 2183 Mysen, B.O., Virgo, D., and Kushiro, I. (1985) Experimental studies at low pressures and high
2184 temperatures: Phase equilibria in the system $\text{CaMgSi}_2\text{O}_6 - \text{H}_2$ in the temperature range $1200^\circ -$
2185 1500°C and the pressure range (PH2) $10^{-6} -$ to 10^{-9} bar. *Earth and Planetary Science Letters*,
2186 75, 139-147.
- 2187 Nagahara, H. (1982) Fe-Ni metals in the type 3 ordinary chondrites. *Symposium on Antarctic*
2188 *Meteorites*, NIPR special Issue, 20, 86-96.
- 2189 Nagahara, H., Kushiro, I., and Mysen, B.O. (1993) Vaporization and condensation of
2190 chondritic materials - experimental studies. In: *Primitive Solar Nebula and Origin of Planets*,
2191 H. Ohya, ed., pp. 427-446, Terra Scientific Publishing Company (TERRAPUB) Tokyo.
- 2192 Newman, S.F., Buratti, B.J., Brown, R.H., Jaumann, R., Bauer, J., and Momary, T. (2008)
2193 Photometric and spectral analysis of the distribution of crystalline and amorphous ices on
2194 Enceladus as seen by Cassini. *Icarus*, 193, 397-406.
- 2195 Noguchi, T. (1994) Petrology and mineralogy of the Coolidge meteorite (CV4). *Proceedings of*
2196 *the NIPR Symposium of Antarctic Meteorites*, 7, 42-72.
- 2197 Nummelin, A., Whittet, D.C.B., Gibb, E.L., Gerakines, P.A., and Chiar, J.E. (2001) Solid carbon
2198 dioxide in regions of low-mass star formation. *The Astrophysical Journal*, 558, 185-193.
- 2199 Öberg, K.I., Boogert, A.C.A., Pontoppidan, K.M., Blake, G.A., Evans, N.J., Lahuis, F., van and
2200 Dishoeck, E.F. (2008) The c2d Spitzer spectroscopic survey of ices around low-mass young
2201 stellar objects. III. CH_4 . *The Astrophysical Journal*, 678, 1032-1041.
- 2202 Omont, A., Moseley, S.H., Forveille, T., Glaccum, W.J., Harvey, P.M., Likkell, L., Lowenstein,
2203 R.F., and Lisse, C.M. (1990) Observation of 40-70 micron bands of ice in IRAS 09371-1212
2204 and other stars. *The Astrophysical Journal*, 355, L27-L30.

- 2205 Palme, H., Hutcheon, I.D., and Spettel, B. (1994) Composition and origin of refractory-metal-rich
2206 assemblages in a Ca,Al-rich Allende inclusion. *Geochimica et Cosmochimica Acta*, 58, 495-
2207 513.
- 2208 Palumbo, M.E. (2005) The morphology of interstellar water ice. *Journal of Physics Conference*
2209 *Series*, 6, 211-216.
- 2210 Palumbo, M.E., Tielens, A.G.G.M., and Tokunaga, A.T. (1995) Solid carbonyl sulphide (OCS) in
2211 W33A. *The Astrophysical Journal*, 449, 674-680.
- 2212 Palumbo, M.E., Geballe, T.R., and Tielens, A.G.G.M. (1997) Solid carbonyl sulfide (OCS) in
2213 dense molecular clouds. *The Astrophysical Journal*, 479, 839-844.
- 2214 Pendleton, Y.J., and Allamandola, L.J. (2002) The organic refractory material in the diffuse
2215 interstellar medium: Mid-infrared spectroscopic constraints. *The Astrophysical Journal*
2216 *Supplement*, 138, 75-98.
- 2217 Podosek, F.A., Zinner, E.K., MacPherson, G.J., Lundberg, L.L., Brannon, J.C., and Fahey, A.J.
2218 (1991) Correlated study of initial $^{87}\text{Sr}/^{86}\text{Sr}$ and Al-Mg isotope systematics and petrologic
2219 properties in a suite of refractory inclusions from the Allende meteorite. *Geochimica et*
2220 *Cosmochimica Acta*, 55, 1083-1110.
- 2221 Pontoppidan, K.M., Dartois, E., van Dishoeck, E.F., Thi, W.-F., and d'Hendecourt, L. (2003)
2222 Detection of abundant solid methanol toward young low mass stars. *Astronomy &*
2223 *Astrophysics*, 404, L17-L20.
- 2224 Pontoppidan, K.M., Boogert, A.C.A., Fraser, H.J., van Dishoeck, E.F., Blake, G.A., Lahuis, F.,
2225 Öberg, K.I., Evans, J., and Salyk, C. (2008) The c2d spitzer spectroscopic survey of ices around
2226 low-mass young stellar objects. II. CO₂. *The Astrophysical Journal*, 678, 1005–1031.

- 2227 Qasim, D., Chuang, K.-J., Fedoseev, G., Ioppolo, S., Boogert, A.C.A., and Linnartz, H. (2018)
2228 Formation of interstellar methanol ice prior to the heavy CO freeze-out stage. *Astronomy &*
2229 *Astrophysics*, 612, A83, 9 pp.
- 2230 Richter, F.M., Davis, A.M., Ebel, D.S., and Hashimoto, A. (2002) Elemental and isotopic
2231 fractionation of Type B calcium-, aluminum-rich inclusions: Experiments, theoretical
2232 considerations, and constraints on their thermal evolution. *Geochimica et Cosmochimica Acta*,
2233 66, 521-540.
- 2234 Richter, F.M., Janney, P.E., Mendybaev, R.A., Davis, A.M., and Wadhwa, M. (2007) Elemental
2235 and isotopic fractionation of Type B CAI-like liquids by evaporation. *Geochimica et*
2236 *Cosmochimica Acta*, 71, 5544-5564.
- 2237 Roser, J.E., Vidali, G., Manicò, G., and Pirronello, V. (2001) Formation of carbon dioxide by
2238 surface reactions on ices in the interstellar medium. *The Astrophysical Journal*, 555, L61-L64.
- 2239 Rubin A. E. (2013) An amoeboid olivine inclusion (AOI) in CK3 NWA 1559, comparison to AOIs
2240 in CV3 Allende, and the origin of AOIs in CK and CV chondrites. *Meteoritics & Planetary*
2241 *Science*, 48, 432-441.
- 2242 Rubin, A.E., and Kallemeyn, G.W. (1989) Carlisle Lakes and Allan Hills 85151: members of a
2243 new chondrite grouplet. *Geochimica et Cosmochimica Acta*, 53, 3035-3044.
- 2244 Rubin, A.E., and Ma, C. (2017) Meteoritic minerals and their origins. *Chemie der Erde*, 77, 325-
2245 385.
- 2246 Rubin, A.E., and Ma, C. (2020) *Meteorite Mineralogy*. Cambridge University Press, in press.
- 2247 Rubin, A.E., Sailer, A.L., and Wasson, J.T. (1999) Troilite in the chondrules of type-3 ordinary
2248 chondrites. *Geochimica et Cosmochimica Acta*, 63, 2281-2298.

- 2249 Russell, S.S., Huss, G.R., Fahey, A.J., Greenwood, R.C., Hutchison, R., and Wasserburg, G.J.
2250 (1998) An isotopic and petrologic study of calcium–aluminum-rich inclusions from CO₃
2251 meteorites. *Geochimica et Cosmochimica Acta*, 62, 689–714.
- 2252 Ruzicka, A. (1997) Mineral layers around coarse-grained, Ca–Al-rich inclusions in CV3
2253 carbonaceous chondrites: Formation by high-temperature metasomatism. *Journal of*
2254 *Geophysical Research*, 102, 13387–13402.
- 2255 Sack, N.J., and Baragiola, R.A. (1993) Sublimation of vapor-deposited water ice below 170 K,
2256 and its dependence on growth conditions. *Physical Review B*, 48, 9973-9978.
- 2257 Sack, R. O., and Ghiorso, M. S. (1994a) Thermodynamic properties of multicomponent pyroxenes:
2258 I. Formulation of a general model. *Contributions to Mineralogy and Petrology*, 116, 277–286.
- 2259 Sack, R. O., and Ghiorso, M. S. (1994b) Thermodynamic properties of multicomponent pyroxenes:
2260 II. Phase relations in the quadrilateral. *Contributions to Mineralogy and Petrology*, 116, 287–
2261 300.
- 2262 Sack, R.O., and Ghiorso, M.S. (1994c) Thermodynamics of multicomponent pyroxenes III:
2263 Calibration of $\text{Fe}^{2+}(\text{Mg})_{-1}$, $\text{TiAl}(\text{MgSi})_{-1}$, $\text{TiFe}^{3+}(\text{MgSi})_{-1}$, $\text{AlFe}^{3+}(\text{MgSi})_{-1}$, $\text{NaAl}(\text{CaMg})_{-1}$,
2264 $\text{Al}^2(\text{MgSi})_{-1}$ and $\text{Ca}(\text{Mg})_{-1}$ exchange reactions between pyroxenes and silicate melts.
2265 *Contributions to Mineralogy and Petrology*, 118, 271-296.
- 2266 Sack, R.O., and Ghiorso, M.S. (2017) Ti^{3+} - and Ti^{4+} -rich fassaïtes at the birth of the solar system:
2267 Thermodynamics and applications. *American Journal of Science*, 317, 807-845.
- 2268 Sahai, R., Zijlstra, A., Sánchez Contreras, C., and Morris, M. (2003) An icy, bipolar proto-
2269 planetary nebula with knotty jets: IRAS 22036+5306. *The Astrophysical Journal Letters*, 586,
2270 L81–L85.

- 2271 Salama, F., Galazutdinov, G.A., Krelowski, J., Biennier, L., Beletsky, Y., and Song, I.-O. (2011)
2272 Polycyclic aromatic hydrocarbons and the diffuse interstellar bands: A survey. The
2273 Astrophysical Journal 728, 154-161.
- 2274 Salzmann, C.G. (2018) Advances in the experimental exploration of water's phase diagram.
2275 arXiv:1812.04333. doi: 1063/1.5085163
- 2276 Sandford, S.A., Allamandola, L.J., Tielens, A.G.G.M., and Valero, G.J. (1988) Laboratory studies
2277 of the infrared spectral properties of CO in astrophysical ices. The Astrophysical Journal, 329,
2278 498-510.
- 2279 Saxena, S.K., and Hrubciak, R. (2014) Mapping the nebular condensates and the chemical
2280 composition of the terrestrial planets. Earth and Planetary Science Letters, 393, 113-119.
- 2281 Schaefer, L., and Fegley, B. (2010) Volatile element chemistry during metamorphism of ordinary
2282 chondritic material and some of its implications for the composition of asteroids. Icarus, 205,
2283 483-496.
- 2284 Schertl, H.-P., Mills, S.J., and Maresch, W.V. (2018) A Compendium of IMA-Approved Mineral
2285 Nomenclature. International Mineralogical Association, Melbourne, Australia.
- 2286 Schutte, W.A., Boogert, A.C.A., Tielens, A.G.G.M., Whittet, D.C.B., Gerakines, P.A., Chiar, J.E.,
2287 Ehrenfreund, P., Greenberg, J.M., van Dishoeck, E.F., and de Graauw, T. (1999) Weak ice
2288 absorption features at 7.24 and 7.41 microns in the spectrum of the obscured young stellar
2289 object W33A. Astronomy & Astrophysics, 343, 966-976.
- 2290 Scott, E.R.D., and Krot, A.N. (2014) Chondrites and their components. In Treatise on
2291 Geochemistry, Vol. 1: Meteorites, Comets, and Planets, Second Edition. A.M. Davis, H.D.
2292 Holland, and K.K. Turekian, Eds., pp. 65-137. Elsevier-Pergamon.

- 2293 Scott, E.R.D., and Rajan, S. (1979) Thermal history of the Shaw chondrite. Proceedings of the
2294 Lunar and Planetary Science Conference, 10, 1031-1043.
- 2295 Seki, J., and Hasegawa, H. (1983) The heterogeneous condensation of interstellar ice grains.
2296 Astrophysics and Space Science, 94, 177-189.
- 2297 Shibata, Y. (1996) Opaque minerals in Antarctic CO3 carbonaceous chondrites: Yamato-74135, -
2298 790992, -791717, -81020, -81025, -82050, and Allan Hills 77307. Proceedings of the NIPR
2299 Symposium on Antarctic Meteorites, 9, 79-96.
- 2300 Shu, F.H., Shang, H., and Lee, T. (1996) Toward an astrophysical theory of chondrites. Science,
2301 271, 1545-1552.
- 2302 Simon, S.B., and Grossman, L. (1992) Low temperature exsolution in refractory siderophile
2303 element-rich opaque assemblages from the Leoville carbonaceous chondrite. Earth and
2304 Planetary Science Letters, 110, 67-75.
- 2305 Simon, S.B., and Grossman, L. (1997) In situ formation of palisade bodies in calcium, aluminum-
2306 rich refractory bodies. Meteoritics & Planetary Science, 32, 61-70.
- 2307 Simon, S.B., Yoneda, S., Grossman, L., and Davis, A.M. (1994) A CaAl₄O₇-bearing refractory
2308 spherule from Murchison: Evidence for very high-temperature melting in the solar nebula.
2309 Geochimica et Cosmochimica Acta, 58, 1937-1949.
- 2310 Simon, S.B., Davis, A.M., and Grossman, L. (1996) A unique ultra-refractory inclusion from the
2311 Murchison meteorite. Meteoritics, 31, 106-115.
- 2312 Smith, R.G., Sellgren, K., and Tokunaga, A.T. (1989) Absorption features in the 3-micron spectra
2313 of protostars. The Astrophysical Journal, 344, 413-426.
- 2314 Smith, D.G.W., Miúra, Y., and Launspach, S. (1993) Fe, Ni, and Co variations in the metals from
2315 some Antarctic chondrites. Earth and Planetary Science Letters, 120, 487-498.

- 2316 Snow, T.P., and McCall, B.J. (2006) Diffuse atomic and molecular clouds. *Annual Review of*
2317 *Astronomy and Astrophysics*, 44, 367-414.
- 2318 Snow, T., and Witt, A. (1995) The interstellar carbon budget and the role of carbon in dust and
2319 large molecules. *Science*, 270, 1455–1460.
- 2320 Snyder, L.E., and Buhl, D. (1971) Observations of radio emission from interstellar hydrogen
2321 cyanide. *The Astrophysical Journal*, 163, L47-L52.
- 2322 Snyder, L.E., Buhl, D., Zuckerman, B., and Palmer, P. (1969) Microwave detection of interstellar
2323 formaldehyde. *Physical Review Letters*, 22, 679-681.
- 2324 Sorrell, W. (1995) Nebular lightning and the chondrule factory. *Comments of Astrophysics*, 18,
2325 151-159.
- 2326 Steele, I.M. (1995) Mineralogy of a refractory inclusion in the Allende (C3V) meteorite.
2327 *Meteoritics*, 30, 9-14.
- 2328 Sylvester, P.J., Grossman, L., and MacPherson, G.J. (1992) Refractory inclusions with unusual
2329 chemical compositions from the Vigarano carbonaceous chondrite. *Geochimica et*
2330 *Cosmochimica Acta*, 56, 1343-1363.
- 2331 Sylvester, P.J., Simon, S.B., and Grossman, L. (1993) Refractory inclusions from the Leoville,
2332 Efremovka, and Vigarano C3V chondrites: Major element differences between Types A and B,
2333 and extraordinary refractory siderophile element compositions. *Geochimica et Cosmochimica*
2334 *Acta*, 57, 3763-3784.
- 2335 Taylor, G.J., Okada, A., Scott, E.R.D., Rubin, A.E., Huss, G.R., and Keil, K. (1981) The
2336 occurrence and implications of carbide-magnetite assemblages in unequilibrated ordinary
2337 chondrites. *Proceedings of the Lunar and Planetary Science Conference*, 12, 1076-1078.

- 2338 Thompson, T. (1818) Scientific intelligence, and notices of subjects connected with science. III.
2339 Notice concerning certain minerals lately discovered. *Annals of Philosophy, or Magazine of*
2340 *Chemistry, Mineralogy, Mechanics, Natural History, Agriculture, and the Arts*, 12, 310-312.
- 2341 Tielens, A.G.G.M. (2008) Interstellar polycyclic aromatic hydrocarbon molecules. *Annual Review*
2342 *of Astronomy and Astrophysics*, 46, 289-337.
- 2343 Ulyanov, A.A., Korina, M.I., Nazarov, M.A., and Sherbovsky, E.Y. (1982) Efremovka CAIs:
2344 Mineralogical and petrological data. *Proceedings of the Lunar and Planetary Science*
2345 *Conference*, 13, 813-814.
- 2346 Urey, H.C. (1955) The cosmic abundances of potassium, uranium, and thorium and the heat
2347 balances of the Earth, the Moon, and Mars. *Proceedings of the National Academy of Sciences*
2348 *USA*, 15, 127-144.
- 2349 Wakelam, V., Bron, E., Cazaux, S., Dulieu, F., Gry, C., Guillard, P., Habart, E., Hornekaer, L.,
2350 Morisset, S., Nyman, G., Pirronello, V., Proce, S.D., Valdivia, V., Vidali, G., and Watanabe,
2351 N. (2017) H₂ formation on interstellar dust grains: The viewpoints of theory, experiments,
2352 models, and observations. *Molecular Astrophysics*, 9, 1-36.
- 2353 Wang, S., Li, A., and Jiang, B.W. (2015) The interstellar oxygen crisis, or where have all the
2354 oxygen atoms gone? *Monthly Notices of the Royal Astronomical Society*, 454, 569-575.
- 2355 Wark, D.A. (1986) Evidence for successive episodes of condensation at high temperatures in a
2356 part of the solar nebula. *Earth and Planetary Science Letters*, 77, 129-148.
- 2357 Wark, D.A. (1987) Plagioclase-rich inclusions in carbonaceous chondrite meteorite: Liquid
2358 condensates? *Geochimica et Cosmochimica Acta*, 51, 221-242.
- 2359 Wark, D.A., and Boynton, W.V. (2001) The formation of rims on calcium–aluminum-rich
2360 inclusions: Step I. Flash heating. *Meteoritics & Planetary Science*, 36, 1135–1166.

- 2361 Wark, D.A., and Lovering, J.F. (1977) Marker events in the early solar system: Evidence from
2362 rims on Ca–Al-rich inclusions in carbonaceous chondrites. Proceedings of the Lunar Science
2363 Conference, 8, 95–112.
- 2364 Wark, D.A., and Lovering, J.F. (1978) Refractory/platinum metals and other opaque phases in
2365 Allende Ca-Al-rich inclusions (CAI's). Proceedings of the Lunar Science Conference, 9, 1214-
2366 1216.
- 2367 Wark, D.A., and Lovering, J.F. (1982a) Evolution of Ca-Al-rich bodies in the earliest solar system:
2368 growth by incorporation. *Geochimica et Cosmochimica Acta*, 46, 2595-2607.
- 2369 Wark, D.A., and Lovering, J.F. (1982b) The nature and origin of type B1 and B2 inclusions in the
2370 Allende meteorite. *Geochimica et Cosmochimica Acta*, 46, 2581-2594.
- 2371 Wark, D.A., Boynton, W.V., Keays, R.R., and Palme, H. (1987) trace element and petrologic clues
2372 to the formation of forsterite-bearing Ca-Al-rich inclusions in the Allende meteorite.
2373 *Geochimica et Cosmochimica Acta*, 51, 607-622.
- 2374 Wasserburg, G.J., Lee, T., and Papanastassiou, D.A. (1977) Correlated O and Mg isotopic
2375 anomalies in Allende inclusions: II. Magnesium. *Geophysical Research Letters*, 4, 299–302.
- 2376 Weber, D., and Bischoff, A. (1994) The occurrence of grossite (CaAl₄O₇) in chondrites.
2377 *Geochimica et Cosmochimica Acta*, 58, 3855-3877.
- 2378 Weber, D., and Bischoff, A. (1997) Refractory inclusions in the CR chondrite Acler 059-El Djouf
2379 001: Petrology, chemical composition, and relationship to inclusion populations in other types
2380 of carbonaceous chondrites. *Chemie der Erde*, 57, 1-24.
- 2381 Weber, D., Zinner, E., and Bischoff, A. (1995) Trace element abundances and magnesium, calcium
2382 and titanium isotopic compositions of grossite containing inclusions from the carbonaceous
2383 chondrite, Acfer 182. *Geochimica et Cosmochimica Acta*, 59, 803-823.

- 2384 Weisberg, M.K., Prinz, M., and Nehru, C.E. (1988) Petrology of ALH85085: A chondrite with
2385 unique characteristics. *Earth and Planetary Science Letters*, 91, 19-32.
- 2386 Weisberg, M.K., Prinz, M., Clayton, R.N., and Mayeda, T.K. (1993) The CR (Renazzo-tyoe)
2387 carbonaceous chondrite group. *Geochimica et Cosmochimica Acta*, 57, 1567-1586.
- 2388 Weisberg, M.K., Connolly, H.C. Jr., and Ebel, D.S. (2004) Petrology and origin of amoeboid
2389 olivine aggregates in CR chondrites. *Meteoritics & Planetary Science*, 39, 1741-1753.
- 2390 Weisberg, M.K., Connolly, H., Zolensky, M., Bland, P., Brearley, A., Bridges, J., Brownlee, D.,
2391 Butterworth, A., and 33 others (2006) Stardust (comet) samples and the meteorite record.
2392 American Geophysical Union, Abstract P51E-1243.
- 2393 Whittet, D.C.B. (2003) *Dust in the Galactic Environment*. Institute of Physics Publishing.
- 2394 Whittet, D.C.B., Pendleton, Y.J., Gibb, E.L., Boogert, A.C.A., Chiar, J.E., and Nummelin, A.
2395 (2001) Observational constraints on the abundance and evolution of “XCN” in interstellar grain
2396 mantles. *The Astrophysical Journal*, 550, 793-798.
- 2397 Widowiak, T.J., Cronin, L.W., Beegle, L.W., and Robinson, M.S. (1995) Plasma processing of
2398 interstellar PAHs into solar system kerogen. *Planetary and Space Sciences*, 43, 1175-1182.
- 2399 Williams, D.A. (2005) Gas and dust in the interstellar medium. *Journal of Physics Conference*
2400 *Series*, 6, 1-17.
- 2401 Wilson, R.W., Jeefferts, K.B., and Penzias, A.A. (1971) Carbon monoxide in the Orion nebula.
2402 *Astrophysical Journal Letters*, 161, 43-44.
- 2403 Winnewisser G., and Churchwell E. (1975) Interstellar formic acid. *Sterne und Weltraum*, 14, 288-
2404 289 [in German].
- 2405 Womack, M., Ziurys, L.M., and Wyckoff, S. (1992) Estimates of N₂ abundances in dense
2406 molecular clouds. *The Astrophysical Journal*, 393, 188–192.

- 2407 Wood, J.A., and Hashimoto, A. (1993) Mineral equilibrium in fractionated nebular systems.
2408 *Geochimica et Cosmochimica Acta*, 57, 2377-2388.
- 2409 Wood, B.J., Smythe, D.J., and Harrison, T. (2019) The condensation temperatures of the elements.
2410 *American Mineralogist*, 104, 844-856.
- 2411 Yan, L., Chary, R., Armus, L., Teplitz, H., Helou, G., Frayer, D., Fadda, D., Surace, J., and Choi,
2412 P. (2005) Spitzer detection of polycyclic aromatic hydrocarbon and silicate dust features in the
2413 mid-infrared spectra of $z \sim 2$ ultraluminous infrared galaxies. *The Astrophysical Journal*, 628,
2414 604–610.
- 2415 Yoneda, S., and Grossman, L. (1995) Condensation of CaO-MgO-Al₂O₃-SiO₂ liquids from cosmic
2416 gases. *Geochimica et Cosmochimica Acta*, 59, 3413-3444.
- 2417 Zasowski, G., Kemper, F., Watson, D.M., Furlan, E., Bohac, C.J., Hull, C., and Green, J.D. (2009)
2418 Spitzer infrared spectrograph observations of Class I/II objects in Taurus: Composition and
2419 thermal history of the circumstellar ices. *The Astrophysical Journal*, 694, 459-478.
- 2420 Zhang, A., Benoit, P.H., and Sears, D.W.G. (1995) The classification and complex thermal history
2421 of the enstatite chondrites. *Journal of Geophysical Research*, 100, 9417-9438.
- 2422 Zhang, A.-C., Ma, C., Sakamoto, N., Wang, R.-C., Hsu, W.-B., and Yurimoto, H. (2015)
2423 Mineralogical anatomy and implications of a Ti-Sc-rich ultra-refractory inclusion from Sayh al
2424 Uhaymir 290 CH3 chondrite. *Geochimica et Cosmochimica Acta*, 163, 27-39.
- 2425 Zinner, E.K., Caillet, C., and El Goresy, A. (1991) Evidence for extraneous origin of
2426 magnesiowustite–metal Fremdlinge from the Vigarano CV3 chondrite. *Earth and Planetary
2427 Science Letters*, 102, 252-264.
- 2428 Zuckerman B., Ball J.A., and Gottlieb, C.A. (1971) Microwave detection of interstellar formic
2429 acid. *The Astrophysical Journal*, 163, L41-L45.

Table 2. Diagnostic properties of circumstellar and interstellar condensed phases. Unconfirmed phases appear in [brackets].

Group	Species (Formula)	Natural Kind	Characteristics	References
NATIVE ELEMENTS				
	<i>Hydrogen (H₂)</i>	[Interstellar hydrogen]	A fraction of H ₂ may condense at T ~ 10 K	1
	<i>Nitrogen (N₂)</i>	[Interstellar nitrogen]	Molecular nitrogen should condense heterogeneously at T < 20 K	2,3
	<i>Oxygen (O₂)</i>	[Interstellar oxygen]	Most molecular oxygen reacts with H ₂ to form H ₂ O	4,5
OXIDES				
	<i>Water (H₂O)</i>	Interstellar cubic ice	Diagnostic sharp IR emission features at 44 and 60 microns	6-8
		Interstellar amorphous H ₂ O	Diagnostic O-H stretch at 3.05 microns	7-10
	<i>Carbon Monoxide (CO)</i>	Interstellar amorphous CO	Diagnostic absorption at 4.67 microns	11,12
		Interstellar CO	Forms when amorphous CO anneals at T > 23 K	13
	<i>Carbon Dioxide (CO₂)</i>	Interstellar amorphous CO ₂	IR absorption features at 4.27 and 15.2 microns	14
	<i>Sulfur Dioxide (SO₂)</i>	[Interstellar SO ₂]	Diagnostic absorption at ~7.6 microns	15,16
ORGANIC MOLECULAR SOLIDS				
	<i>Methanol (CH₃OH)</i>	Interstellar amorphous CH ₃ OH	Diagnostic absorption at 3.54, 3.95, 8.9, and 9.75 microns	8,17
	<i>Methane (CH₄)</i>	Interstellar amorphous CH ₄	Diagnostic 7.676-micron absorption	8,18

<i>Cyanide (XCN; X = H,O)</i>	[Interstellar XCN]	Diagnostic absorption at 4.62 microns	8,19,20
<i>Formaldehyde (H₂CO)</i>	[Interstellar H ₂ CO]	5.81 and 5.83-micron absorption; 4830 MHz emission	8,21
<i>Formic Acid (HCOOH)</i>	[Interstellar HCOOH]	Diagnostic absorption at 5.85 and 7.243 microns	8,22,23
<i>Acetaldehyde (CH₃HCO)</i>	[Interstellar CH ₃ HCO]	Diagnostic 7.414-micron absorption	8,23
<i>Carbonyl Sulfide (OCS)</i>	[Interstellar OCS]	Diagnostic 4.91-micron absorption	8,24,25
<i>Ammonia (NH₃)</i>	[Interstellar NH ₃]	Suggested by bands at 3.5 and ~9 microns	8,26
<i>Kerogen (C,H,N,O)</i>	Interstellar kerogen	Preserved in relatively unaltered carbonaceous chondrites; Diagnostic absorption at 3.3, 3.47, 6.2, 8.6, and 11.3 microns	8,27-31

References: 1. Allamandola et al. (1999); 2. Maret et al. (2006); 3. Daranlot et al. (2012); 4. Hollenbach et al. (2009); 5. Wang et al. (2015); 6. Omont et al. (1990); 7. Whittet (2003); 8. Gibb et al. (2004); 9. Hagen et al. (1981); 10. Newman et al. (2008); 11. Chiar et al. (1996); 12. Elsila et al. (1997); 13. Kouchi (1990); 14. Pontoppidan et al. (2008); 15. Boogert et al. (1997); 16. Zasowski et al. (2009); 17. Pontoppidan et al. (2003); 18. Boogert et al. (1996); 19. Clark et al. (1974); 20. Whittet et al. (2001); 21. Grim et al. (1991); 22. Bisschop et al. (2007); 23. Schutte et al. (1999); 24. Palumbo et al. (1995); 25. Palumbo et al. (1997); 26. Smith et al. (1989); 27. Cronin & Pizzarello (1990); 28. Greenberg et al. (1995); 29. Widowiak et al. (1995); 30. Ehrenfreund & Cami (2010); 31. Ehrenfreund et al. (1991).

Table 3. Properties of primary phases in the solar nebula formed by condensation, melt crystallization, and solid-state reactions.

CAI = calcium-aluminum-rich inclusion; AOA = amoeboid olivine aggregate; URI = ultra-refractory inclusion.

Group	Species (Formula)	Natural Kind	Characteristics	References
NATIVE ELEMENTS				
Pt group alloys (Pt,Ru,Os, etc.)		<i>CAI PGE alloy</i>	Nano- to micro-scale alloys, space group <i>P63/mmc</i> .	1,2
		<i>URI PGE alloys</i>	Often Os-dominant	3-5
Iron (Fe,Ni) [also called “kamacite”]		<i>CAI iron</i>	Occurs as a primary phase in type A, B, and C CAIs	1,6-8
		<i>AOA iron</i>	Ubiquitous in AOAs, typically with 5 to 7 wt % Ni	9-11
		<i>URI iron</i>	Sub-micron grains associated with ultra-refractory minerals	6
Taenite (Fe,Ni)		<i>CAI taenite</i>	Occurs in type A and B CAIs; typically 10 to 50 wt. % Ni	1,6,8
Fe-Mo alloys (Fe,Mo,Ru,Os,etc.)		<i>CAI Fe-Mo alloys</i>	Includes IMA-approved hexaferrum and hexamolybdenum	12-14
		<i>URI Fe-Mo alloys</i>	Includes IMA-approved hexaferrum and hexamolybdenum	4,5,14
CARBIDES				
Khamrabaevite (TiC)		<i>URI khamrabaevite</i>	Associated with corundum and tistarite	15
NITRIDES				
Osbornite (TiN)		<i>CAI osbornite</i>	As a rare phase in CAIs	16,17
PHOSPHIDES				
Monipite (MoNiP)		<i>CAI monipite</i>	Known from micron-scale grains in the Allende meteorite	18
OXIDES				
Ice (H ₂ O)		<i>Nebular cubic ice</i>	Condenses at 50 < T < 150 K in the outer nebula	19

Corundum (Al ₂ O ₃)	<i>CAI corundum</i>	Near end-member; in CAI cores, inclusions in hibonite or spinel	1,20,21
	<i>URI corundum</i>	Associated with khrambaevite and tistarite	15
Tistarite (Ti ₂ O ₃)	<i>URI tistarite</i>	Associated with khrambaevite and corundum	15,22
Kaitianite (Ti ³⁺ ₂ Ti ⁴⁺ O ₃)	<i>URI kaitianite</i>	Known from two grains, both micron-scale	15,22
Rutile (TiO ₂)	<i>URI rutile</i>	Associated with tistarite and kaitianite	15,22
Baddeleyite (ZrO ₂)	<i>URI baddeleyite</i>	Associated with zirkelite	23
Anosovite [(Ti ⁴⁺ ,Ti ³⁺ ,Mg,Sc,Al) ₃ O ₅]	<i>URI anosovite</i>	Known from two grains, both micron-scale	14
Spinel (MgAl ₂ O ₄)	<i>CAI spinel</i>	Ubiquitous in CAIs; a component of Wark-Lovering rims	1,2
	<i>AOA spinel</i>	Associated with perovskite, fassaite, and anorthite	10,11
	<i>URI spinel</i>	Associated with Sc-rich fassaite, REE-enriched perovskite	5,24,25
Hibonite (CaAl ₁₂ O ₁₉)	<i>CAI hibonite</i>	Common in CAIs and Wark-Lovering rims	1,2
Perovskite (CaTiO ₃)	<i>CAI perovskite</i>	Common in CAIs and Wark-Lovering rims	1,2
	<i>AOA perovskite</i>	Common as sub-micron grains associated with spinel	1,11
	<i>URI perovskite</i>	Typically enriched in REE; associated with Sc minerals	4,5,24-26
Lakargiite (CaZrO ₃)	<i>URI lakargiite</i>	Sub-micron grains as inclusions in hibonite	4
Grossite (Ca ₂ Al ₄ O ₇)	<i>CAI grossite</i>	5- to 10-micron grains as inclusions in major CAI phases	27,28
Krotite (CaAl ₂ O ₄)	<i>CAI krotite</i>	One occurrence; in association with major CAI phases	29,30
Machiite (Al ₂ Ti ₃ O ₉)	<i>URI machiite</i>	Known from a single 4.4-micron diameter crystallite	31

Zirkelite [(Ti,Ca,Zr)O _{2-x}]	<i>URI zirkelite</i>	Found in association with baddeleyite	23
Kangite [(Sc,Ti,Al,Zr,Mg,Ca) _{1.8} O ₃]	<i>URI kangite</i>	Cation-deficient, cubic bixbyite structure	25
Panguite [(Ti,Sc,Al,Mg,Zr,Ca) _{1.8} O ₃]	<i>URI panguite</i>	Cation-deficient, orthorhombic bixbyite structure	12,14,32,33
Zirconolite (CaZrTi ₂ O ₇)	<i>URI zirconolite</i>	Associated with tazheranite and metal alloys	3
Tazheranite [(Zr,Sc,Ca,Y,Ti)O _{1.75}]	<i>URI tazheranite</i>	Associated with zirconolite and metal alloys	3,13
Allendeite (Sc ₄ Zr ₃ O ₁₂)	<i>URI allendeite</i>	Contains spinel and refractory metal inclusions	5
SILICATES			
Quartz (SiO ₂)	<i>AOA quartz</i>	Associated with fassaite, forsterite, anorthite, and spinel	34
Olivine Group [(Mg,Fe,Ca,Mn) ₂ SiO ₄]			
Forsterite Mg ₂ SiO ₄	<i>CAI forsterite</i>	A minor primary CAI phase; with spinel and fassaite	1,2
	<i>AOA forsterite</i>	Defining major phase of AOAs	1,2
Garnet Group [Ca,(Al, Ti ³⁺ ,V,Sc) ₂ Si ₃ O ₁₂]			
Rubinite (Ca ₃ Ti ³⁺ ₂ Si ₃ O ₁₂)	<i>CAI rubinite</i>	From type A CAIs	35
	<i>URI rubinite</i>	Significantly enriched in Y, Sc, and Zr; with eringaite	35
Eringaite (Ca ₃ Sc ₂ Si ₃ O ₁₂)	<i>URI eringaite</i>	Occurs with rubinite	13,35
Melilite Group [gehlenite (Ca ₂ Al ₂ SiO ₇) to åkermanite (Ca ₂ MgSi ₂ O ₇)]			
	<i>CAI melilite</i>	Common in CAIs and Wark-Lovering rims	1,2

	<i>AOA melilite</i>	Gehlenite-rich, associated with anorthite and spinel	1,10
	<i>URI melilite</i>	Gehlenite-rich, associated with davisite, perovskite, spinel	26
Clinopyroxene Group [Ca(Mg,Al,Ti ³⁺ ,Sc,V)(Al,Ti ⁴⁺ ,Si)SiO ₆]			
Fassaite [Ca(Mg,Al,Ti ³⁺)(Si,Al,Ti ⁴⁺)SiO ₆]	<i>CAI fassaite</i>	Common in CAIs and Wark-Lovering rims	1,2
	<i>AOA fassaite</i>	Common in association with forsterite and anorthite	10,11
	<i>URI fassaite</i>	Sub-millimeter grains with davisite, spinel, etc.	5,24,36
Burnettite (CaV ³⁺ AlSiO ₆)	<i>CAI burnettite</i>	Identified by from one fluffy type A CAI	37
Davisite (CaSc ³⁺ AlSiO ₆)	<i>URI davisite</i>	Associated with fassaite, perovskite, and spinel	12,15,24
Feldspar Group [(Na,Ca)(Al,Si) ₄ O ₈]			
Anorthite (CaAl ₂ Si ₂ O ₈)	<i>CAI anorthite</i>	Commonly as laths in CAIs; Primary anorthite is Na-free	1,2
	<i>AOA anorthite</i>	Common minor phase in AOAs	11
Dmisteinbergite (CaAl ₂ Si ₂ O ₈)	<i>CAI dmisteinbergite</i>	A rare high-T, low-P polymorph of anorthite	38
Baghdadite [Ca ₃ (Zr,Ti)Si ₂ O ₉]	<i>CAI baghdadite</i>	Known from a single 0.8-micron euhedral grain	39
Rhönite [Ca ₂ (Mg,Al,Ti) ₆ (Si,Al) ₆ O ₂₀], Addibischoffite [Ca ₂ (Al,Mg,V,Ti) ₆ (Al,Si) ₆ O ₂₀], and Warkite [Ca ₂ (Sc,Ti,Al,Mg,Zr) ₆ Al ₆ O ₂₀]			
	<i>CAI rhönite</i>	A rare constituent of A and B CAIs	40,41
	<i>URI warkite</i>	Micron-scale crystals with perovskite and davisite	26
Paqueite [Ca ₃ TiSi ₂ (Al,Ti,Si) ₃ O ₁₄]	<i>CAI paqueite</i>	From a fluffy type A CAI	37
Thortveitite (Sc ₂ Si ₂ O ₇)	<i>URI thortveitite</i>	Micron-scale crystals with fassaite and davisite	12

Silicate Glass (Ca,Mg,Al,Si,O)

CAI silicate glass

A component of hibonite-silicate spherules

2,42,43

References: 1. Brearley & Jones (1998); 2. MacPherson (2014); 3. Ma & Rossman (2008); 4. Ma (2011); 5. Ma et al. (2014a); 6. Campbell et al. (2005); 7. Scott & Krot (2014); 8. Rubin & Ma (2017); 9. Chizmadia et al. (2002); 10. Krot et al. (2004); 11. Weisberg et al. (2004); 12. Ma et al. (2011a); 13. Ma (2012); 14. Zhang et al. (2015); 15. Ma & Rossman 2009c; 16. Grokhovsky (2006); 17. Weisberg et al. 1988; 18. Ma et al. (2014b); 19. Omont et al. (1990); 20. Bar-Matthews et al. (1982); 21. Greshake et al. (1996); 22. Ma (2019); 23. Krot et al. 2019; 24. Ma & Rossman (2009b); 25. Ma et al. (2013b); 26. Ma et al. (2015); 27. Greenwood et al. (1992); 28. Simon et al. (1994); 29. Ivanova et al. (2002); 30. Ma et al. (2011b); 31. Krot et al. (2020); 32. El Goresy et al. (2002); 33. Ma et al. (2012); 34. Komatsu et al. (2018); 35. Ma et al. (2017a); 36. Ma and Rossman (2009a); 37. Ma and Beckett (2016); 38. Ma et al. (2013a); 39. Ma (2018); 40. Fuchs (1971); 41. Ma et al. (2017b); 42. Kimura et al. (1993); 43. Beckett and Stolper (1994)
